# A LDA+U study of selected iron compounds

Thesis submitted for the degree of
Doctor Philosophiae

CANDIDATE:
Matteo Cococcioni

SUPERVISOR:
Stefano de Gironcoli

October 2002

# Contents

# Introduction

Since its theoretical foundation in the mid-1960's [1, 2], Density Functional Theory (DFT) has demonstrated a large predictive power in the study of the ground states properties of real materials, so that it has soon become the most important tool (if not the only one) for first principles calculations. Though exact in principle, this theoretical scheme needs some approximations to be used in practical calculations. In fact, the many body problem concerning an interacting electron system is far too complicated to be approached directly, so that it is usually treated in a simpler one body formalism which describes a fictitious non interacting electron gas with the same density of the real interacting one. In this simplified scheme the many body contributions to the electronic interactions are usually modeled in some approximations.

The simplest of these simplified (and the first historically introduced) is the Local (Spin) Density Approximation (LSDA) which is based on the assumption that the electronic system can be locally represented by a uniform electron gas with the same density. Using L(S)DA the structural, electronic and magnetic ground state properties of a large class of materials, including, for instance, nearly-free-electron-like (simple) metals, covalent semiconductors, ionic solids, and even rather complex intermetallic transition metal compounds, could be described and understood very deeply and usually within a fair agreement with experimental results.

A possible extension to the LDA method is represented by (spin-polarized) Generalized Gradient Approximation (GGA approaches) which, in the modeling of the effective electronic interactions, also accounts for the possible inhomogeneity of real electron systems. The introduction of this approach could solve indeed some open questions within LSDA and even improve the descriptive power of DFT calculations about the structural and the electronic properties of some real non homogeneous systems as, for instance, the transition metal compounds.

However GGA functionals brought out very little enlargement of the class of materials whose properties could be successfully described by DFT, so that there still remains

quite a large group of systems (of growing scientific interest) whose study cannot be accurately addressed by standard DFT approaches: the strongly correlated materials. The reason why ordinary LDA or GGA methods are not able to correctly describe this class of materials mainly consists in the fact that their energy functionals are built treating the real interacting electron system as a (possibly homogeneous) electron gas, and thus result to be not accurate enough to deal with situations in which strong localization of the electrons is likely to occur. The description and understanding of the electronic structure of strongly correlated materials is indeed a very long standing problem and the transition metal oxides (which, in contrast with the observed insulating behavior, are incorrectly predicted to be metals or small gap semiconductors by LSDA or GGA) have represented for long time the most notable failure of DFT. When the high-$T_c$ superconductors entered the scene (their parent materials are also strongly correlated systems) the study of new approaches which could allow to describe this kind of systems with first principle calculations received a new impulse, and in the last fifteen years many methods were proposed in this direction.

One of the most popular approaches of this kind is LDA+U for which a variety of different functionals were introduced and developed. Although the different formulations can differ, to some extent, from each other for their theoretical construction and the technical details concerning their practical implementation, the main idea they all rely on is the same and mainly consists in trying to correct the standard (LDA or GGA) energy functionals with a mean field Hubbard-like term which is meant to improve the description of the electronic correlations. The formal expression of this additional energy functional is generally taken from the model hamiltonians (the Hubbard model is just one example) that represent the "natural" theoretical framework to deal with strongly correlated materials. These models, however, are strongly dependent on the choice of the interaction parameters which sometimes have been evaluated using ab-initio (constrained) calculations. Anyway, no general procedure is well established to calculate these effective interaction parameters entering the theory and this situation is also reflected in the LDA+U-like approaches. In fact, the few method which have been proposed to extract the effective electronic interactions from first principle (constrained) calculations, did not give very reliable results, so that their value is usually determined by seeking a good agreement of the calculated properties with the experimental results in a semiempirical way.

In this work a critical study of the LDA+U approach is proposed, which starting from the formulation of Anisimov al. [3, 4, 5], and its further improvements [6, 7, 8], develops

a simpler approximation that appears, to our opinion, a more "natural" extension of the LDA (or GGA) description we aim to correct and complete. In this context a method to calculate the interaction parameters is also introduced which is based on a linear response approach and allows to fix the parameters entering the LDA+U correction in close relationship with the behaviour of the system under consideration, without any aprioristic assumption.

This methodology is then applied to the study of the electronic, magnetic and structural properties of some iron compounds, chosen as representative of "normal" (bulk iron) and strongly correlated (iron oxide and fayalite) situations.

The present thesis is organized as follows. After having devoted a first chapter to a brief overview of the standard DFT techniques and approximations, in the second chapter we present results about the electronic, magnetic, and structural properties of some iron compounds obtained within the GGA framework. We underline the merits of this approach in describing these crystals, but also point out the aspects which need a further improvement to be correctly described because the relevance of strong electronic correlation. In the second chapter the LDA+U method and its implementation within a pseudopotential-plane wave framework are introduced. We start from a brief historical overview about this theoretical method and discuss the goals it was built for. Then we focus on the particular approximation we actually use and underline the motivations which led us to consider this simpler expression for the LDA+U functional. To complete the theory and make our approach self-sustaining, a linear response approach to calculate the effective electronic interactions entering the LDA+U correction is also presented, together with a discussion about the differences with the approaches presented in other works. In the fourth chapter we deal with the same systems studied in the second chapter but using LDA+U. We focus on the improvements we obtain with respect to the GGA calculations and discuss the role of LDA+U corrections in describing the electronic structure of these materials and their structural properties. A conclusive discussion about merits and defects of the presented simplified LDA+U scheme and of the linear response approach to calculate the effective interactions is presented in the last chapter together with some possible perspectives of improvement and still remaining problems.

# Chapter 1

# Theoretical tools and approximations

In this chapter the theoretical approaches and approximations used in standard first principles calculations will be briefly described. Our motivation is twofold: on one hand the most commonly used tools employed in the study of the physical properties of real materials are reminded; on the other hand a more complete description is given to the theoretical background our LDA+U approach is built on. This will provide a better understanding of the starting point of the new theoretical approach and a good knowledge of the many technical details required for its practical implementation.

## 1.1 The Born Oppenheimer approximation

The possibility of treating separately the electrons and the ions of a real system, ab-initio calculations generally rely on, is the result of the adiabatic approximation of Born and Oppenheimer [11] which is a consequence of the large mass difference between the two families of particles. In other words, being much lighter than the ions, the electrons can move in a solid much faster than the nuclei and the electronic configuration can be considered as completely relaxed in its ground state at each position the ions assume during their motion. In mathematical terms we would say that the time scale for the electron excitations, the inverse of their bandwidth, is usually much smaller than the one for the ions, namely the inverse of the phonon frequencies. This means that while studying the electronic degrees of freedom the ions can be considered at rest; thus the total wavefunction of the system can (approximately) be written as the product of a function describing the ions and another for the electrons depending only parametrically

upon the ionic positions:

$$\Psi(\mathbf{R},\mathbf{r}) = \Phi(\mathbf{R})\psi_{\mathbf{R}}(\mathbf{r}) \tag{1.1}$$

where $\mathbf{R} = \{\mathbf{R}_I\}$ is the set of all the nuclear coordinates, and $\mathbf{r} = \{\mathbf{r}_i\}$ is the same quantity for all the electrons in the system (though not explicitly indicated, the many particle wavefunction $\psi_{\mathbf{R}}(\mathbf{r})$ also depends on the electronic spin degrees of freedom). Within this approximation, the ionic wavefunction $\Phi(\mathbf{R})$ is the solution of the Schrödinger equation:

$$\left(-\sum_I \frac{\hbar^2}{2M_I}\frac{\partial^2}{\partial \mathbf{R}_I^2} + E(\mathbf{R})\right)\Phi(\mathbf{R}) = \varepsilon\Phi(\mathbf{R}) \tag{1.2}$$

where $M_I$ is the mass of the $I^{\text{th}}$ nucleus and $E(\mathbf{R})$ is the so called *Born-Oppenheimer potential energy surface* corresponding to the ground state energy of the electronic system when the nuclei are fixed in the configuration $\mathbf{R}$. More generally electronically excited potential energy surfaces can be defined which are important when electronic transitions driven by ionic motion, through the non adiabatic coupling terms (electron-phonon interaction), are considered. The potential energy surface can be computed solving the Schrödinger problem for the electrons:

$$\left(-\sum_i \frac{\hbar^2}{2m}\frac{\partial^2}{\partial \mathbf{r}_i^2} + \frac{e^2}{2}\sum_{i\neq j}\frac{1}{|\mathbf{r}_i-\mathbf{r}_j|} - \sum_{iI}\frac{Z_I e^2}{|\mathbf{r}_i-\mathbf{R}_I|} + \frac{e^2}{2}\sum_{I\neq J}\frac{Z_I Z_J}{\mathbf{R}_I-\mathbf{R}_J}\right)\psi^{\alpha}_{\mathbf{R}}(\mathbf{r}) = \\ = E_\alpha(\mathbf{R})\psi^{\alpha}_{\mathbf{R}}(\mathbf{r}) \tag{1.3}$$

where $Z_I$ is the charge of the $I^{\text{th}}$ nucleus, $-e$ and $m$ are the electronic charge and mass, and $\alpha$ is an index for the electronic state.

The equations describing the electronic and the ionic problems are obtained from the equation for the total system assuming the wavefunction factorization of eq. 1.1 and neglecting the *non adiabatic* terms which come from the kinetic operator for the nuclei acting on the electronic wavefunction $\psi_{\mathbf{R}}(\mathbf{r})$. This is expected to be a good approximation for most real materials since the neglected terms are of the order of the ratio $m_e/M$ between the (effective) electronic mass and the ionic one. The separation among electronic and ionic degrees of freedom is a very useful simplification of the problem and allows to treat the ions within a classical formalism as generally done in molecular dynamics calculations. However the electronic problem is a quantum many body problem; the total wavefunction of the system depends on the coordinates of all the electrons and cannot be decoupled in single particle contributions because of their mutual interaction, so that the problem is still far too complicated to be solved exactly in practical computations. Owing to this difficulty, further developments are required to perform ab-initio calculations for real materials. Density Functional Theory provides a framework for these developments.

## 1.2 Density Functional Theory

The first important conceptual advantage introduced by Density Functional Theory (DFT) [1] is the possibility to describe the ground state properties of a real system in terms of its ground state electronic charge density (which depends on just one spatial variable) instead of the far more complicated wavefunctions (which depends on the coordinates of all the electrons in the system). Dealing with the charge density allows to reformulate the problem in a mean-field-like language which is however based on an exact result. If we consider an interacting electron gas, the external potential acting on the particles determines the ground state of the system and the corresponding charge density. Thus, all the physical quantities concerning this state (like, for instance, the total energy) are functionals of the external potential. As it was first demonstrated by Hohenberg and Kohn [1], due to a one to one correspondence among the external potential and the ground state density (which allows to express the former as a functional of the latter), there also exists a unique universal functional $F[n(\mathbf{r})]$ of the ground state electron density alone such that a variational principle exists with respect to the electron density for the total energy functional

$$E[n(\mathbf{r})] = F[n(\mathbf{r})] + \int V_{ext}(\mathbf{r}) n(\mathbf{r}) d\mathbf{r} \tag{1.4}$$

where $F[n(\mathbf{r})]$ contains the kinetic energy and the mutual Coulomb interaction of the electrons, and $V_{ext}(\mathbf{r})$ represents the external potential acting on the particles. The minimization of this functional with the condition that the total number of particles, $N$, is preserved:

$$\int n(\mathbf{r}) d\mathbf{r} = N, \tag{1.5}$$

directly gives the ground state energy and charge density, from which all the other physical properties can be extracted. This variational principle is very important from a conceptual point of view as it suggests a procedure to access all the interesting quantities.

Unfortunately, the universal functional $F[n(\mathbf{r})]$ (which is independent on $V_{ext}(\mathbf{r})$) is not known in practice and in order to transform DFT into a useful tool Kohn and Sham [2] introduced a further development which consists in mapping the original interacting problem into an auxiliary non interacting one. For this fictitious system of non interacting electrons the Hohenberg and Kohn theorem also applies and the unique functional $F[n(\mathbf{r})]$ corresponds in this case to the kinetic energy of the non interacting electrons, $T_0[n(\mathbf{r})]$. The density functional $F[n(\mathbf{r})]$ for the interacting system can then be expressed as the sum of the kinetic energy of a non interacting electron gas with

the same density of the real one and the additional terms describing the interparticle interaction:

$$F[n(\mathbf{r})] = T_0[n(\mathbf{r})] + \frac{e^2}{2}\int \frac{n(\mathbf{r})n(\mathbf{r}')}{|\mathbf{r}-\mathbf{r}'|}d\mathbf{r}d\mathbf{r}' + E_{xc}[n(\mathbf{r})]. \tag{1.6}$$

The second term in the right hand side of eq. 1.6 is the classical Coulomb interaction among the electrons described through their charge density (the Hartree term), whereas $E_{xc}[n(\mathbf{r})]$ is the so called exchange-correlation energy and accounts for all the many body effects which are not described in the other terms. In practice this term contains all the differences among the non interacting fictitious system and the real interacting one (here including corrections for the Coulomb interaction and for the kinetic energy also) so that what we do is confining our ignorance about $F[n(\mathbf{r})]$ into one single, hopefully small, term. This is particularly useful when we minimize the functional $F[n(\mathbf{r})]$ with the constraint given by the conservation of the total number of particle to obtain the ground state physical properties of the real system. In fact from eq. 1.6 it is quite easy to extract the effective potential $V_{KS}$ acting on the electrons of the fictitious non interacting system. If we impose the total energy functional for the non interacting electron gas

$$E^0[n(\mathbf{r})] = T_0[n(\mathbf{r})] + \int V_{KS}(\mathbf{r})n(\mathbf{r})d\mathbf{r} - \mu'\left(\int n(\mathbf{r})d\mathbf{r} - N\right) \tag{1.7}$$

to be minimized by the same electron density which also minimizes the total energy of the interacting electron system

$$\begin{aligned} E[n(\mathbf{r})] &= T_0[n(\mathbf{r})] + \\ \frac{e^2}{2}\int \frac{n(\mathbf{r})n(\mathbf{r}')}{|\mathbf{r}-\mathbf{r}'|}d\mathbf{r}d\mathbf{r}' + E_{xc}[n(\mathbf{r})] &+ \int V_{ext}(\mathbf{r})n(\mathbf{r})d\mathbf{r} - \mu\left(\int n(\mathbf{r})d\mathbf{r} - N\right) \end{aligned} \tag{1.8}$$

the expression for the effective Kohn-Sham potential results:

$$V_{KS}(\mathbf{r}) = V_{ext}(\mathbf{r}) + e^2\int \frac{n(\mathbf{r}')}{|\mathbf{r}-\mathbf{r}'|}d\mathbf{r}' + v_{xc}(\mathbf{r}), \tag{1.9}$$

$$v_{xc}(\mathbf{r}) = \frac{\delta E_{xc}[n]}{\delta n(\mathbf{r})}, \tag{1.10}$$

which is defined within an unimportant additive constant corresponding to the difference among the chemical potentials $\mu$ and $\mu'$, which were introduced in the total energy functionals as Lagrange multipliers to ensure the conservation of the total number of particles. The resulting effective hamiltonian for the system is the one describing a non interacting electron gas feeling the effective potential $V_{KS}$ in which all the interparticle interactions for the real system are contained. The electronic problem can thus be

approached using (fictitious) one particle wavefunctions which allow the charge density to be written as:

$$n(\mathbf{r}) = \sum_i f_i |\psi_i(\mathbf{r})|^2, \tag{1.11}$$

where $i$ is an index for the single particle state, and $f_i$ is the Fermi distribution (which corresponds to $\theta(\epsilon_F - \epsilon_i)$ for $T = 0$). The kinetic energy for the non interacting auxiliary system is also straightforward to compute within this formalism:

$$T_0[n(\mathbf{r})] = -\sum_i f_i \int \psi_i^*(\mathbf{r}) \frac{\hbar^2 \nabla^2}{2m} \psi_i(\mathbf{r}) d\mathbf{r}. \tag{1.12}$$

From the minimization of the non interacting energy functional with respect to $\psi_i^*$ with the constraint of fixed number of electrons, the following set of Schrödinger-like equations (called Kohn-Sham equations) can be obtained:

$$\hat{H}_{KS}\psi_i(\mathbf{r}) = \left[ -\frac{\hbar^2 \nabla^2}{2m} + V_{KS}(\mathbf{r}) \right] \psi_i(\mathbf{r}) = \epsilon_i \psi_i(\mathbf{r}) \tag{1.13}$$

where the hermeticity of the operators appearing in this expression ensures the possibility of choosing the constraints in such a way the orthonormality conditions for the fictitious wavefunctions are satisfied:

$$\int \psi_i^*(\mathbf{r}) \psi_j(\mathbf{r}) d\mathbf{r} = \delta_{ij}. \tag{1.14}$$

It is worth to remark that the wavefunctions appearing in the Kohn-Sham equations have no direct physical meaning: they are the eigenstates of the one body density matrix we use in the theory but cannot be considered the wave functions for the electrons of the real system as they are the electronic orbitals for the auxiliary non interacting gas.

The set of the Kohn-Sham equations is a strongly non linear one since the electronic wavefunctions, which are to be obtained as the solutions of the problem, also enter the expression of the effective potential as they are used in building the charge density on which $V_{KS}$ depends.

This means that, in order to solve this system, we have to adopt an iterative method which, starting from an initial guess for the wavefunctions and the potential, evolves both quantities up to self consistency. Owing to the fact that solving the Kohn-Sham equations corresponds to minimize the total energy functional of the $N$-electrons system on a set of orthonormal single particle wavefunction, the ground state total energy can also be expressed as:

$$E_0[n(\mathbf{r})] = \sum_i f_i \epsilon_i - \frac{e^2}{2} \int \frac{n(\mathbf{r}) n(\mathbf{r}')}{|\mathbf{r} - \mathbf{r}'|} d\mathbf{r} d\mathbf{r}' + E_{xc}[n(\mathbf{r})] - \int v_{xc}(\mathbf{r}) n(\mathbf{r}) d\mathbf{r} + E_{ion} \tag{1.15}$$

where the Hartree ($H$) and the exchange-correlation ($xc$) contributions respectively account for the double counting and the miscounting of the same quantities in the sum of the eigenvalues, whereas $E_{ion}$ is the energy term accounting for the direct Coulomb interaction among the ionic cores. The variational principle the theory relies on, eq. 1.8, implies that the total energy functional is quadratic, near the self consistent point, in the fluctuations of the wavefunctions (or the charge density) around their self consistent value. This variational properties is not shared by eq. 1.15 which displays a linear error near the self consistent point. In fact, at any intermediate step of the minimization, the $Hxc$ potential entering the expression of the Kohn-Sham hamiltonian, eqs. 1.13 and 1.9, is calculated from the charge density $n^{in}$ obtained in the previous iteration. This charge density is generally different from the analogous quantity obtained in the current diagonalization $n^{out}$. The sum of the eigenvalues thus reads:

$$E_{band} = \sum_i f_i \epsilon_i = T_0[n^{out}] + \int (V_{ext}(\mathbf{r}) + V^{in}_{Hxc}(\mathbf{r})) n^{out}(\mathbf{r}) d(\mathbf{r}) \tag{1.16}$$

which behaves at most linearly in the above mentioned fluctuations of the quantity $n^{out}$ around its self consistent value. To obtain a variational total energy we can add some corrections to the band energy which eliminate the undesired dependence on $n^{in}$. The final expression results:

$$\begin{aligned}
&\tilde{E}_{band}[n^{out}] = \sum_i f_i \epsilon_i + \int (V^{out}_{Hxc}(\mathbf{r}) - V^{in}_{Hxc}(\mathbf{r})) n^{out}(\mathbf{r}) d(\mathbf{r}) = \\
&T_0[n^{out}] + \int (V_{ext}(\mathbf{r}) + V^{in}_{Hxc}(\mathbf{r})) n^{out}(\mathbf{r}) d(\mathbf{r}) + \int (V^{out}_{Hxc}(\mathbf{r}) - V^{in}_{Hxc}(\mathbf{r})) n^{out}(\mathbf{r}) d(\mathbf{r}) = \\
&T_0[n^{out}] + \int (V_{ext}(\mathbf{r}) + V^{out}_{Hxc}(\mathbf{r})) n^{out}(\mathbf{r}) d(\mathbf{r})
\end{aligned} \tag{1.17}$$

where it is evident that the correction (to be added to $E_0$ in eq. 1.15) completely vanish when self consistency is reached (full details can be found in [12]).

The theoretical approach described so far is expected to be very efficient when the dominant part of the energy consists of the kinetic and the electrostatic terms because they are described without any approximation. However the success in studying real materials depends very strongly on how the (hopefully small) exchange-correlation contribution is described and this is particularly true with systems (like the strongly correlated materials studied in this thesis) where the many body effects are expected to be important.

### 1.2.1 Approximations for the exchange-correlation energy functionals: LDA and GGA

Up to this point no approximation was introduced into the theory, but there still exists a term (the exchange-correlation energy) which, though well defined (and exact) in principle, has a very complicated expression which is not known explicitly. Some assumptions are thus needed in the definition of $E_{xc}$ to convert the DFT in a practical tool for ab-initio calculations and this modeling necessarily introduce in the theory some approximations.

The simplest of these descriptions is called the Local Density Approximation (LDA) and is obtained assuming that the $xc$ energy of a real system behaves locally as in a uniform (homogeneous) electron gas having the same density. The $xc$ energy thus depends only on the local density of the system and actually reads:

$$E_{xc}^{LDA}[n] = \int \varepsilon_{xc}^{hom}(n(\mathbf{r}))n(\mathbf{r})d\mathbf{r} \tag{1.18}$$

where $\varepsilon_{xc}^{hom}(n(\mathbf{r}))$ is the $xc$ energy density of the above mentioned homogeneous system. The $xc$ potential can be easily obtained from the $xc$ energy functional and results:

$$v_{xc}^{LDA}(\mathbf{r}) = \frac{\delta E_{xc}^{LDA}[n]}{\delta n(\mathbf{r})} = \frac{\partial F_{xc}(n)}{\partial n}|_{n=n(\mathbf{r})} \tag{1.19}$$

where $F_{xc}(n) = \varepsilon_{xc}^{hom}(n)n$. This approximation was designed to work with systems in which the electronic charge density is expected to be smooth (like, for instance, in nearly free-electron-like (simple) metals, intrinsic semiconductors and so on) but it gives indeed quite good results also with non homogeneous systems like covalently bonded materials and (some) transition metals. It typically produces good agreement with experiments about structural and vibrational properties, but usually overestimates bonding energies and predicts shorter equilibrium bond lengths than found in experiments. In order to overcome these and other difficulties of LDA, some extensions of the original approximation were introduced among which the Generalized Gradient Approximation (GGA) family is one of the most successful. Within GGA the $xc$ energy is a functional not of the density alone, but also of its local spatial variations:

$$E_{xc}^{GGA}[n] = \int \varepsilon_{xc}^{GGA}(n(\mathbf{r}), |\nabla n(\mathbf{r})|)n(\mathbf{r})d\mathbf{r}. \tag{1.20}$$

Several expressions of the $xc$ energy density have been described in different formulations of the GGA functionals. Among these, the Perdew-Burke-Ernzherof (PBE) expression was chosen in this work [13].

The potential corresponding to the energy functional $E_{xc}^{GGA}[n]$ can be expressed as:

$$v_{xc}^{GGA}(\mathbf{r}) = \frac{\delta E_{xc}^{GGA}[n]}{\delta n(\mathbf{r})} = \left( \frac{\partial F_{xc}}{\partial n} - \sum_{\alpha=1}^{3} \partial_\alpha \left( \frac{\partial F_{xc}}{\partial(\partial_\alpha n)} \right) \right) |_{n=n(\mathbf{r})} \tag{1.21}$$

where $F_{xc}(n, |\nabla n|) = \varepsilon_{xc}^{GGA}(n, |\nabla n|)n$, $\partial_\alpha$ stands for the $\alpha^{\text{th}}$ component of the gradient and the rule of integration by parts was used to obtain the last equality. This improved approximation is actually able to cure some defects of LDA and generally produces better description of the structural properties of real materials. In particular it improves significantly the results about the binding energy of real system. It is also expected to give a better description of non homogeneous systems, like transition metals, producing correct results in some cases where LDA completely fails. One example is bulk iron which in agreement with experiments, is predicted by GGA to have a ferromagnetic (FM) bcc ground state rather than a paramagnetic fcc one as found in LDA.

Despite the theory is exact in principle, the approximations we have to adopt for the exchange and correlation energy both in LDA and GGA introduce a mean-field-like formalism which can be expected to work well for systems with rather delocalized electrons but is not sufficiently accurate when dealing with materials with localized electrons for which many body effects are expected to be more important.

### 1.2.2 The Local Spin Density Approximation

A formulation of the $xc$ functional depending only on the total electron density should allow an exact description of real materials; however the treatment of magnetic systems is much simpler if the $xc$ energy functional is explicitly considered as dependent on the two spin populations separately. In this case the Kohn Sham equations can be written independently for the two spin polarizations:

$$\left[ -\frac{\hbar^2 \nabla^2}{2m} + V_{KS}^{\sigma}(\mathbf{r}) \right] \psi_i^{\sigma}(\mathbf{r}) = \epsilon_i^{\sigma} \psi_i^{\sigma}(\mathbf{r}) \tag{1.22}$$

where we have:

$$V_{KS}^{\sigma}(\mathbf{r}) = V_{ext}(\mathbf{r}) + e^2 \int \frac{n(\mathbf{r}')}{|\mathbf{r} - \mathbf{r}'|} d\mathbf{r}' + v_{xc}^{\sigma}(\mathbf{r}) \tag{1.23}$$

$$v_{xc}^{\sigma}(\mathbf{r}) = \frac{\delta E_{xc}[n^{\uparrow}, n^{\downarrow}]}{\delta n^{\sigma}(\mathbf{r})} \tag{1.24}$$

$$n^{\sigma}(\mathbf{r}) = \sum_i f_i^{\sigma} |\psi_i^{\sigma}(\mathbf{r})|^2, \quad n(\mathbf{r}) = \sum_{\sigma} n^{\sigma}(\mathbf{r}). \tag{1.25}$$

Of course the two spin populations interact with each other through the Hartree and $xc$ potentials and the effective field acting on one of them depends on the opposite-spin charge density also. As it can be observed from the expression of the effective

potential, the Coulomb part of the potential doesn't change at all with respect to LDA; the unbalance between up and down spin states, which originates the magnetization, is indeed produced by the exchange and correlation potential which accounts for the differences between like-spin and unlike-spin interactions. The exchange and correlation functionals of this generalized spin-dependent approach (whose simplest variant is the so called Local Spin Density Approximation) are usually given separate expressions. In fact, the exchange contribution is diagonal in the spin and can be obtained extending the non polarized expression:

$$E_x^{LSDA}[n] = \sum_\sigma \int F_x^{LSDA}(n_\sigma(\mathbf{r}))d\vec{r} = \sum_\sigma \frac{1}{2}\int F_x^{LDA}(2n_\sigma(\mathbf{r}))d\vec{r} \tag{1.26}$$

where $F_x^{LDA}$ is the same functional used for the unpolarized case. The correlation functional, instead, is obtained interpolating the results for the homogeneous electron gas at different spin polarizations and can be written as dependent on both the (total) charge density $n(\mathbf{r})$ and the magnetization $m(\mathbf{r})$ which is defined as:

$$m(\mathbf{r}) = \mu_B(n^\uparrow(\mathbf{r}) - n^\downarrow(\mathbf{r})). \tag{1.27}$$

If we define the magnetic polarization,

$$\xi(\mathbf{r}) = \frac{\frac{1}{\mu_B}|m(\mathbf{r})|}{n(\mathbf{r})}, \tag{1.28}$$

so that $0 \leq \xi \leq 1$, this contribution to the total energy actually results:

$$E_c^{LSDA}[n,\xi] = \int \left[\epsilon_c^U(n(\mathbf{r})) + f(\xi(\mathbf{r}))\left(\epsilon_c^P(n(\mathbf{r})) - \epsilon_c^U(n(\mathbf{r}))\right)\right] n(\mathbf{r})d\mathbf{r} \tag{1.29}$$

where $f(\xi)$ is a smooth interpolating function with $f(0) = 0$ and $f(1) = 1$, and the $\epsilon_c^P$ and $\epsilon_c^U$ functionals represent respectively the correlation energy densities for the polarized and the unpolarized systems. The contribution to the Kohn-Sham potential coming from the exchange and correlation functionals described so far corresponds to an effective magnetic field. In fact, by calculating the first derivative of these quantities with respect to the spin polarized charge densities, we obtain a first term equal for the two spin polarizations and a second one (depending on the magnetization) which has the same absolute value but changes sign according to the spin it is applied on. This latter term introduces differences in the two effective fields thus producing the spin unbalances from which the magnetic properties of the system derive.

A similar extension to the spin polarized case is also possible within the GGA approximation. However, within this approach, the correlation contribution usually does

not contain the gradient of the magnetic polarization [13] and the functionals finally reads:

$$E_x^{\sigma-GGA} = \frac{1}{2}\sum_\sigma \int F_x(2n_\sigma, |2\nabla n_\sigma|)d\mathbf{r} \tag{1.30}$$

$$E_c^{\sigma-GGA} = \int F_c(n, \xi, |\nabla n|)d\mathbf{r} \tag{1.31}$$

where $F_x$ and $F_c$ are the gradient-dependent analogues of the quantity defined in the LDA case.

## 1.3 Periodic systems: the Bloch theorem

The description of real (bulk) materials within ab-initio calculations is based on the assumption that the atoms which compose them are at rest in their equilibrium positions and these form an infinite, periodically repeated structure. In mathematical terms, if we call $V$ the external potential acting on the electrons, we have:

$$V(\mathbf{r} + \mathbf{R}) = V(\mathbf{r}) \tag{1.32}$$

where $\mathbf{R}$ is a direct lattice vector corresponding to an integer linear combination of three fundamental vectors determining the periodicity of the lattice in three independent directions. The whole electronic hamiltonian and all the physical quantities describing the periodical system also share the translational invariance of the lattice and this allows to use the Bloch theorem which states that the single particle electronic wave function can be expressed in the form

$$\psi_{\mathbf{k}v}(\mathbf{r}) = e^{i\mathbf{k}\cdot\mathbf{r}} u_{\mathbf{k}v}(\mathbf{r}) \tag{1.33}$$

where $\mathbf{k}$ is the crystal momentum of the electrons (it actually describes the translational properties of the wavefunction), $v$ is a discrete index (called the band index) classifying states corresponding to the same $\mathbf{k}-$vector and $u_{\mathbf{k}v}(\mathbf{r})$ is a function with the same periodicity of the crystal:

$$u_{\mathbf{k}v}(\mathbf{r} + \mathbf{R}) = u_{\mathbf{k}v}(\mathbf{r}). \tag{1.34}$$

Due to the translational invariance of the system different $\mathbf{k}-$points can be treated independently. In fact, the hamiltonian commutes with the operators which generate translations through the points of the lattice and is thus block diagonal on the basis set of the eigenvectors of these latter operators which corresponds to Bloch wavefunction of the form given in 1.33 and are classified by $\mathbf{k}$. In this context the band index $v$ numbers the eigenvalues of the hamiltonian belonging to the same $\mathbf{k}-$block.

The $\mathbf{k}-$vectors are defined within the so called first Brillouin Zone (BZ) of the reciprocal space which has a periodic structure whose fundamental lattice vectors $\mathbf{b}_i$ are related to the ones of the real (direct) space $\mathbf{u}_i$ as follows:

$$\mathbf{b}_i \cdot \mathbf{u}_j = 2\pi\delta_{ij} \qquad\qquad i,j = 1,2,3. \tag{1.35}$$

The sums over the electronic states which define many physical quantities as, for instance, $E_{band}$ and $n(\mathbf{r})$, actually correspond to integrals over the BZ (and sums over the band index $v$). Using the symmetry of the crystal, the integration can be conveniently confined in a smaller region of the BZ, the so called irreducible wedge of the Brillouin zone (IBZ). This result can be further improved by the use of the special point integration technique which allows to perform reciprocal space integration (needed for example when calculating the charge density or the sum of the eigenvalues) using generally a small set of $\mathbf{k}$-vectors in the IBZ. These points can be chosen according to different techniques [14](in this thesis we use the Monkhorst and Pack recipe) and in general the accuracy of the (approximate) method can be checked by the convergence properties of the physical properties of interest upon increasing their number. As an example, the reciprocal space integration for the charge density is performed as a sum over a discrete set of vectors:

$$\tilde{n}(\mathbf{r}) = \sum_{\mathbf{k}\in IBZ} \omega_{\mathbf{k}} \sum_{v} f_{\mathbf{k}v} |\psi_{\mathbf{k}v}(\mathbf{r})|^2 \tag{1.36}$$

from which the electronic charge density results through a symmetrization procedure:

$$n(\mathbf{r}) = \frac{1}{N_S} \sum_{S} \tilde{n}(S^{-1}\mathbf{r} - \mathbf{f}) \tag{1.37}$$

where $N_S$ is the number of symmetry operations $S$ in the space group of the crystal and $\mathbf{f}$ a possible fractional translation. In eq. 1.36 the $\omega_{\mathbf{k}}$ coefficient is the $\mathbf{k}$-point weight calculated within the special point technique.

The special points technique is very efficient in the description of semiconductors or insulators but gives poor results when directly applied to metals. This happens because the region around the Fermi level (which is crossed by some electronic states) needs to be sampled quite accurately and in general a larger number of vectors is required. If the used $\mathbf{k}$-point grid is not fine enough, there could also be problems of instability during the self-consistent run because even small shifts in the Fermi energy could include or exclude in the reciprocal space sums (like the one in eq. 1.36) a finite number of electronic states thus producing considerable fluctuations in the corresponding quantities. A possible solution to this problem can be achieved using the tetrahedron method which consists in

decomposing the BZ into symmetry breaking elemental volumes and connecting the energy bands between neighboring **k**-points by linear interpolation. However this method presents some important drawbacks [15] so that we choose to use another approach to the problem of describing metallic systems. This technique consists in introducing a finite smearing of the Fermi distribution (actually corresponding to consider a finite effective temperature) which smoothes the weight of the states around this level and avoids large fluctuations in the calculated quantities. The convoluting function used to introduce the smearing can be chosen in many ways: finite temperature Fermi distribution, Lorentzian, Gaussian [16], cold smearing factors [17], and so on. In this thesis the Methfessel and Paxton smearing technique [18] is used which adopts a combination of Gaussians and polynomials as spreading functions. This approximation works quite well for metals (even if a larger number of **k**-points is usually required than for semiconductors) and the accuracy of the reciprocal space integrations at finite smearing can be checked by their convergence properties upon increasing the number of the special **k**-vectors in the IBZ and reducing the broadening width $\sigma$. The main drawback introduced by the smearing technique is the dependence of the ground state total energy on the chosen $\sigma$. The Methfessel and Paxton methods allows to considerably reduce this dependence by accurately choosing the convoluting function to smear the Fermi distribution.

## 1.4 The plane wave pseudopotential method

In order to solve the KS equations by practical calculations we need to transform the original integro-differential problem into a more tractable algebraic one. This can be achieved by expanding the electronic wavefunctions on a basis set and using this representation in all operators in the hamiltonian. The one chosen in this work (and one of the most used in ab-initio calculations) is the Plane Wave (PW) basis set [12] which takes advantage from efficient algorithms, like the Fast Fourier Transform (FFT), to move back and forth from real to reciprocal space. The Bloch electronic wave function in eq. 1.33 can thus be represented in the form:

$$\psi_{\mathbf{k}v}(\mathbf{r}) = \frac{1}{(N\Omega)^{\frac{1}{2}}} \sum_{\mathbf{G}} e^{i(\mathbf{k}+\mathbf{G})\cdot\mathbf{r}} c_v(\mathbf{k}+\mathbf{G}) \tag{1.38}$$

where $\Omega$ is the volume of the unit cell, the $\mathbf{G}$ vectors are the reciprocal lattice vectors, and the $c_v(\mathbf{k}+\mathbf{G})$ coefficients are normalized in such a way that:

$$\sum_{\mathbf{G}} |c_v(\mathbf{k}+\mathbf{G})|^2 = 1. \tag{1.39}$$

Using this expansion, the KS equations can be written in reciprocal space as:

$$\sum_{\mathbf{G}'}\left[\frac{\hbar^2}{2m}|\mathbf{k}+\mathbf{G}|^2+v_h(\mathbf{G}-\mathbf{G}')+v_{xc}(\mathbf{G}-\mathbf{G}')+v_{ext}(\mathbf{G},\mathbf{G}')\right]c_v(\mathbf{k}+\mathbf{G}')=\epsilon_{\mathbf{k}v}c_v(\mathbf{k}+\mathbf{G}). \tag{1.40}$$

It is evident from this expression that the hamiltonian has block diagonal form with respect to the $\mathbf{k}$ vectors and the diagonalization can thus be performed within each of these block separately. As we are studying the ground state properties of the system, for each $\mathbf{k}-$point only a finite number of the lowest-energy electronic states on which all the electrons of the system can be accommodated, need to be computed to obtain the charge density. This quantity is then used to construct a new guess of the potential to be reintroduced in the Kohn-Sham equations for the successive step of the iterative diagonalization. Of course the PW expansion is exact in the limit of infinite number of $\mathbf{G}$-vectors. In practical calculations one can deal only with a finite number of plane waves and usually chooses those contained in a sphere of maximum kinetic energy $E_{cut}$ (the energy cut-off):

$$\frac{\hbar^2}{2m}|\mathbf{k}+\mathbf{G}|^2\leq E_{cut}. \tag{1.41}$$

The accuracy we obtain in resolving the KS equation under the condition in eq. 1.41 has to be checked each time by increasing the value of the energy cut-off and studying the convergence of the properties we are interested in. The big advantage of using the PW expansion mainly consists in the fact that $E_{cut}$ is the only parameter in the theory which controls the accuracy of the description of the system under consideration. This means that, once $E_{cut}$ is fixed, all the wavefunctions of the system whose variation takes place over distances larger than (and up to) $2\pi\hbar/\sqrt{2mE_{cut}}$ can be well described.

Unfortunately, the PW expansion uses the same resolution in each region of space so that, to describe the ionic cores and the electronic states partially localized around them, we would need an intractably large number of $\mathbf{G}$ vectors. One possible way around this difficulty is the Pseudopotential (PP) technique, which is based on the assumption that the most relevant physical properties of a system, as far as bonding and chemical reactivity are concerned, are brought about by its valence electrons only, while the ionic cores (the nuclei dressed by the most internal electronic cloud) can be considered as frozen in their atomic configurations. The valence electrons thus move in the effective external field produced by these inert ionic cores and the pseudopotential tries to reproduce the interaction of the true atomic potential on the most external (valence) states without explicitly including the core states in the calculations. There exist different procedures to build a pseudopotential but the general ideas they rely on are similar. Once a full

potential calculation is performed for the isolated atom, the electronic states are divided into two categories: the internal states and the valence ones. The internal electrons remain frozen in their ground state atomic configuration whereas for the external ones a pseudowavefunction is built (which matches the corresponding full potential one in the region external to a fixed core radius) which is chosen to be smooth and nodeless inside the core, while conserving the total valence charge in this region (norm conserving condition). Given a choice for both the core radius and the shape of the pseudowavefunction, a pseudopotential is built (inverting the Schröndinger-like equation for the considered electronic state) which reproduces the scattering properties of the "real" valence states of the reference atomic configuration in a region of energies which has to be as large as possible in order to give good transferability of the pseudopotential when used in different chemical environments. Owing to the smoothness of the pseudowavefunction, the calculations can be performed with a reasonable number of plane waves. However in order to reproduce the scattering properties of the all-electrons (AE) wavefunctions of several angular momenta, it is usually necessary to split the pseudopotential in a local part (matching the real full potential outside the core) and a non local one (vanishing outside the core) which acts in different ways on each different angular momentum channel. The first expression for this non local contribution was given in a semi-local form [19, 20, 21] where the non-locality is built just on the angular coordinates:

$$V(\mathbf{r},\mathbf{r}') = V_{loc}(r)\delta(\mathbf{r}-\mathbf{r}') + \sum_{l=0}^{l_{max}} V_l(r)\delta(r-r')P_l(\mathbf{r},\mathbf{r}'), \tag{1.42}$$

where $P_l$ is the projector operator onto the $l^{\text{th}}$ angular momentum subspace. However, in order to make the PW calculation more efficient, Kleinman and Bylander (KB) [22] replaced the above semilocal expression with a fully separable form:

$$V(\mathbf{r},\mathbf{r}') = V_{loc}(r)\delta(\mathbf{r}-\mathbf{r}') + \sum_i |i\rangle V_i \langle i|. \tag{1.43}$$

where the wavefunctions $|i\rangle$ are (modified) atomic pseudo-states such that the KB potential reproduces the action of the original semilocal one on the reference atomic pseudowavefunctions.

The most complete generalization (and improvement) of this scheme was introduced by Vanderbilt [23, 24] who found a method to increase the transferability of the PPs while reducing the workload necessary to describe the pseudowavefunctions inside the cores. The region of energy corresponding to occupied states in the crystals is sampled with more than one projector so that the index $i$ in eq. 1.43 runs not just on the atomic

reference states but also, for each angular momentum, on a set of (usually two) energy values around them used to reproduce the correct scattering properties of the ion. This requires a generalization of the expression 1.43 whose non local part becomes:

$$V_{nl} = \sum_{i,j} B_{ij} |\beta_i\rangle\langle\beta_j| \tag{1.44}$$

where the functions $|\beta_i\rangle$ are built from the *chosen* pseudowavefunctions (corresponding to the *chosen* energy $\epsilon_i$) and local pseudopotential and are localized in the core region (they vanish at a *chosen* core radius of the atom on that site), while the matrix $B_{ij}$ is an hermitian operator built using the same quantities. This is already a very useful improvement as it allows to increase the PP transferability, but the most important reduction of the computational load introduced by the ultrasoft (US) PPs comes from the relaxation of the norm conserving condition on the pseudowavefunctions and the possibility of choosing them as smooth as possible inside the core regions. This is possible by introducing a generalized overlap operator:

$$S = 1 + \sum_{i,j} q_{i,j} |\beta_i\rangle\langle\beta_j| \tag{1.45}$$

so that the orthonormality condition to be satisfied in the solution of the KS equations is:

$$\langle\psi_i|S|\psi_j\rangle = \delta_{ij}. \tag{1.46}$$

In these expressions $q_{i,j}$ is the integral of the augmentation charge density,

$$q_{i,j} = \int Q_{i,j}(\mathbf{r}) d\mathbf{r} \tag{1.47}$$

$$Q_{i,j}(\mathbf{r}) = \psi_i^{AE*}(\mathbf{r})\psi_j^{AE}(\mathbf{r}) - \psi_i^{PS*}(\mathbf{r})\psi_j^{PS}(\mathbf{r}) \tag{1.48}$$

where the wavefunctions appearing in eq.1.48 are the atomic (all-electrons and pseudo) states used to build the crystal electronic ones. Owing to this generalization of the overlap, the charge density has to be completed with the augmentation part on the ionic cores:

$$n(\mathbf{r}) = \sum_{\mathbf{k},v} f_{\mathbf{k}v} \left[ |\psi_{\mathbf{k}v}(\mathbf{r})|^2 + \sum_{I,i,j} Q_{ij}^I(\mathbf{r} - \mathbf{R}_I) \langle\psi_{\mathbf{k}v}|\beta_i^I\rangle\langle\beta_j^I|\psi_{\mathbf{k}v}\rangle \right]. \tag{1.49}$$

In this expression an index, I, counting the different ions, in position $\mathbf{R}_I$ has been added to the augmentation charges $Q_{ij}^I$ and to the $\beta$ functions. This modification in $n(\mathbf{r})$ also involves the expression of the potential in the KS equations. If we describe the external potential in the form:

$$V(\mathbf{r}, \mathbf{r}') = V_{loc}(r)\delta(\mathbf{r} - \mathbf{r}') + \sum_{I,i,j} D_{ij}^{Iion} |\beta_i^I\rangle\langle\beta_j^I| \tag{1.50}$$

the coefficient $D_{ij}^{Iion}$ have to be calculated as:

$$D_{ij}^{Iion} = B_{ij}^{I} + \epsilon_j q_{ij}^{I} \tag{1.51}$$

and the KS equations (which have to be solved with the generalized orthonormality condition 1.46) finally read:

$$\left[ -\frac{\nabla^2}{2} + \sum_{I,i,j} D_{ij}^{I} |\beta_i^I\rangle\langle\beta_j^I| + V_{eff} \right] |\psi_{\mathbf{k}v}\rangle = \epsilon_{\mathbf{k}v} S |\psi_{\mathbf{k}v}\rangle \tag{1.52}$$

where

$$V_{eff} = V_{loc} + V_{Hxc} \quad \text{and} \quad D_{ij}^{I} = D_{ij}^{Iion} + \int V_{eff}(\mathbf{r}) Q_{ij}^{I}(\mathbf{r} - \mathbf{R}) d\mathbf{r}. \tag{1.53}$$

As evident from the last expression, the pseudopotential needs to be updated at each iteration (the effective potential $V_{eff}$ is built with the electronic charge density) and this makes it participate to the screening process, further increasing its transferability. The prize to be paid to obtain the advantages introduced by US PPs (beside updating the $D_{ij}^{I}$ coefficients each time) consists in the fact that we need a very large cut-off energy to describe the augmentation contribution to the charge density. However this term is important just in the calculation of $n(\mathbf{r})$ and does not enter the diagonalization problem which has the dimension fixed by the (smaller) wave function energy cut-off.

### 1.4.1 The non linear core correction

The PW PPs method is based on the assumption that the electronic charge density can be separated into a valence term $n_v(\mathbf{r})$ and a frozen core contribution $n_c(\mathbf{r})$. In its original form $H$ and $xc$ potentials in the solid are calculated using $n_v(\mathbf{r})$ only. This is not an approximation for the Hartree potential because it's linear in the charge density and the contribution coming from the core term can be easily separated from the other (and included in the local part of the pseudo potential). The problem exists instead for the $xc$ potential which is not linear in the density. Thus separating the $xc$ energy density as

$$\epsilon_{xc}(n_v(\mathbf{r}) + n_c(\mathbf{r})) \sim \epsilon_{xc}(n_v(\mathbf{r})) + \epsilon_{xc}(n_c(\mathbf{r})) \tag{1.54}$$

introduces a systematic error which is more serious when the two contributions to the charge density considerably overlap with each other. It follows that the systems having valence electrons strongly penetrating in the core regions (they usually are very localized external states like $d$ bands for transition metals or $f$ states in rare earths compounds)

may be affected by this problem. The exact solution would be to include the core states with strong overlap with the valence ones in the valence manifold, but this would become very expensive from a computational point of view, also requiring a larger space for the wavefunctions to be stored. The non linear core correction (NLCC) approximately overcomes this difficulty including the core contribution in the charge density when computing the $xc$ energy and potential. The $xc$ energy thus results:

$$E_{xc}[n_v + n_c] = \int (n_v(\mathbf{r}) + n_c(\mathbf{r}))\epsilon_{xc}(n_v(\mathbf{r}) + n_c(\mathbf{r}))d\mathbf{r} \tag{1.55}$$

where the core contribution is still fixed in its frozen atomic configuration (it is not updated during iteration). The need of introducing the NLCC formalism is particularly evident when dealing with magnetic crystals: without including the core contribution (which is spin unpolarized), into the charge density, the magnetic polarization $\xi$, introduced in eq. 1.28,

$$\xi(\mathbf{r}) = \frac{n^{\uparrow} - n^{\downarrow}}{n^{\uparrow} + n^{\downarrow}} \tag{1.56}$$

could be significantly overstimated thus spuriously enhancing the tendency of the system to acquire a finite magnetization.

# Chapter 2

# Some $d$-open shell systems studied with GGA

## 2.1 introduction

The present chapter is devoted to the study of selected compounds using standard DFT methods. All the chosen systems contain Iron whose electronic configuration (for the isolated atom) is [Ar]$3d^6 4s^2$. Both the $3d$ and the $4s$ electrons of iron (which populate the most external shells) play an important role in the chemistry of this element. Being weakly bound to the ionic core (composed by the nucleus and the most internal electronic clouds) the $4s$ electrons are easily lost by the atoms in presence of other elements with (even slightly) higher electronegativity (as oxygen, for instance). A different behaviour is observed instead for the $3d$ electrons which, being more localized than the $4s$ ones, are more bound to the ionic cores. Despite this fact, they are deeply involved in the chemical bonds that ions form and, being usually the highest energy occupied states, they are frequently responsible for the conduction properties of iron compounds, as they represent the incomplete manifold crossed by the Fermi energy. However, despite the fact that the electrons which are responsible for the possible metallic behaviour of iron compounds are mainly accommodated on these states, the $d$ levels strongly retain their atomic character which (usually) produces quite narrow bands, very localized charge densities and magnetic moments.

The localization of the $d$ (open) shell electrons may cause electronic correlations on the atomic sites to play a very important role in the physical behaviour of iron (and, in general, of transition metal) compounds and create some troubles to conventional LDA or GGA approaches which are not designed to deal with rather localized strongly

correlated electrons.

The motivation of the present chapter is thus twofold: from one side we study the physical properties of some representative systems that are correctly addressed within GGA and whose good description we would like to be preserved (as much as possible) also when using our LDA+U scheme; on the other hand we can consider the aspects that are not well reproduced by the conventional *xc* functionals and possibly need a better treatment of the electronic correlations.

The chapter is divided in three sections each one devoted to a different material: (bulk) iron, FeO iron oxide and $Fe_2SiO_4$ fayalite.

The computational approach adopted to study these compounds is GGA used in its spin polarized version together with NLCC. For each of these systems, we present the band structure, the magnetic moment arrangement, and the structural properties (determined from the fit of our total energy calculations to the Murnaghan's equation of state) and comparison is made with the experimental results (when available) to underline successes and defects of this preliminary study.

Bulk iron has been studied extensively using ab-initio calculations and we know that $\sigma$-GGA together with NLCC pseudopotentials are required to obtain the bcc ferromagnetic (FM) phase as the ground state (LDA without NLCC predicts a paramagnetic fcc structure to be the most stable) [25]. Within this approximation it is quite well described by standard DFT which is able to correctly reproduce structural, magnetic, and also vibrational properties [26]. Thus the strong correlations existing for the *d* electrons around the Fermi level are not expected to be very important for this material and this is the aspect we want to investigate in this thesis.

Iron oxide, FeO, (as many other transition metal oxides) is a material which can be poorly described within GGA. Even if this theoretical approach can give reasonably good results for the magnetic moments and the equilibrium lattice spacing, it is less accurate in describing its behaviour under pressure (in particular the distortion along the [111] direction) and, more seriously, fails in reproducing the observed insulating ground state. In fact, as other compounds of this class (the transition metal oxides), FeO is an insulator of supposedly Mott kind where the band gap is actually due to the strong on site Coulomb repulsion which forbids the electrons to hop from one site to another. The approximated expression of the conventional GGA functionals is thus not sufficiently accurate to give a good description of the electronic properties of this compound, and this is probably the reason for the failure in describing its physical behaviour which will be presented in this chapter.

$Fe_2SiO_4$ fayalite is a mineral of geophysical interest in the study of the Earth's upper mantle. We present some calculations (using, in this case, both LDA and GGA) for this compound and we eventually obtain both magnetic and structural properties in quite good agreement with experiments (the best results were produced by GGA). However, despite the observed insulating behaviour, we obtain a metal with a narrow band of iron *d*-levels crossing the Fermi energy. The charge density of the states around this level was found to be extremely localized on iron sites thus revealing the strong atomic-like character of these electrons and the possible importance of on site correlations. Comparing GGA calculations to a simplified Hubbard model we will be able indeed to roughly estimate the average Hubbard $U$, and to obtain a value of 2.4 eV consistent with a Mott-Hubbard behaviour of this compound.

## 2.2 Bulk iron

In this paragraph we report some results about the equilibrium structural, magnetic and electronic properties of bulk iron as obtained by DFT calculations.

In order to describe electron-ion interactions we use an ultrasoft pseudopotential generated according to a modified Rappe-Rabe-Kaxiras-Joannopoulos (RRKJ) scheme [27] which has been used previously in a structural and vibrational study of iron [26]. As the LSDA is known to give wrong results about the ground state structural properties of this material, we adopt the $\sigma$-GGA framework using the Perdew-Burke-Ernzherof (PBE) [13] expression for both the exchange and correlations functionals. An energy cut off of 35 Ry is chosen to describe the electronic pseudo wavefunctions while the augmented part of the charge density is expanded up to 420 Ry. The wave function energy cut-off is larger than the one used in other works for iron [26], but this will be required in LDA+U calculations and we adopt the same choice here in order to obtain consistent results in both schemes. To perform reciprocal space integrations we adopt the Monkhorst and Pack special point technique [14] and a mesh of 8×8×8 special points (corresponding to 29 inequivalent points within the Irreducible wedge of the Brillouin Zone) is found to sample the BZ quite accurately. The Methfessel and Paxton smearing technique [18] is used to smooth the Fermi distribution and a broadening of 0.005 Ry, which is smaller than required in "ordinary" DFT calculations, gives good accuracy for our LDA+U calculations whose results will be presented in the last chapter and compared with the ones obtained in this section.

In its ground state this material has a ferromagnetic (FM) spin arrangement and

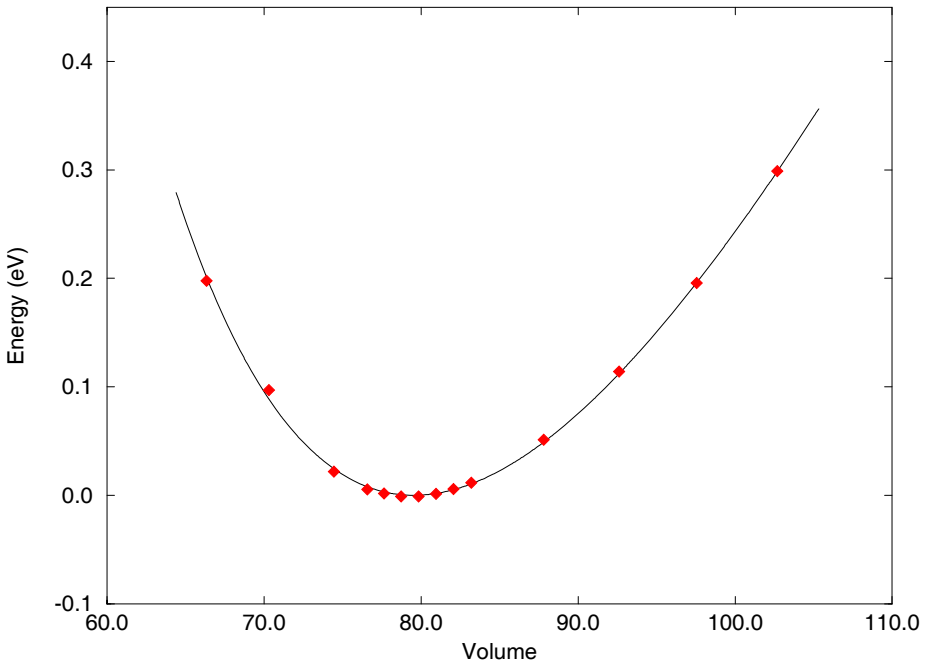


Figure 2.1: The fit to the Murnaghan equation of state for bcc FM Iron. The volume is given in $(\text{a.u.})^3$ while the zero of the energy coincides with the minimum of the energy-volume fit.

Table 2.1: The calculated lattice constant ($a_0$), bulk modulus ($B_0$) and magnetic moment ($\mu_0$) in comparison with LSDA (from ref. [26] and experimental results (from ref. [28].)

| | $a_0$ (a.u.) | $B_0$ (Mbar) | $\mu_0$ ($\mu_B$) |
|---|---|---|---|
| $\sigma$-GGA | 5.42 | 1.45 | 2.46 |
| LSDA | 5.22 | 2.33 | 2.10 |
| Expt. | 5.42 | 1.68 | 2.22 |

a body centered cubic structure. In order to study the structural properties of this FM bcc phase, we change the volume of the unit cell (while keeping its cubic shape fixed) and study the behaviour of the total energy of the system. The result is shown in fig. 2.1 where a fit of the calculated points to the Murnaghan equation of state is also introduced to estimate the equilibrium lattice spacing and the bulk modulus. In table 2.1 a comparison is made between the experimental and the theoretical results

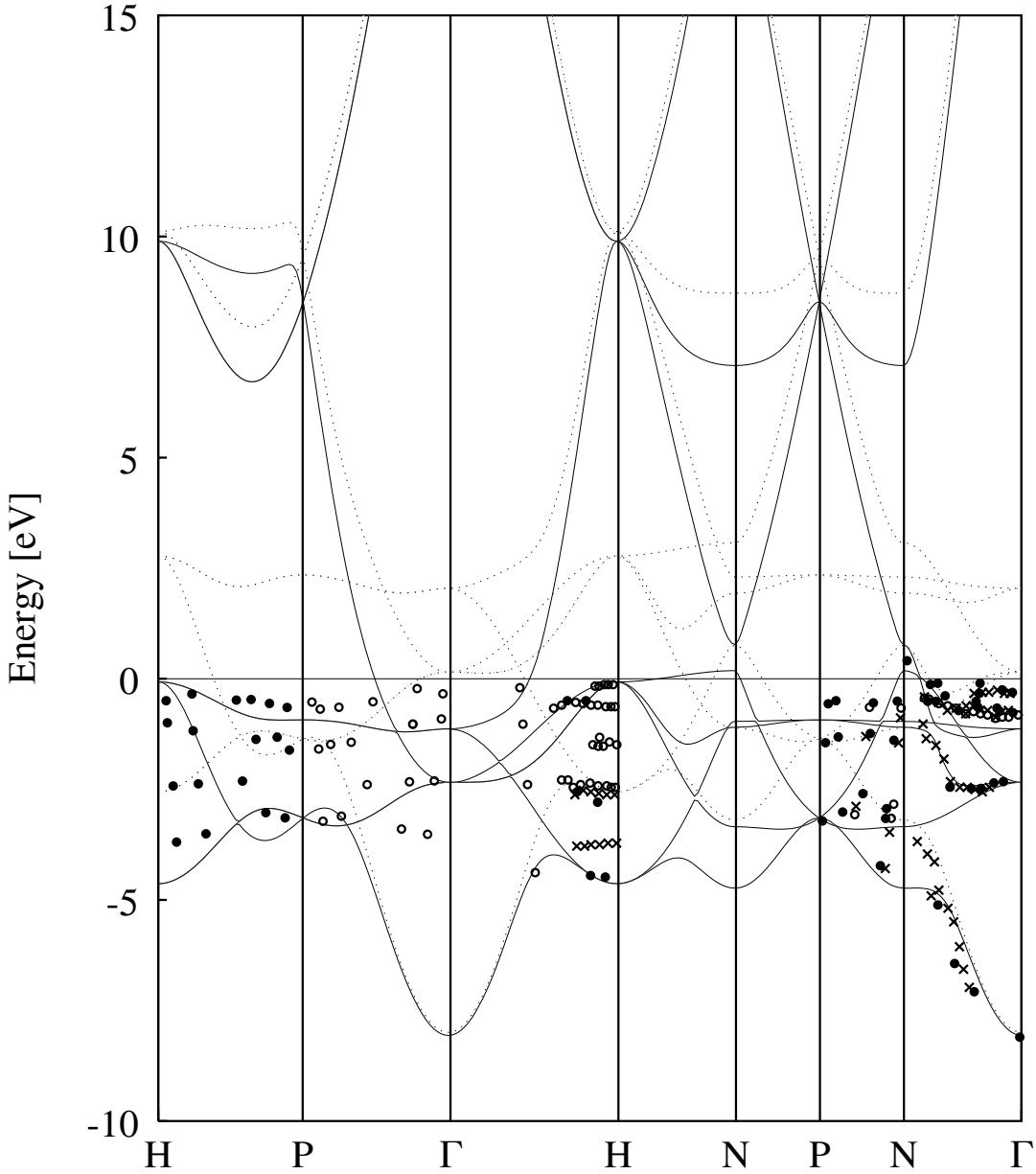


Figure 2.2: The band structure of bcc iron. Solid line for majority spin bands, dotted line for minority spin bands. The 0 of the energy is set at the Fermi level. The experimental results were taken from [55].

for these quantities and for the magnetic moment on each ion. The agreement with the experiments is fairly good for the cell parameter, while there are large discrepancies (but much smaller than those produced by LSDA [26]) for the bulk modulus and the magnetic moments. The electronic structure obtained at the equilibrium lattice parameter is

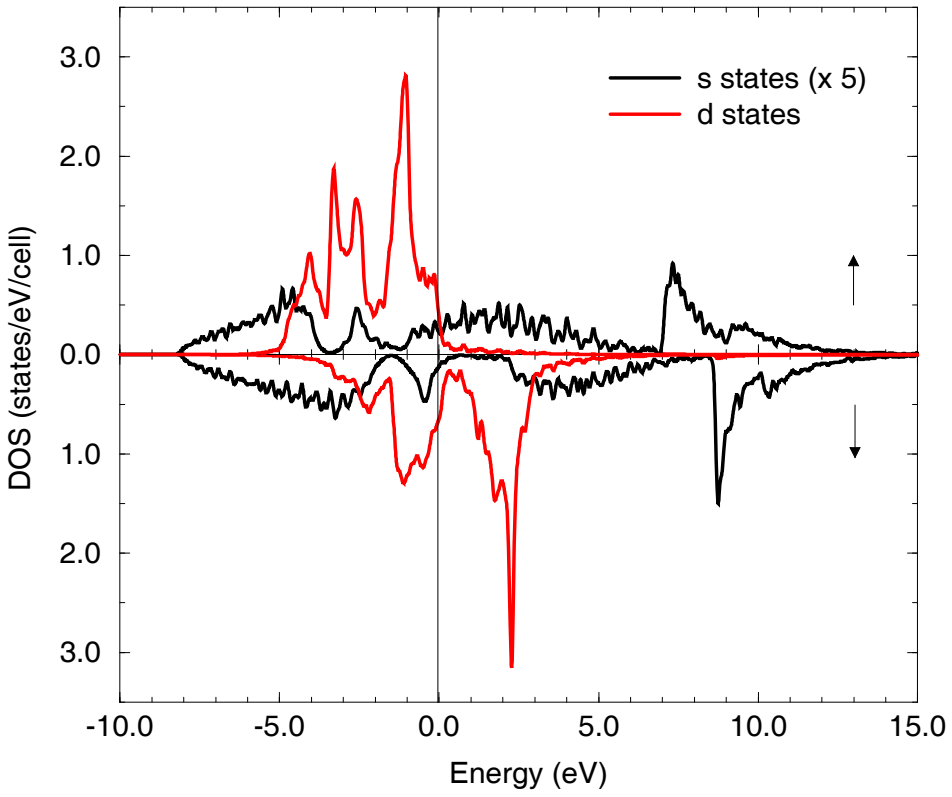


Figure 2.3: The projected density of states of bcc iron. Red lines are for $d$ states, black lines for $s$ states. The top panel is for majority spin states, the down panel for minority spin states. The $s$ density of states is multiplied by a factor of 5 in order to have an integral comparable with the one of the $d$ density of states.

shown in fig. 2.2 where a finite splitting among the two spin populations (which is the origin of the ferromagnetic character of the material) is evident and larger in the region around the Fermi level. In the same plot some experimental results obtained by photoemission techniques by Turner et al. [55] are also shown. The comparison with our calculated band structure seems to be quite good especially in the Γ-N-P region, while a somewhat looser correspondance is obtained around the H point and in the Γ-P-H zone. In this plot a clear distinction can be made among two groups of levels as also evident from the projected density of states in fig. 2.3: the first group, extended in the region around the Fermi energy (approximately from 5 eV below the Fermi energy to 3eV above it), is mainly composed by the $3d$ levels of iron; the second group, with a much larger dispersion, consists of the $4s$ states which extend between 8 and 4 eV below

the Fermi level, and above the region occupied by the $d$ states. The magnetization of the ions (generated by the relative shift among the two spin populations) is due, to a large extend, to the $d$ states. Thus, the same electrons which are responsible for the metallic behaviour, also give rise to the magnetic properties of this material (itinerant ferromagnetism). However a very small contribution also comes from the $s$ states because, as it can be observed in figure 2.3, they have slightly different density of states in the two spin channel which produces unbalance among their populations (the integrals of the two density of states are 0.39 and 0.45 electrons/cell for the majority and the minority spin $s$ states respectively). As it can be observed from fig. 2.3, in the region around the Fermi level states of both kind coexist, but the $s$ density of states is strongly depleted (for both the spin channels) in the region where the $d$ levels are located, and is quite small in proximity of the Fermi level. The mixing among the two is thus expected not to be very important so that the metallic character of the material mainly arises from the strongly atomic-like $d$ states.

As evident from the study about electronic, magnetic and structural properties, the GGA approach gives a very good description of bulk iron; some questions, however, still remains about its physical behaviour as, for instance, the mechanism which leads to atomic like magnetic moments. The magnetism produced by itinerant electrons, in fact, is still an open problem and the importance of the electronic correlations in this context is one of the points under debate [29].

## 2.3 Iron oxide

Iron oxide (FeO) is a much more problematic material than Fe to be studied with state-of-the-art numerical techniques. As it happens in most transition metal oxides, LDA completely fails in reproducing the observed insulating behaviour (expected to be produced by a Mott-like mechanism); nevertheless it can describe the structural and magnetic properties of this compound in reasonable agreement with experimental results, at normal pressure and temperature conditions.

In this paragraph some results of a $\sigma$-GGA study of FeO will be presented and particular care will be devoted to its structural and electronic properties, to be compared with the LDA+U results presented in a later chapter of the thesis.

The calculations are performed describing iron with the same US GGA (PBE) NLCC pseudopotential already used for the bulk material, while for oxygen an US PBE (non NLCC) potential has been chosen. The same smearing amplitude (0.005 Ry) as for bulk

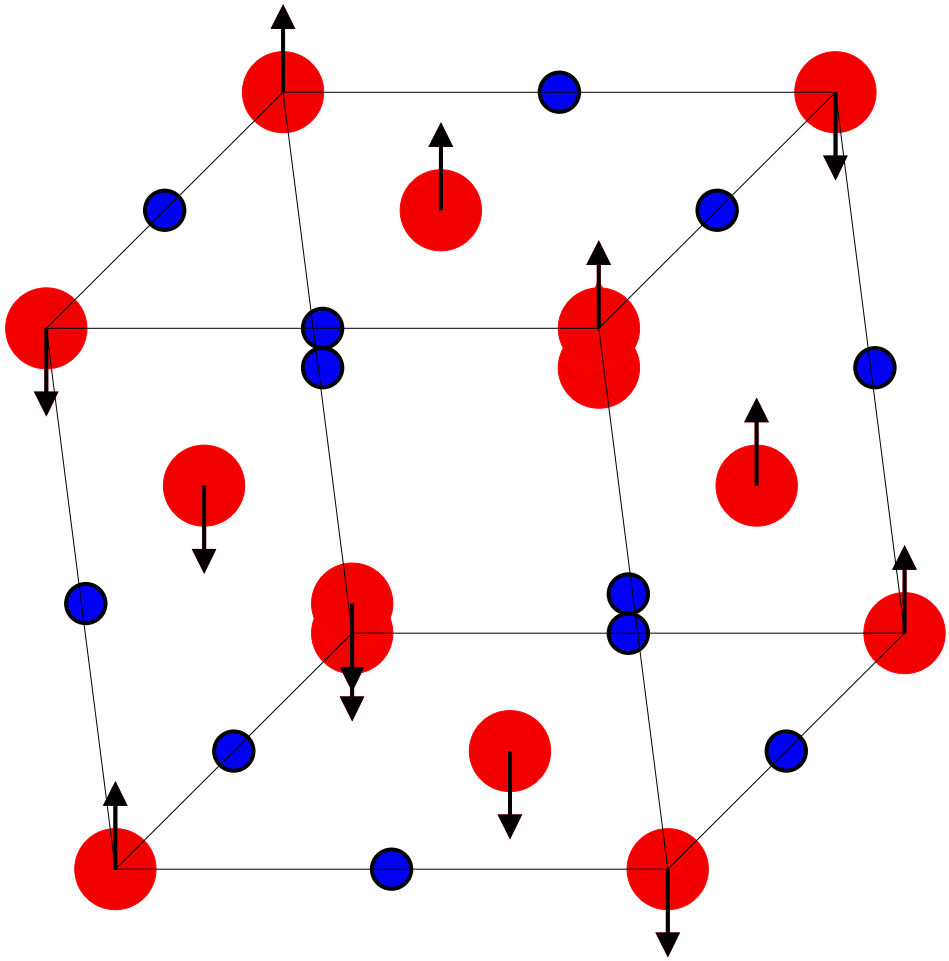

Figure 2.4: The unit cell of FeO. Red balls are Fe, blue are O, while the arrows represent the spin polarization of the magnetic ions

iron is also used to smooth the Fermi distribution (we know that GGA describes this compound as a metal) and a 4×4×4 mesh **k**-points (corresponding to 13 independent vectors within the IBZ) is found to be enough for reciprocal space summations. An energy cut-off of 40 Ry is chosen to describe the electronic wave functions, while the augmented contribution to the charge density requires a 400 Ry cut-off. These are again larger values than strictly required in "normal" GGA (or LDA) calculations, but we choose them in order to compare directly these results with those obtained in LDA+U approach in which they are necessary.

The unit cell of FeO (in the undistorted phase) has a cubic rock salt (B1) structure with rhombohedral symmetry originating from the magnetization of the iron. The ground state spin configuration, shown in fig. 2.4, is ferromagnetic for ions belonging to

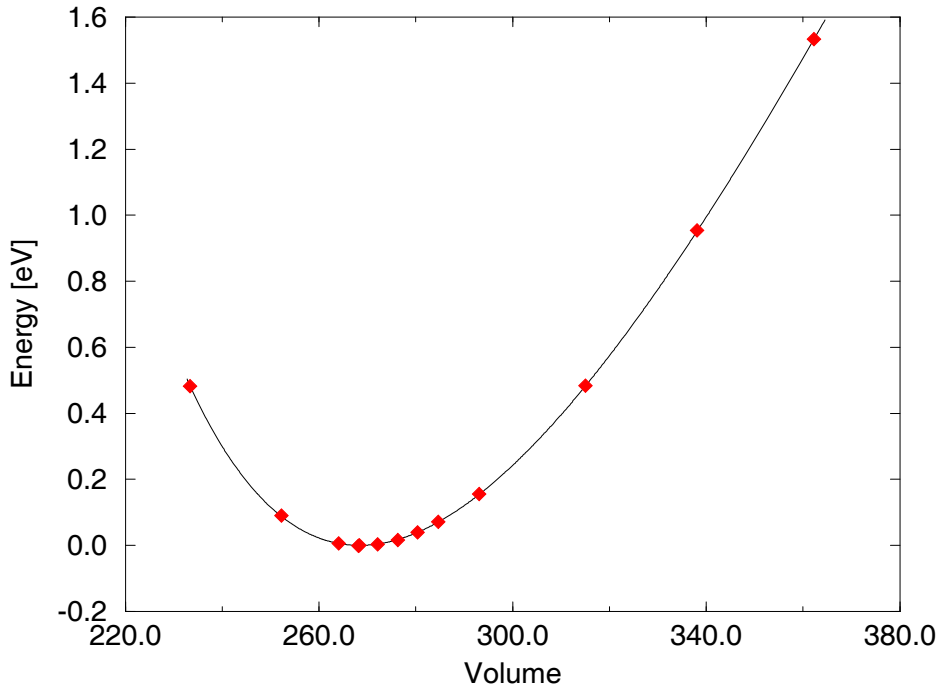


Figure 2.5: The fit to the Murnaghan equation of states for iron oxide. The volume is given in $(\text{a.u.})^3$ while the zero of the energy coincides with the minimum of the energy-volume fit.

the same [111] planes, while nearest neighbor magnetic planes are in an antiferromagnetic configuration with each other because of a superexchange interaction mediated by the oxygen ions lying in between [30]. At ambient pressure a rhombohedral stretching of the crystal structure along the [111] body diagonal is also observed upon lowering the temperature below the Néel value ($\approx$ 198 K). The distortion is found to increase under pressure loading and the Néel temperature is also observed to increase; at higher pressure the system transform to other structural phases whose nature has been recently studied [31, 32] and which will not be addressed here. We begin studying the undistorted structure in the ground state rhombohedral AF spin configuration. The results of our calculations can be seen in fig. 2.5 where the curve resulting from a Murnaghan fit to the calculated points is also drawn and used to extract some structural parameters of this material. In the table 2.2 a comparison is made with the experimental results about the lattice parameter, the bulk modulus and the magnetic moment of each iron. Despite some scattering in the experimental results, the agreement is reasonable especially for

Table 2.2: Calculated lattice constant ($a_0$), bulk modulus ($B_0$) and magnetic moment ($\mu_0$) in comparison with experimental results (taken from ref. [31].)

| | $a_0$ (a.u.) | $B_0$ (Mbar) | $\mu_0$ ($\mu_B$) |
|---|---|---|---|
| $\sigma$-GGA | 4.30 | 1.73 | 3.61 |
| Expt. | 4.33 | 1.42-1.80 | 4.20 |

the lattice parameter (we report the side of the conventional cubic cell of fig. 2.4 which is not a fundamental direct lattice vector) and the bulk modulus. A larger discrepancy is obtained for the magnetic moment of each iron which is anyway in better agreement with experimental result than in other theoretical studies [31].

The electronic band structure of iron oxide has been calculated at the equilibrium lattice parameter (of the undistorted cubic structure) for the AF spin configuration depicted in fig. 2.4. The result is plotted in fig. 2.6 where the zero of the energy scale is set to the Fermi energy. As it can be noticed from the plot, there is a complete degeneracy among the spin up (solid lines) and the spin down (dotted lines) electronic levels due to the antiferromagnetic ground state spin configuration. The majority spin $d$ states of each iron are located between 4 and 1 eV below the Fermi energy, while the (partially filled) minority bands are extended around the Fermi level (between -1 to 2 eV) and cross it in several points thus producing the metallic behaviour. This is at variance with experimental results which show an insulating ground state for this compound at low pressure and temperature, and represents the most evident failure of LDA (or GGA) in describing this class of compounds. However, the itinerant character of the $d$ electrons of iron is not in contradiction with the non zero magnetization which actually results from the finite (exchange) splitting between majority and minority spin states. Thus, while failing in reproducing the conduction properties, LDA and GGA can give appreciable results about the magnetization on each ion. Four groups of states in the electronic band structure can be distinguished: the oxygen $s$ and $p$ states lying at about 20 eV and between 9 and 4 eV below the Fermi energy respectively, the iron $d$ levels from -4 to 2 eV around the Fermi energy, and the iron $s$ states which are completely empty in the region above the Fermi level. In a perfectly cubic environment the $d$ states of the magnetic ions could be further divided into two subgroups: the low lying $t_{2g}$ levels ($xy$, $yz$ and $xz$) and the higher energy $e_g$ states ($x^2 - y^2$ and $3z^2 - r^2$). The rhombohedral ligand field felt by the iron in the AF spin configuration lifts the

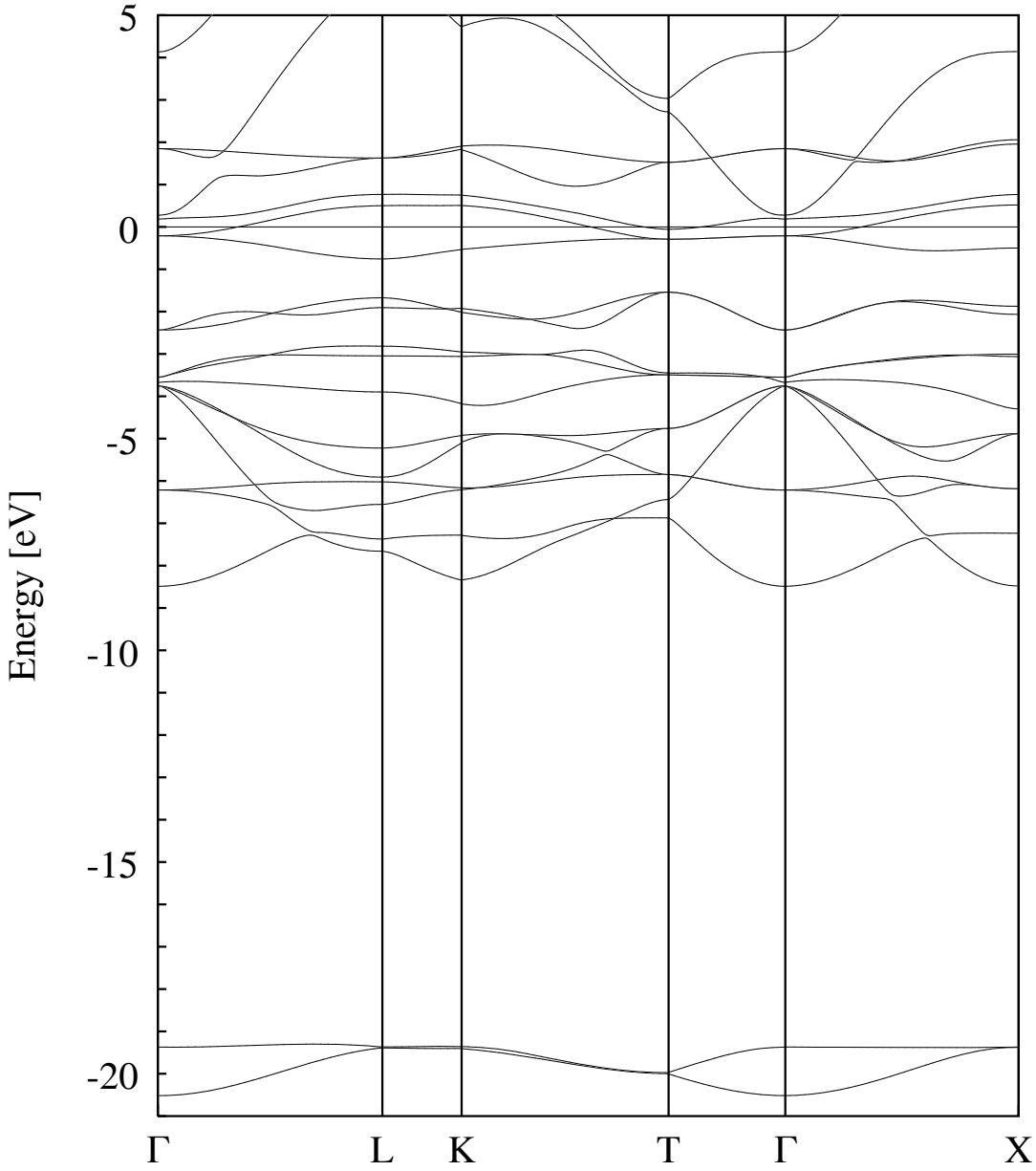


Figure 2.6: The band structure of iron oxide corresponding to the spin configuration of fig. 2.4. Solid lines, for majority spin bands, are completely degenerate with the dotted line for minority spin bands. The zero of the energy is is set to the Fermi level.

$t_{2g}$ degeneracy of the cubic structure and produces one state of $A_{1g}$ symmetry, which corresponds to the linear combination $\frac{1}{\sqrt{3}}(xy+yz+xz)$ of $3Z^2-r^2$ symmetry where $Z$ is taken along the [111] rhombohedral axis, and two other states of $E_g$ symmetry lying on the FM [111] planes corresponding to $E_g^1 = \frac{1}{\sqrt{6}}(2xy-yz-zx)$ and $E_g^2 = \frac{1}{\sqrt{2}}(yz-zx)$. The

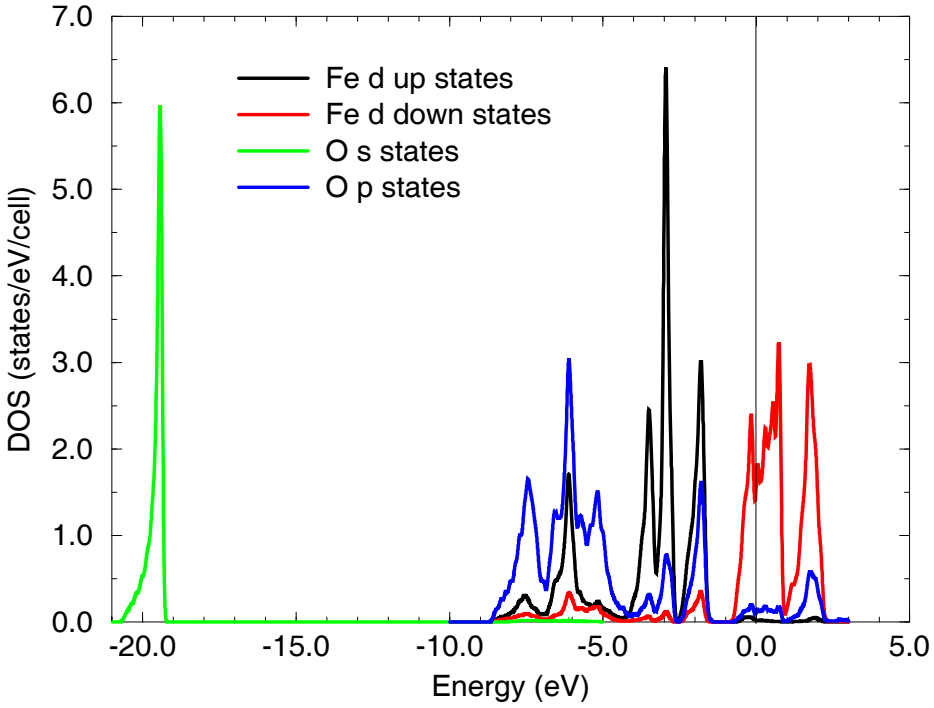


Figure 2.7: The projected density of states of AF undistorted iron oxide. The zero of the energy is set to the Fermi level.

insulating gap could not be realized without rhombohedral symmetry [31] [33] because in this case the degenerate $t_{2g}$ states would all sit at the Fermi level thus producing a 1/3 filled band. In the rhombohedral symmetry, in order the gap opening to take place, the $A_{1g}$ state should correspond to a lower energy with respect to the other two states originating from the $t_{2g}$ triplet (the six $d$ electrons of iron would completely fill in this case the five majority spin states and the lowest energy minority-spin state thus leaving the other states above the Fermi energy). This is not realized within the GGA which thus also fails in ordering the $d$ orbitals of the magnetic ions. Furthermore, even if this order were correct, the gap in the band structure would have been too small [31] (as it happens for MnO and NiO) because it is not just produced by the ligand field acting on the iron, but rather it is expected to be due to electronic correlations which are not properly described within "ordinary" mean-field-like LDA or GGA approaches.

A related aspect which is, however, somehow well described by GGA calculations is the spectroscopical nature of the (unrealized) gap opening at the Fermi level: pho-

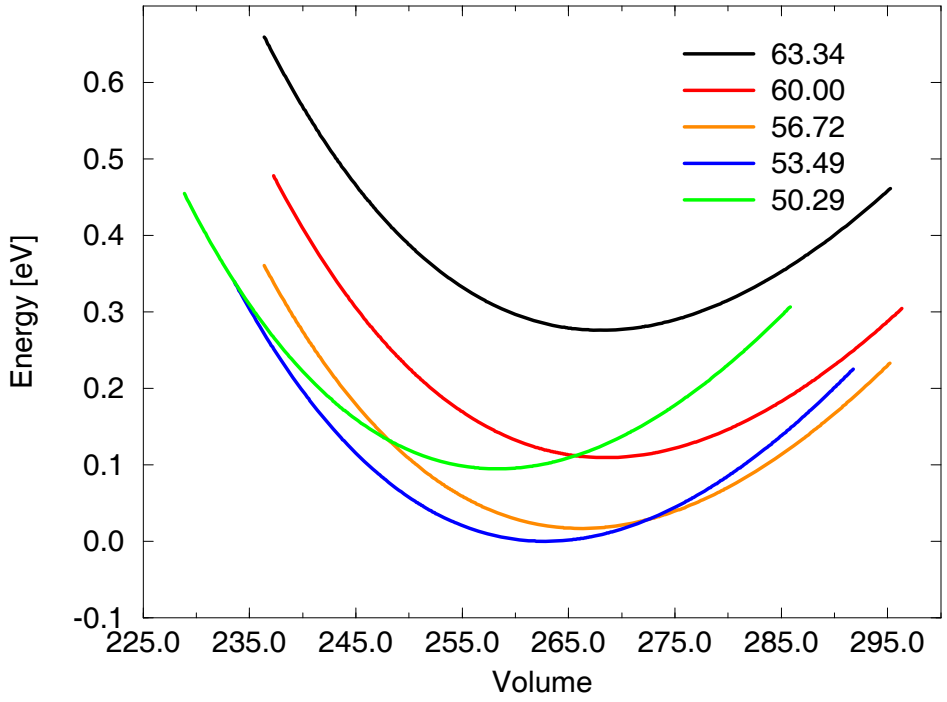


Figure 2.8: The Murnaghan fits for different distorted structures. smaller angles correspond to larger rhombohedral distortions. The volume is given in (a. u.)$^3$.

toemission and optical experiments on iron oxide both reveal that the valence band of this compound is of mixed O $2p$-Fe $3d$ character [33] so that transitions between the valence and the conduction band should also involve electrons hopping from oxygen to iron (charge transfer insulator). A strong mixing between the oxygen $p$ states and the iron $d$ levels should therefore be observed on the top of the valence band. Despite the gap is not obtained within GGA, the mixing among these states is somehow realized in our calculation as evident from fig. 2.7 where the projected density of states describing different atomic contributions has been plotted. Neglecting the states at the Fermi energy, mainly originating from the minority-spin $d$ states, we can see, in fact, that a considerable overlap of oxygen $p$ states and majority-spin $d$ states exists in the region near to 2 eV below the Fermi level. However, the spectral weight of this overlap region is mainly due to iron $d$ levels while a stronger interaction among oxygen $p$ and iron $d$ states can be observed only between 5 and 9 eV below the Fermi level where oxygen states give the ominant contribution. In other words, even if some finite overlap exists, the two atomic contributions are centered in different regions of the energy spectrum.

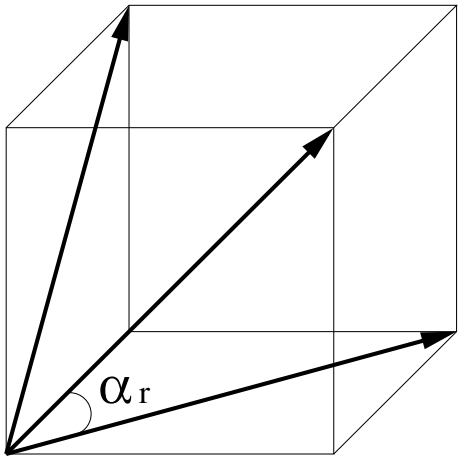


Figure 2.9: The rhombohedral angle is the one among any two of the face diagonal vectors. In the undistorted structure its value is 60°.

Despite GGA is quite successful in reproducing the lattice spacing and the bulk modulus of FeO in the cubic (undistorted) structure, the failure in describing its electronic properties is possibly the reason of quantitatively wrong results for the rhombohedrally distorted phase. In fact the cubic structure of FeO is found to be unstable with respect a rhombohedral stretching along the [111] cubic diagonal and the reason of this is a strong interplay among electronic/conduction properties, orbital ordering, and crystal symmetry, producing very efficient magnetocrystalline interactions [31]. In fact, the distortion is observed at ambient conditions when temperature is decreased below the Néel threshold (which is of about 198 K) and found to even increase under pressure loading. The GGA approach to the study of FeO correctly predicts the distorted structure to be the ground state at normal conditions (calculations are always performed at zero temperature) and also reproduces the enhancement of the rhombohedral stretching under pressure loading. In fig. 2.8 the fitting curves corresponding to different rhombohedral distortions are plotted (the distortion parameter is the rhombohedral angle $\alpha_r$ among any two face diagonal vectors shown in fig. 2.9) and it can be seen that increasing pressure favours larger and larger distortions. In order to study the increase of distortion from a quantitative point of view we calculated the pressure corresponding to each point of the Murnaghan curves and explored a pressure range from 0 to 200 kbars. At each chosen pressure (we divided this interval in 20 parts) we calculated the enthalpy of the

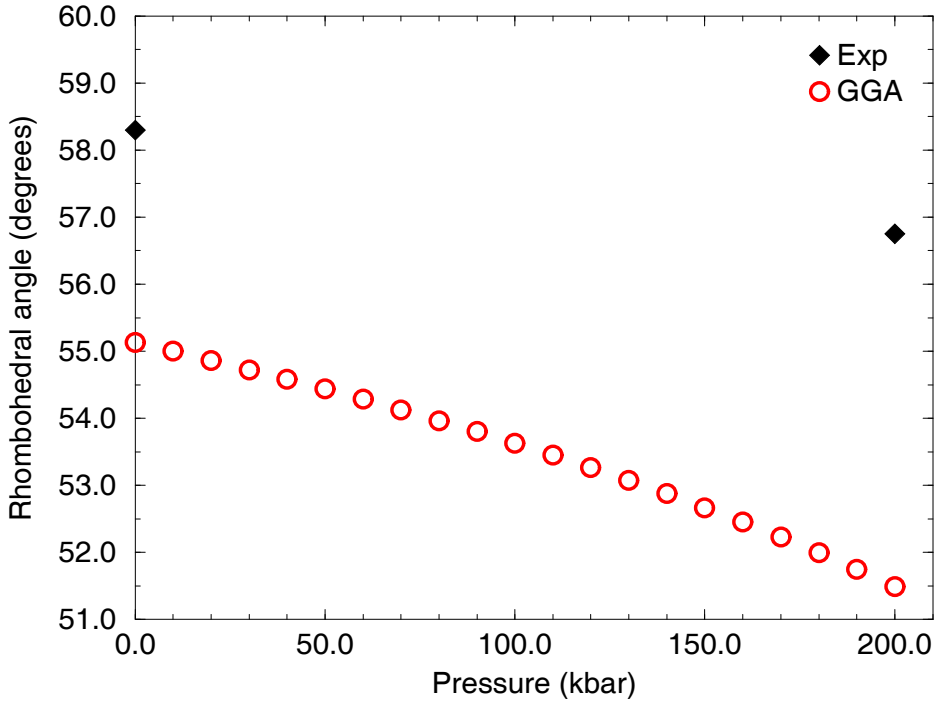


Figure 2.10: The rhombohedral angle as a function of pressure.

system $(E + PV)$ and fitted its dependence on $\cos\alpha_r$ with a quadratic curve finally obtaining the rhombohedral angle corresponding to the minimum of the enthalpy. The result is shown in fig. 2.10 where a clear tendency toward the enhancement of the rhombohedral distortion can be observed as predicted by [31] and references quoted therein. In the same picture two experimental points are also presented. The ambient pressure experimental result was extracted from ref. [34], whereas the 200 kbar one was obtained from ref. [35]. Both of them were obtained for non stoichiometric compounds so that we extrapolated the experimental results up to the composition with the same amount of iron and oxygen using the linear dependence of the rhombohedral angle with iron concentration obtained in ref. [34] from measurements at 90 K and ambient pressure. The use of the same linear dependence on ion concentration may not be very accurate for the point at 200 kbars. In any case the amount of stretching (the deviation of the rhombohedral angle from its cubic structure value of 60°) predicted within GGA is far too large if compared with experimental points even if we consider the results obtained for the non stoichiometric compound which is used in experiments. In ref. [36] the same agreement with experimental results led the authors to conclude that the behaviour of

the rhombohedral distortion under pressure loading is correctly described within GGA, but we think this is true just on a qualitative ground. Thus, GGA does not describe accurately the structural properties of this compound in its ground state both at ambient and higher pressure regimes. As we expect this failure to be connected to the incorrect description of the electronic structure, the rhombohedral distortion will be a further aspect (beside, of course, the band gap opening and its spectroscopical nature) our LDA+U approach will be tested on.

## 2.4 $Fe_2SiO_4$ Fayalite

Fayalite is the iron-rich end member of $(Mg,Fe)_2SiO_4$ olivine (orthorhombic structure), one of the most abundant minerals in Earth's upper mantle. Modeling the physical behaviour of this compound is thus very important for geophysics which requires considering high pressure and temperature conditions. However the study of this material at room temperature and pressure is also very interesting because it allows to understand the starting point of the structural phase transitions it undergo at upper mantle conditions. At normal pressure and temperature, fayalite shows insulating behaviour and experimental work indicates a Mott-Hubbard type mechanism [37, 38]. The magnetic structure of $Fe_2SiO_4$ Fayalite has been also studied with Mössbauer spectroscopy and neutron diffraction and it is reported to be a (noncollinear) antiferromagnetic compound below a Néel temperature of $T_N \approx 65$ K [39]. Strong anisotropy in the measured magnetic susceptibility (and also the noncollinearity of the spin arrangement) support the idea of strong correlations among the crystal structure and the electronic/magnetic properties.

In this work we will consider the ambient pressure, low temperature ($T<T_N$) phase of fayalite, which will be described (within standard spin polarized LDA or GGA approaches) in its ground state AF spin configuration. The neglect of spin orbit coupling and of the orbital contribution (found to be not completely quenced) to the magnetization does not allow to consider the noncollinear spin arrangement of this compound, nor the important magnetocrystalline effects which lead to the strong anisotropies in the measured magnetic susceptibility. Nevertheless an ab initio study of this compound within a collinear spin polarized description could be useful to understand the role of the electronic degrees of freedom on both magnetic and structural properties. In this context, to reproduce the observed insulating behaviour could be of crucial importance in the study of this material and, due to the strong interplay between electronic, mag-

Table 2.3: The Wyckoff parameters for each ionic species

| Ion | Class | Coordinates |
|---|---|---|
| Fe1 | 4a | (0,0,0), (1/2,0,1/2) |
| | | (0,1/2,0), (1/2,1/2,1/2) |
| Fe2, Si, O1, O2 | 4c | ±(u,1/4,v), |
| | | ±(u+1/2,1/4,1/2-v) |
| O3 | 8d | ±(x,y,z), ±(x,1/2-y,z), |
| | | ±(x+1/2,1/2-y,1/2-z), |
| | | ±(x+1/2,y,1/2-z) |

netic and crystal properties, also contribute to a deeper understanding of the structural phase transitions it undergoes under pressure loading.

In the present investigation the physical properties of $Fe_2SiO_4$ fayalite are studied from first principles using LSDA and $\sigma$-GGA approximations. The comparison among the results obtained in the two approaches will allow to establish the relative merit of the two schemes and to identify those properties of Fayalite that are reasonably described by these electron-gas based schemes and which ones are instead poorly described and point toward strong correlation effects.

From X-rays diffraction studies it is known that Fayalite has an orthorhombic cell, whose experimental lattice parameters are (in atomic units) a = 19.79, b = 11.50, c = 9.11. The unit cell (depicted in fig. 2.11) contains four formula units, 28 atoms: 8 iron, 4 silicon, and 16 oxygen atoms. Silicon ions are tetrahedrally coordinated to oxygens, whereas iron ions occupy the centers of distorted oxygen octahedra. The point group symmetry of the non magnetic crystal is mmm ($D_{2h}$ in the Schoenflies notation) and the space group is Pnma. The magnetization of iron reduces the original symmetry and only half of the symmetry operations survive. The general expression for the internal structural degrees of freedom is given in table 2.3 in the Wyckoff notation [40]. Iron sites can be divided in two classes (see fig. 2.11 and tab. 2.3): Fe1 centers which are structured in chains running parallel to the $b$, [010], side of the orthorhombic cell, and Fe2 sites which belong to mirror planes for the non magnetic crystal structure perpendicular to the $b$ side and cutting it at 1/4 and 3/4 of its length. The main structural units are the iron centered oxygen octahedra which are distorted from the cubic symmetry and tilted with respect to each other both along the chains and on nearest Fe2 sites.

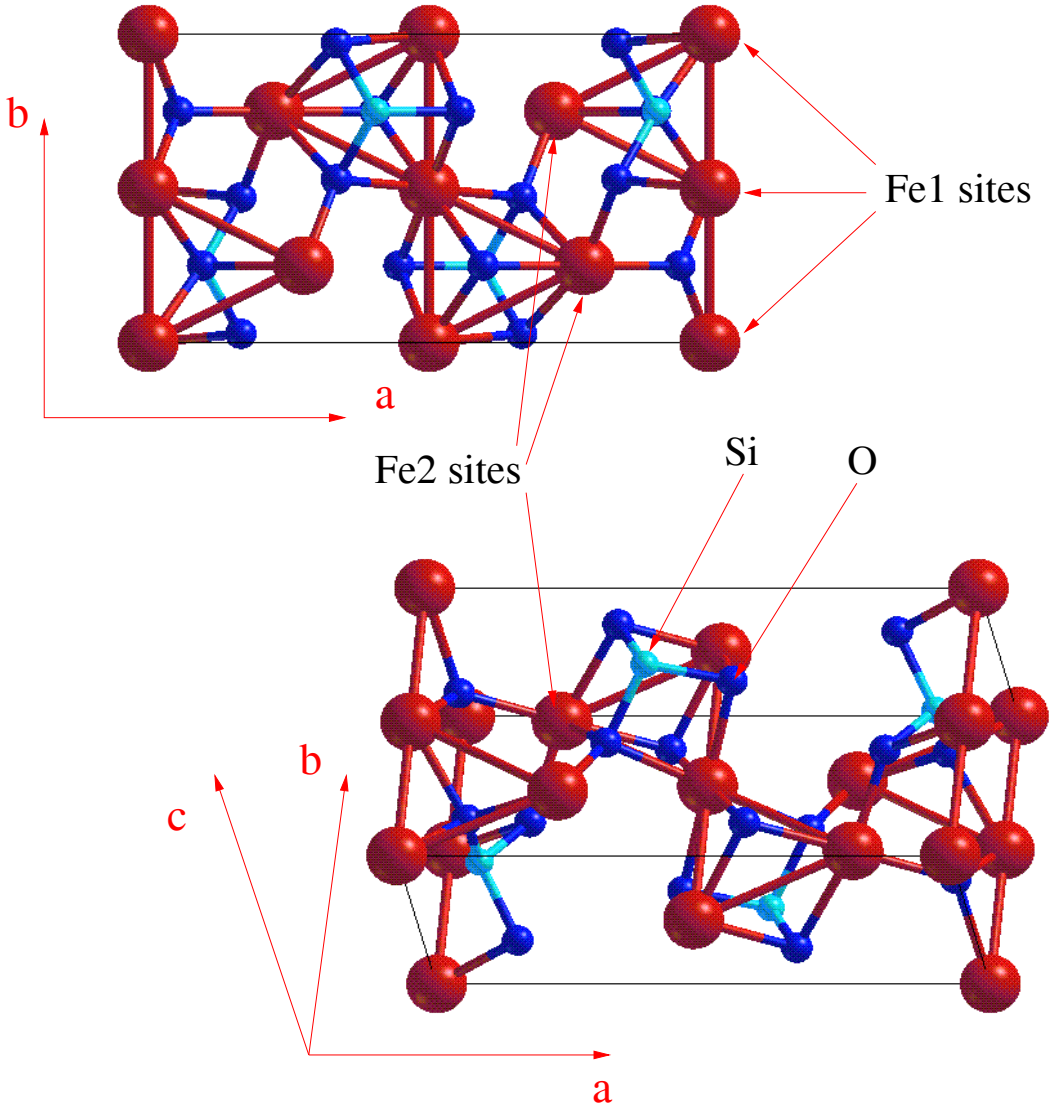


Figure 2.11: The unit cell of Fayalite. Light blue ions are Si, darker blue O, red Fe.

As for the magnetic structure, Fayalite is known to be an antiferromagnetic (AF) compound with slightly non collinear arrangement of spin on Fe1 iron sites. This non collinearity (expected to be due to the coupling of spin-orbit with the crystal field of the tilted octahedra [39]) will not be addressed here. Magnetic moments along the central and the edge Fe1 chains are antiferromagnetically oriented, but no constraint about the relative orientation of moments on iron belonging to different classes comes from experiment.

Table 2.4: The relaxed lattice parameters and the total energy for spin configuration 1 and 2

| | a [a.u.] | b [a.u.] | c [a.u.] | Δ E [Ry/cell] |
|---|---|---|---|---|
| Exp. | | | | |
| | 19.79 | 11.50 | 9.11 | |
| LSDA | | | | |
| 1 | 19.23 (−2.8%) | 11.09 (−3.6%) | 8.99 (−1.2%) | 0.0598 |
| 2 | 18.36 (−7.2%) | 10.77 (−6.3%) | 9.42 (+3.4%) | — |
| $\sigma$-GGA | | | | |
| 1 | 19.96 (+0.9%) | 11.45 (−0.4%) | 9.21 (+1.1%) | 0.0113 |
| 2 | 19.78 (−0.1%) | 11.29 (−1.8%) | 9.36 (+2.7%) | — |

In order to investigate the ground-state spin configuration of Fayalite density functional theory (DFT) calculations were performed both in the LSDA and $\sigma$-GGA approximations (the PBE functional is used in this case). The same ultrasoft pseudopotentials used for bulk iron and iron oxide were adopted for Fe and O while a norm-conserving pseudopotential was used for Si atoms. A 31 Ry kinetic-energy cutoff was found sufficient for the plane-wave expansion of the electronic states, while a 248 Ry cutoff for the augmented charge density was used. As the electronic structure of Fayalite turns out to be metallic, the smearing technique was adopted to smooth the Fermi distribution with a broadening width of 10 mRy, while 16 points in the IBZ (2×4×8 Monkhorst-Pack grid) were found to give a good convergence of the total energy and the ionic forces.

Two spin configurations, shown in fig. 2.12, are compatible with experiments: in the first one the magnetization of Fe2 ion is opposite to the one of the closest Fe1 iron, and one obtains AF order between ions at the center of edge-sharing oxygen octahedra and ferromagnetic order between corner sharing octahedra. In the second spin configuration the opposite is true and AF order occurs between corner sharing octahedra. This second magnetic structure is consistent with an iron-iron magnetic interaction via a superexchange mechanism through oxygen $p$ orbitals. This mechanism provides AF coupling when the Fe-O-Fe angle is close to 180 degrees (corner sharing octahedra) and a weak ferromagnetic interaction when this angle is about 90 degrees (edge sharing octahedra). For each spin configuration (and both exchange-correlation functionals) a structural relaxation of the internal ionic degrees of freedom and of the unit cell lattice parameters

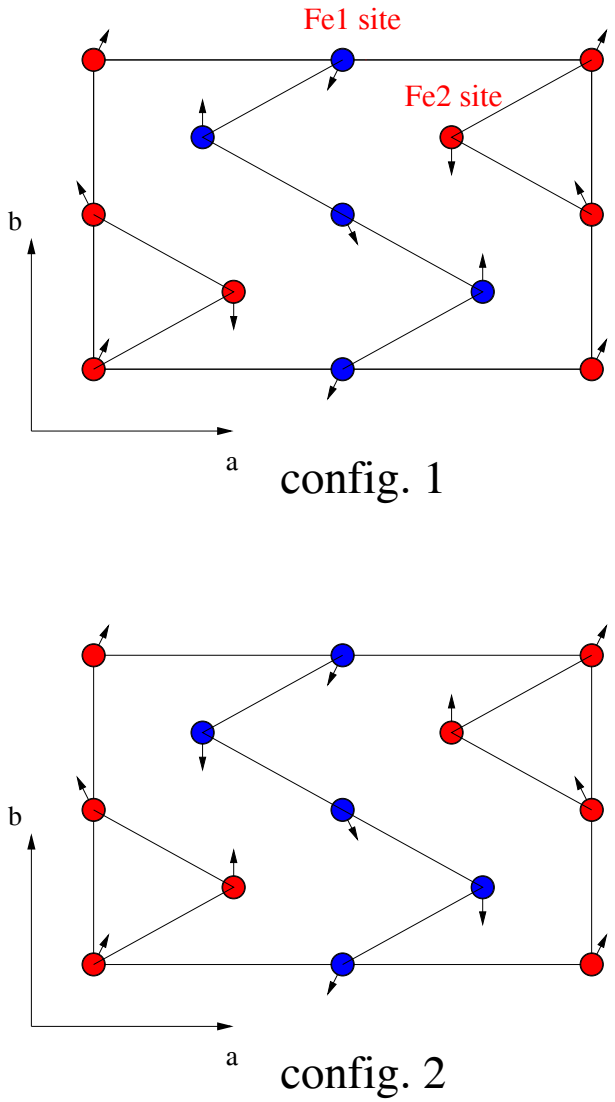


Figure 2.12: The two possible spin configurations. 1) AF interaction between edge-sharing octahedra; 2) AF interaction between corner-sharing octahedra. The zig zag lines connect first neighbor Fe1-Fe2 iron sites (almost on the same 001 plane).

was performed. In the final relaxed geometries force components did not exceed $10^{-3}$ a.u. and the stress tensor vanished within 4-5 kbar corresponding to errors in both the atomic positions and the lattice parameters of about (and usually less than) two parts per thousand. For both exchange-correlation functionals the second spin configuration has lower total energy and is therefore the magnetic ground state of the system. Su-

perexchange mechanism is thus confirmed to be responsible of magnetic interaction and the difference between the total energies of the spin configurations (about 10 mRy/cell in $\sigma$-GGA) gives a measure of the exchange parameters between Fe1 and Fe2 iron (it is about sixteen times the average $J_{Fe1,Fe2}$). This small value is consistent with the low value of Néel temperature ($\sim$65 K at ambient pressure). Despite the fact the canting of the magnetic moments on iron sites cannot be accounted for (because only collinear magnetism is allowed in the calculation and spin-orbit coupling is not included), their absolute value is found to be in good agreement with experimental results [39]. Our average value of 3.8 $\mu_B$ per magnetic ion compare quite well with the experimental result of 4.4 $\mu_B$ (both for Fe1 and Fe2 ions) at a temperature of about 10 K if we consider that this latter moment contain a residual orbital contribution (the spin-only value is 4 $\mu_B$) [39].

Although both LSDA and $\sigma$-GGA functionals provide a reasonable description of the structural properties of the system it can be observed that for both spin configurations $\sigma$-GGA gives lattice parameters which are in better agreement with experimental data than LSDA does. Moreover $\sigma$-GGA structural properties are not very sensitive to spin ordering while LSDA appears to be more sensitive.

The result of our calculations are collected in table 2.4. A detailed comparison of the internal structural degrees of freedom is given in table 2.5 where the theoretical value of these quantity obtained for the ground-state spin-configuration using LSDA and $\sigma$-GGA are compared with the experimental data. An overall good agreement between theory and experiment can be observed but again $\sigma$-GGA results are in closer agreement with experimental results.

Using $\sigma$-GGA approximation, a good description was obtained for the ground-state crystal structure and spin configuration of Fayalite. However, as in the case of iron oxide, the same can not be said for its electronic band structure. In fig. 2.13 the $\sigma$-GGA band structure of Fayalite around Fermi energy is shown where it appears to be a band metal, with two iron $d$ bands crossing the Fermi level, in spite of the fact that experimentally it is found to be insulating. A finite density of state (DOS) is present at the Fermi energy, see fig. 2.14. All the electronic bands displayed in fig. 2.13 originate from iron $d$ levels. As in FeO, due to the AF ordering, spin up and spin down levels are degenerate. $Fe^{2+}$ ions occupy the center of distorted oxygen octahedra. The quasi-cubic local symmetry determines a crystal field splitting of the $d$ levels in two groups: a lower energy $t_{2g}$ (three-fold) level and an higher energy $e_g$ (two-fold) level. It is convenient to refer to the simple scheme reported in fig. 2.15 and compare it to fig. 2.14. Every

Table 2.5: The relaxed ionic positions in the unit cell described by the Wyckoff parameters.

| | Ion | u | v | x | y | z |
|---|---|---|---|---|---|---|
| Exp. | | | | | | |
| | Fe2 | 0.7800 | 0.5147 | | | |
| | Si | 0.5975 | 0.0708 | | | |
| | O1 | 0.5929 | 0.7313 | | | |
| | O2 | 0.9530 | 0.2923 | | | |
| | O3 | | | 0.1637 | 0.0384 | 0.2885 |
| LSDA | | | | | | |
| | Fe2 | 0.7591 | 0.5080 | | | |
| | Si | 0.5905 | 0.0716 | | | |
| | O1 | 0.5886 | 0.7471 | | | |
| | O2 | 0.9353 | 0.2878 | | | |
| | O3 | | | 0.1663 | 0.0224 | 0.2822 |
| $\sigma$-GGA | | | | | | |
| | Fe2 | 0.7766 | 0.5170 | | | |
| | Si | 0.5955 | 0.0710 | | | |
| | O1 | 0.5964 | 0.7376 | | | |
| | O2 | 0.9467 | 0.2979 | | | |
| | O3 | | | 0.1650 | 0.0292 | 0.2782 |

iron ion in Fayalite is in its high spin configuration because the crystal field splitting, $U_{CF}$, due to the oxygen octahedra, is smaller than the exchange splitting, $U_X$ due to the first Hund's rule. From an analysis of the band structure it results that $U_{CF} \sim \frac{1}{2}U_X$. Therefore five electrons per iron fill up completely the majority spin $d$ states (Hund's rule is fulfilled) whereas one more electron per iron atom partially fills the minority spin $t_{2g}$ bands that are crossed by the Fermi level. The distortion of the Fe-O octahedra from cubic symmetry induces a partial mixing of majority spin $t_{2g}$ and $e_g$ states and a small splitting of the minority spin $t_{2g}$ levels in two groups of 12 bands each (visible in fig. 2.14 only as a very deep dip in the DOS at $\approx$0.3 eV above the Fermi level due to the finite smearing width used in the plot). The $t_{2g}$ bandwidth around the Fermi level is about 1.5 eV (or about 1 eV if only the 12 lowest $t_{2g}$ bands are considered).

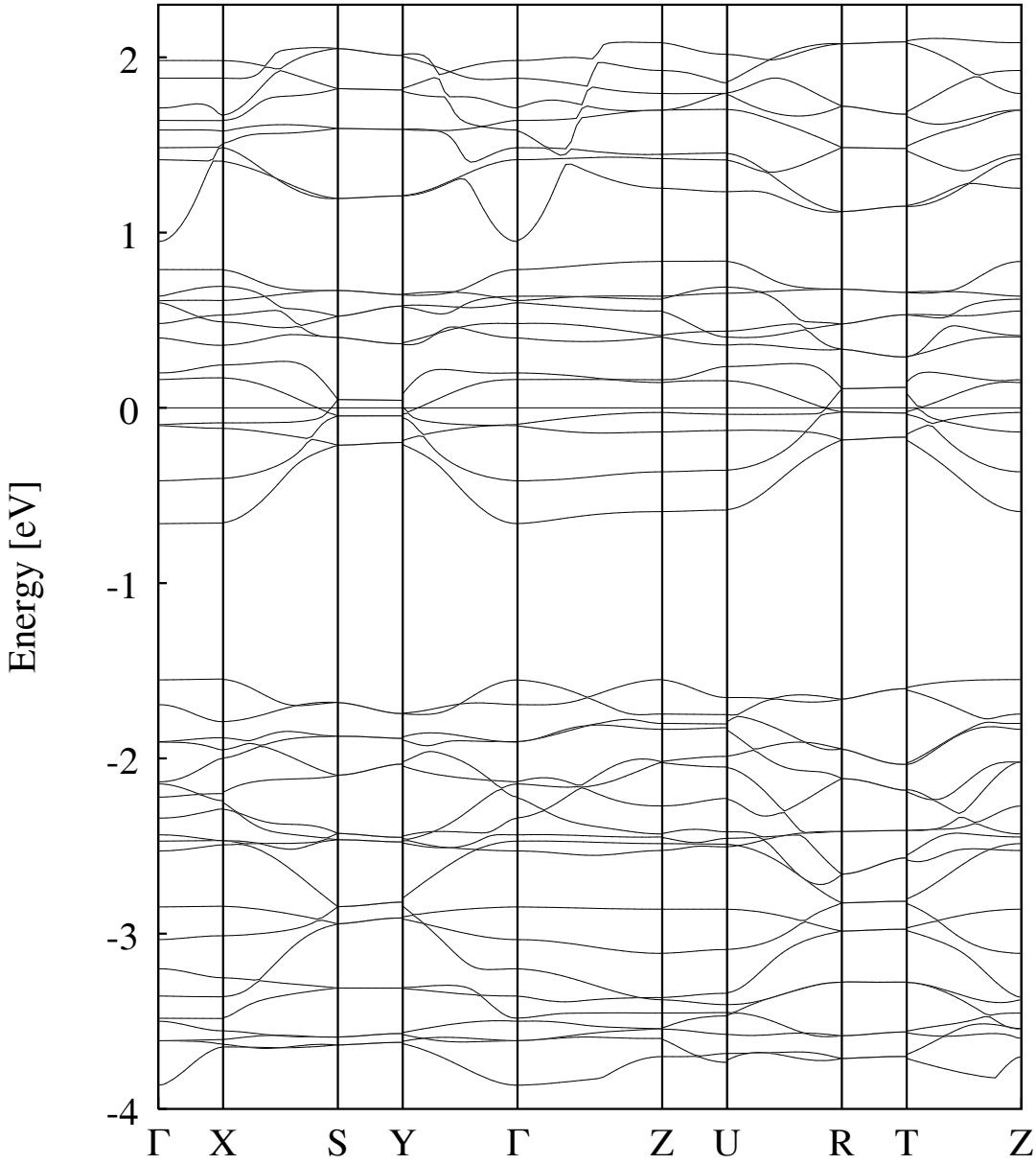


Figure 2.13: The electronic band structure originated from the iron $d$ levels.

One important feature of the electronic band structure is the marked flatness of the bands around the Fermi surface along [001] (ΓZ line in fig. 2.13) and [100] (ΓX, SY, ZU, RT) directions and the relative large dispersion in the [010] direction (ΓY, XS, ZT, UR). This means that the calculated electronic states in the minority-spin $t_{2g}$ bands are rather localized in the x an z direction and mainly extend along the zig-zag chains in the y direction.

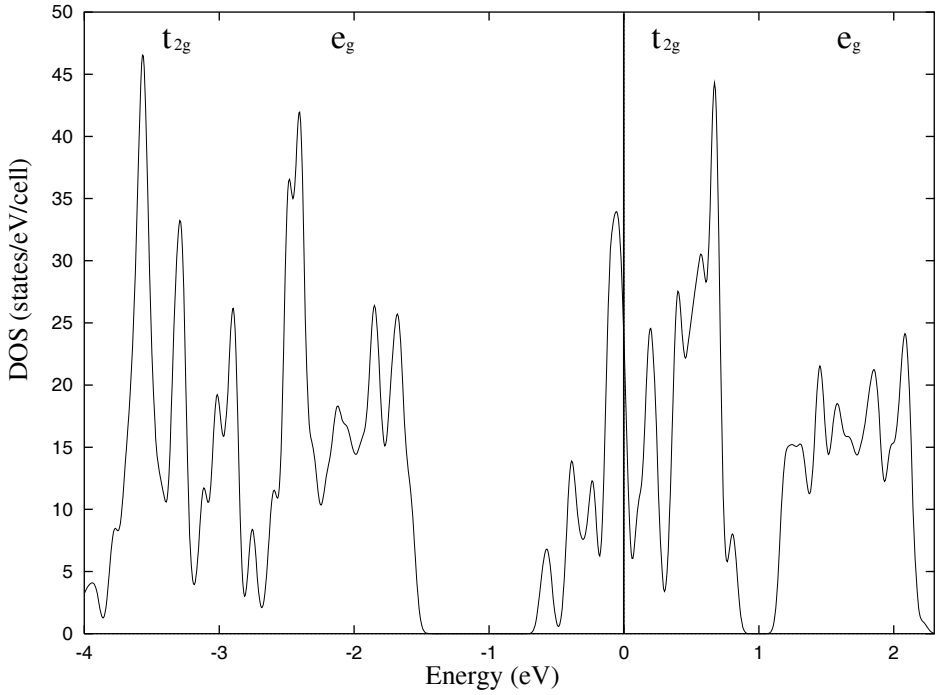


Figure 2.14: The electronic density of states. The zero of the energy is set to the Fermi level.

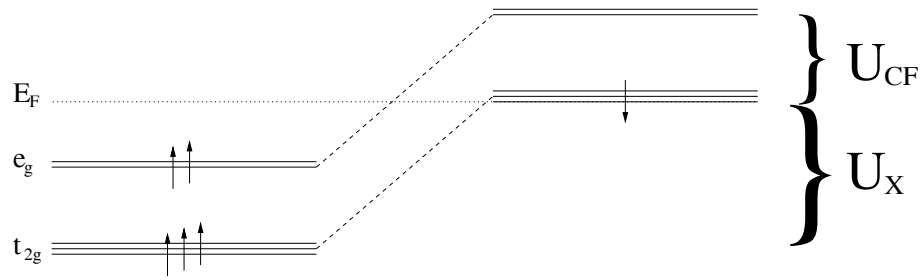


Figure 2.15: A simple scheme about the splitting of the iron $d$ levels in the crystal.

This scenario is confirmed by fig. 2.16 where the charge density corresponding to the electronic states at the Fermi energy is shown by isosurfaces drawn at a value equal to 2 % of the maximum charge density. As evident from the plot, electronic states at the Fermi-level actually belong to both Fe1 and Fe2 irons but extreme localization occurs on iron sites so that electrons are very little extended away from the atomic sites. The

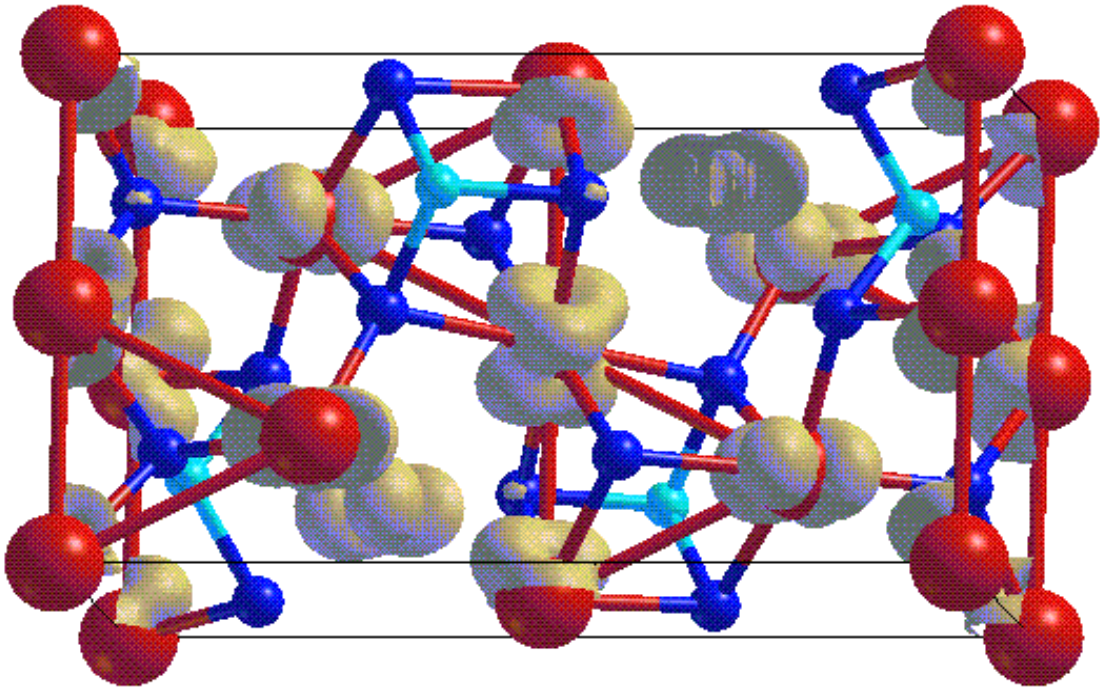

Figure 2.16: The charge density generated by states around the Fermi level.

spatial localization of these states suggests that correlation effect due to on-site Hubbard repulsion, treated only at the mean-field level in the LSDA and $\sigma$-GGA calculations, may be important and may explain the insulating behavior of Fayalite.

Let us make a first crude estimate of the on-site repulsion for electrons on the iron sites and compare the result with the relevant bandwidth around the Fermi level. Let us assume that GGA provides a good mean-field-like solution for the electronic states around the Fermi energy and compare its electronic compressibility with the RPA result obtained for a simplified Hubbard model that describes the physics of the electrons responsible for conduction (or lack of it) in Fayalite. This is given in the following expression:

$$H = \sum_{<i,j>} \sum_{l,l'} t_{ij} c^{\dagger}_{i,l} c_{j,l'} + \frac{U}{2} \sum_{i} \sum_{l} \sum_{l'(\neq l)} n_{i,l} n_{i,l'} \tag{2.1}$$

where $t_{ij}$ is the hopping amplitude between two nearest iron on the same zig-zag chain (the model is therefore effectively unidimensional), $U$ is the average on-site repulsion, $c^{\dagger}_{il}$ and $c_{il}$ are creation and annihilation fermionic operators on the l-th orbital of the i-th site, while $n_{il}$ $(= c^{\dagger}_{il} c_{il})$ are the corresponding occupation numbers. The spin degrees of freedom never appear in this simple model because we consider only the three $t_{2g}$

minority spin levels for each iron atom and thus, fixing the site, actually fixes also the spin. This simple model contains the two competing parameters (the hopping term and the on site repulsion) which describe the physics of the electrons around the Fermi level. In order to establish a connection between the parameter in this model and the DFT calculation we need to treat it at the same level of approximation, *i.e.* at the mean-field level. One can thus assume that

$$E_{DFT} \approx \langle H \rangle_{MF} = T[\langle n \rangle] + \frac{N_s U}{2} \frac{(m-1)}{m} \langle n \rangle^2 + E_{bg} \tag{2.2}$$

where T is the average kinetic energy, $m$ is the number of states per site (3 $t_{2g}$ levels on each ion in our case), $\langle n \rangle$ is the average electronic occupation of each iron site, and $N_s$ is the number of iron site in the unit cell (8). The total energy does not allow to extract a value for $U$ due to the presence in the actual system not only of the mentioned states close to the Fermi energy but also of all the other electrons that determine the structural stability of the system and are hidden in Eq. (2.2) in the background energy, $E_{bg}$. The electronic response to long wavelength external perturbing potential is however insensitive to the background and we can therefore compare the electronic compressibility obtained from the DFT calculation (which is proportional to $\lim_{q \to 0} \chi(q, 0)$ where $\chi$ is the density response function of the electronic system [41]) with the second order derivative of the total energy in Eq. (2.2) with respect to $\langle n \rangle$. We obtain:

$$U = \frac{m}{(m-1)} \left[ \frac{\partial \mu}{\partial < n >} - \frac{1}{\nu(0)} \right]. \tag{2.3}$$

In this expression the quantities in square bracket can be easily calculated in the DFT approach: $\nu(0)$ is the electronic DOS at the Fermi level per iron atom, whereas $\partial\mu/\partial\langle n \rangle$ is the linear variation of the Fermi energy when the number of electron in the unit cell is changed (a uniform compensating background is added when changing the number of electrons in order to keep the system neutral). This derivative is computed numerically adding $\pm 0.01$ electrons per unit cell. From Eq. 2.3 we obtain $U = 2.4$ eV which is much larger than the electronic bandwidth ($\approx 1.5$ eV) around the Fermi level.

This implies that the electrons in the minority $t_{2g}$ bands do not have enough kinetic energy to overcome the repulsion they experience on each iron site and thus a Mott localization is likely to occur giving rise to the observed insulating behavior. We will come back to this issue in the last chapter of this thesis devoted to LDA+U calculations.

# Chapter 3

# The LDA+U method within a PW PP framework

## 3.1 Introduction

As we learned from the few case studies presented in the previous chapter and from very abundant literature, LSDA actually fails in describing the electronic structure, and thus the conduction properties, of strongly correlated systems. Slight improvements can sometimes be achieved using GGA functionals which indeed provides better results about the physical properties of non homogeneous systems, like transition metal compounds, proving particularly useful to correctly describe their binding energies and, in some cases, their magnetic and structural properties. Two examples are NiO and MnO [30, 42]. The former is described as an insulator within GGA because the crystal field due to the oxygens around the transition metal ions splits the (minority spin) $t_{2g}$ $d$ states (which are fully occupied) from the $e_g$ empty bands left above the Fermi level. With the latter a similar situation occurs because the exchange interaction among spin up and spin down populations (the first Hund's rule) pushes the five $d$ bands with one spin below the Fermi energy (completely filled with the five $d$ electrons of Mn) and pulls the opposite spin states above it. However, even in these lucky situations, where the gap opening occurs because the number of $d$ electrons is such as to completely fill the lower energy $d$ bands, the obtained gap between valence and conduction states is far too small if compared with the results of photoemission experiments on these materials, and its spectroscopic nature is also wrong as the oxygen $p$ states are not present at the top of the valence band (as experiments point out), but below the highest occupied $d$ states [43]. It seems to be a scenario similar to the one occurring in semiconductors which are also known

to display theoretically a smaller band gap than experimentally observed. However with the strongly correlated materials (such as transition metal or rare earth oxides) LSDA (or GGA) shows indeed a different behaviour because, while completely failing in describing their conduction properties, it can generally achieve reasonable results for the magnetic and the crystal structures (some completely wrong cases are also known as, for example, $\delta$-Pu [44]).

So what is the reason of such a failure in describing the electronic structure of strongly correlated materials? To answer this question we can think of what would happen if we described, using band structure calculations, the valence states of a simple metal while increasing the interatomic distances. We would observe electronic states of vanishing width crossing the Fermi level but, while retaining the metallic character, we would approach the insulating state corresponding to the infinite distance among the atoms. The electronic states around (and crossing) the Fermi level would produce a charge distribution extremely localized around the atoms (similar to the one of $d$ electrons in fayalite) such that band conduction would be hindered. The problem thus seems to be due to an inadequate description based on the use of band structure calculations. To solve this paradoxical situation we should be able to measure the relative "strength" of two competing factors: the kinetic energy of the electrons (their bandwidth) and the energy cost (the Coulomb repulsion) they have to pay when approaching regions where other electrons are localized (i.e. the ionic cores). In fact, strongly correlated materials (usually systems with partially filled $d$ or $f$ valence shells belong to this family) are such that their electrons (or some of them) are supposed to spend their time in regions (around the ions) where the presence of other particles would make them feel strong Coulomb repulsion, thus making their motion "correlated". This is quite a different situation from what we have in simple metal (especially simple ones) where electron-electron scattering is expected to be weak and particles spend vanishing amount of time in the regions around the ions. So we have two extreme scenarios (actually continuously connected to each other). When the kinetic energy is the dominant contribution (beside the attraction to the nuclei), the electrons can overcome the (on-site) Coulomb cost and actually delocalize in extended states giving metallic behaviour. On the other hand, when the bands on which they move are quite narrow (high effective mass, low kinetic energy), correlation wins and electrons actually localize in some regions (they cannot move to other ones because this is too expensive) while the system acquires insulating character (of so called Mott-Hubbard type [45]).

The band structure calculations are not the best approach to observe this phys-

ical behaviour, as they are manifestation of a one body problem (even the formally exact Kohn Sham equation in DFT), whereas correlation is the result of many body interactions. Furthermore the exchange and correlation functionals currently used are built from a homogeneous electron gas so that interactions are treated in a mean field approach which is not accurate enough to properly describe correlations or account for other many body effects. The "natural" theoretical framework for studying such systems (Mott insulators and strongly correlated materials in general) are the model hamiltonians (the Mott-Hubbard model and the Anderson impurity model are just two examples) in which the bandwidth (related to the hopping terms) and the electronic correlations are explicitly considered. This approach allows to directly take into account the behaviour of the system in regimes with different relative strength of these two factors. Unfortunately these models are strongly parameter dependent (the hopping amplitudes $t$ and the on site repulsion $U$ have to be given as input) and usually too much simplified to include effects coming from crystal structure or the different kind of ions. So we cannot use them if we want to obtain accurate numerical results and study how the electronic, magnetic, and crystal structures of a system result from the nature of the ions, their spatial arrangement, the kind of state they build to accommodate valence electrons, the importance of the ion cores and their finite size, and so on.

Owing to these difficulties in the direct use of these models, a number of methods was presented in the last 15 years which attempt to link the two theoretical frameworks discussed so far (model hamiltonian and ab initio calculations). For some time (after the discovery of high $T_c$ superconductors) constrained LDA was performed to obtain a realistic evaluation of the interaction parameters entering the model hamiltonians [46, 47]. However, the most recent theoretical methods aim to directly approach the study of strongly correlated materials from first principles [48, 49, 50]. The main idea they all have in common is to use some hints from the many body formalism to (try to) correct some of the defects of DFT and go beyond the mean field approach in which electronic interactions are treated. However the way of obtaining this extension differs from one model to the other and also depends on the particular inefficiency they propose to cure (as for example self interaction, orbital polarization and so on).

One of the most popular methods in this family is LDA+U which is the one adopted in this thesis. The present chapter is indeed devoted to introduce the LDA+U method as implemented in a PW PP framework. In the first part, starting from the (early) approach of Anisimov and coworkers [3, 4, 5], we discuss the main idea and the most important features of the method. Then, presenting the most recent rotationally invari-

ant formulation [6, 7], we extract from it the simple approximation we actually use in our calculations. At this point, a separate discussion is introduced for our simplified approach which underlines some differences among our theoretical construction and that presented in other works. The following paragraph is devoted to the development of a method to calculate the effective Coulomb on site repulsion starting from the linear response of the system under consideration (as described by LSDA or GGA) to fluctuations in the $d$ levels occupancy of the "Hubbard" sites. A possible extension of the linear response approach to determine the on site repulsion parameter is also discussed in comparison with other methods presented in the literature. In the last section, after introducing our definition of $d$ levels occupancy, some technical details are described about the use of LDA+U formalism in a PW PP code.

## 3.2 Rotational invariant LDA+U method

The main idea proposed by the LDA+U method is to correct the LDA (or GGA) approach in order to make it able to approximately describe strong electronic correlations. As underlined in the introduction, in order to obtain this, we have to go beyond the electron gas approximation used to model electron-electron interactions. One way to introduce such a correction is the Hartree-Fock (HF) approach which is based on the use of Slater determinants (built from atomic orbital) to represent the many body wave function. This method includes in the Hamiltonian both one body (external potential) and two body (electron-electron) interactions, but actually results in unphysically too large couplings due to the absence of screening.

Screening is instead included (at least in principle) in LDA+U. This approach is essentially based on an Hartree-Fock-like expression for the effective (screened) electronic interactions which is introduced as a mean field Hubbard-like correction to the standard $Hxc$ functionals. The starting point of the method is the description of the system within LDA (from now on we use LDA to mean standard LSDA or $\sigma$-GGA) which is supposed to contain (screened) correlations in some average way. This "wrong" contribution (modeled in some mean field approximation) is then subtracted from the energy functional, and finally a correction term, in which correlations are supposed to be treated properly, is added. The total energy functional thus reads

$$E_{LDA+U}[n(\mathrm{r})] = E_{LDA}[n(\mathrm{r})] + E_{Hub}[\{n^{I\sigma}_{mm'}\}] - E_{dc}[\{n^{I\sigma}\}] \tag{3.1}$$

where $n(\mathrm{r})$ is the electronic density, $n^{I\sigma}_{mm'}$ are generalized atomic orbital occupations (to

be defined later) for the "Hubbard" atom (the atom with strongly correlated orbitals) at site $I$, and $n^{I\sigma} = \sum_m n^{I\sigma}_{mm}$. In this equation $E_{LDA}[n(r)]$ is the "ordinary" energy functional used in DFT calculations, whereas $E_{Hub}[\{n^{I\sigma}_{mm'}\}]$ and $E_{dc}[\{n^{I\sigma}\}]$ represent respectively the term containing the "correct" on-site correlation functional and the Mean Field (MF) approximation to it, which modeling the LDA contribution to the on-site electronic interactions, has to be subtracted in order to avoid double counting.

This first expression of the LDA+U approach was formulated by Anisimov et al. [3, 4, 5]. A recent important contribution was given by Pickett et al. [8] who, while slightly refining the functionals, introduced a linear response technique for calculating the Hubbard parameters. Despite some different details occurring among these approaches, the main physical idea behind them can be captured in a very elementary formulation of the total energy functional:

$$E = E_{LDA} + \sum_I \left[ \frac{U}{2} \sum_{m,\sigma \neq m',\sigma'} n^{I\sigma}_m n^{I\sigma'}_{m'} - \frac{U}{2} n^I (n^I - 1) \right] \tag{3.2}$$

where $n^I_{m\sigma} = n^I_{mm\sigma}$, $n^I = \sum_{m,\sigma} n^I_{m\sigma}$, $U$ is the parameter (the Hubbard $U$) describing on site correlations and the second and third terms in the right hand side are, respectively, $E_{hub}$ and $E_{dc}$. If we derive this equation with respect to the orbital occupation to obtain the corresponding orbital energy, we have:

$$\epsilon^I_{m\sigma} = \frac{\partial E}{\partial n^{I\sigma}_m} = \epsilon^{0I}_{m\sigma} + U(\frac{1}{2} - n^{I\sigma}_m) \tag{3.3}$$

($\epsilon^0$ is the corresponding LDA quantity) from which it is evident that a gap of width $\approx U$ opens between occupied ($n^I_i \approx 1$) and unoccupied ones ($n^I_i \approx 0$) orbitals. If we define the atomic orbital occupation as the projection of the occupied valence manifold over the corresponding atomic state ($n^I_{m\sigma} = \sum_{k,v} \langle \psi^\sigma_{k,v} | P^I_m | \psi^\sigma_{k,v} \rangle$) we can easily extract the potential entering the Kohn-Sham equation which reads:

$$V|\psi^\sigma_{k,v}\rangle = V_{LDA}|\psi^\sigma_{k,v}\rangle + \sum_{I,m} U(\frac{1}{2} - n^{I\sigma}_m) P^I_{m\sigma} |\psi^\sigma_{k,v}\rangle. \tag{3.4}$$

From this expression we can see that if the occupation of a particular atomic orbital is initially larger than 1/2 then the Hubbard contribution to the potential is attractive and encourages the electrons to localize on that particular atomic state, whereas the opposite happens when the initial occupation is smaller than 1/2. In practical calculations, the final result does not actually depend very strongly on the initial conditions as occupations greatly evolve during the self consistent iterations with possible changes in the sign of the Hubbard potential. In the final self consistent configuration completely

empty or completely filled atomic orbitals are not necessarily obtained because the LDA contribution to the energy functional contains the competing factor (the tendency to minimize kinetic energy through delocalization) which sometimes could result stronger than the effect due to the Hubbard $U$ term. Fractional occupation numbers (for atomic orbitals around the Fermi level) is indeed the situation we would expect when applying this functional to a normal metal. Furthermore, even for localized electrons we could observe fractional $n_m^{I\sigma}$ because localization may occur on hybridized orbital built by $d$ levels with states of other atoms (this situation is actually not taken into account by most models).

Despite the fact that this simple scheme already contains the main physical mechanism that could lead to gap opening in strongly correlated materials, it actually neglects the exchange coupling and the possible non spherical character of the effective interactions (the dependence of $U$ on the magnetic quantum number $m$) entering the model. Its most serious inconsistency is, however, that the expression given in eq. 3.2 is not invariant under rotation of the atomic orbital basis set used to define the occupancies $n_{i\sigma}^I$. To solve these problems, Anisimov and coworkers [6, 7] introduced a basis set independent formulation of LDA+U in which $E_{Hub}$ and $E_{dc}$ are given a more general expression:

$$E_{Hub}[\{n^I_{mm'}\}] = \frac{1}{2}\sum_{\{m\},\sigma,I}\{\langle m,m''|V_{ee}|m',m'''\rangle n^{I\sigma}_{mm'}n^{I-\sigma}_{m''m'''} + (\langle m,m''|V_{ee}|m',m'''\rangle - \langle m,m''|V_{ee}|m''',m'\rangle)n^{I\sigma}_{mm'}n^{I\sigma}_{m''m'''}\} \tag{3.5}$$

$$E_{dc}[\{n^I\}] = \sum_I\{\frac{U}{2}n^I(n^I-1) - \frac{J}{2}[n^{I\uparrow}(n^{I\uparrow}-1) + n^{I\downarrow}(n^{I\downarrow}-1)]\} \tag{3.6}$$

where $U$ and $J$ are screened Coulomb and exchange parameters. The $V_{ee}$ integrals in eq. 3.5 describe the Coulomb interaction among ($d$) electrons sitting on the same site. Their expression is borrowed from the expansion of the $e^2/|r-r'|$ Coulomb potential in terms of spherical harmonics (see [6] and references quoted therein):

$$\langle m,m''|V_{ee}|m',m'''\rangle = \sum_k a_k(m,m',m'',m''')F^k \tag{3.7}$$

where $0 \le k \le 2l$ ($l$ is the angular moment of the Hubbard electrons which is equal to 2 in our case) and

$$a_k(m,m',m'',m''') = \frac{4\pi}{2k+1}\sum_{q=-k}^{k}\langle lm|Y_{kq}|lm'\rangle\langle lm''|Y^*_{kq}|lm'''\rangle. \tag{3.8}$$

The $F^k$ coefficients, that in HF theory are the radial Slater integrals describing the electron-electron (bare) interaction, in the present formulation represent parameters to

be related to the $U$ and $J$ of the LDA+U approach. For $d$ electrons we just need $F^0$, $F^2$, and $F^4$ which can be related to the on site and exchange interaction parameters as follows:

$$U = \frac{1}{(2l+1)^2} \sum_{m,m'} \langle m, m' | Vee | m, m' \rangle = F^0 \tag{3.9}$$

$$J = \frac{1}{2l(2l+1)} \sum_{m \neq m', m'} \langle m, m' | Vee | m', m \rangle = \frac{F^2 + F^4}{14} \tag{3.10}$$

where $m$ and $m'$ describe electronic (atomic) orbitals with the same $l$. In these formulas the $Vee$ integrals have the same angular dependence of HF electronic interactions, but they are evaluated using an indirect procedure which allows to account for the screening [9]. At first, the effective $U$ and $J$ are calculated (usually extracting their value from LDA) from which $F^0$, $F^2$ and $F^4$ are obtained (assuming the atomic value for $F^4/F^2$ = 0.625 for $d$ electrons) using eqs. 3.9 and 3.10. As the factors $a_k(m, m', m'', m''')$ are products of Clebsh-Gordan coefficients (the $|lm\rangle$ are also spherical harmonics), once the effective Slater integrals are obtained, the $V_{ee}$ interactions entering the $E_{Hub}$ functional can be directly evaluated and, being extracted from effective average Coulomb and exchange interactions, they result to be *screened* quantities as well.

It is worth notice that the ingredients used in this rotationally invariant formulation are strongly atomic-HF-like (it is evident in the procedure to obtain the $V_{ee}$ integrals from the effective interactions $U$ and $J$) and so we can expect it to be valid in the case the electronic states are effectively localized around the ions. This is indeed a limitation of the model (actually designed for a localized basis set approach) because, if we want to apply this scheme to a generic material, we cannot be sure that localization will occur, and furthermore, if it actually takes place, there is no guarantee that the $V_{ee}$ values (computed in this HF-like approximation) will be the correct ones. In other words, the physics of the system could lead to a kind of localization that these (atomic like) effective interactions are not able to enforce.

## 3.3 LDA+U simplified scheme

Owing to this unsatisfactory theoretical construction of the model, the lack of formal justification of its formulation, and the technical difficulties arising from the use of plane waves instead of localized basis set, we decided to extract from it a simpler scheme, whose theoretical foundation is possibly easier to understand, and we tried to construct a functional that could be applied to the study of real materials without any aprioristic

assumption. Formally, this new functional can be obtained from the basis set invariant formulation described so far by setting $F^2 = F^4 = J = 0$. This corresponds to neglect the non sphericity of the electronic interactions ($a_0(m, m', m'', m''') = \delta_{m,m'}\delta_{m'',m'''}$) and the differences among the interactions in like-spin and unlike-spin channels (described by $J$). The energy functional can be easily recalculated from expressions 3.5 and 3.6 and we obtain:

$$\begin{aligned} E_U[\{n^{I\sigma}_{mm'}\}] &= E_{Hub}[\{n^{I}_{mm'}\}] - E_{dc}[\{n^{I}\}] \\ &= \frac{U}{2}\sum_{I}\sum_{m,\sigma}\{n^{I\sigma}_{mm} - \sum_{m'} n^{I\sigma}_{mm'}n^{I\sigma}_{m'm}\} \\ &= \frac{U}{2}\sum_{I,\sigma} Tr[n^{I\sigma}(1 - n^{I\sigma})]. \end{aligned} \tag{3.11}$$

Despite this model can be obtained from the rotationally invariant LDA+U, we observe that we got rid of its HF-like assumptions in the evaluation of the electronic interactions, and the average (effective) $U$ can be defined in some more physically transparent way. In this sense the approach formulated in eq. 3.11 is not a restriction of the one given by eqs. 3.5 and 3.6, but rather a quite independent one. The model can indeed be thought of as the generalization to crystals of constrained occupation calculations in atomic problems. An atom in contact with a reservoir of electrons (as, for instance, another atom in its neighborhood, or a metallic surface to which it can adhere) can only exchange integer numbers of particle with its environment. This means, that intermediate situations with fractional occupations of one (or more) of its orbitals may only arise, in the open atomic system, as time averages over states with integer number of electrons on the atomic orbitals [10, 51]. In quantum mechanics an open system with a fluctuating number of particles is described not by a pure state or wave function, but rather by a statistical mixture so that, for instance, the total energy should be given as:

$$E_n = (1 - \omega)E_N + \omega E_{N+1} \tag{3.12}$$

where $E_N$ and $E_{N+1}$ are the energies of the system corresponding to states with $N$ and $N + 1$ particles respectively, while $\omega$ represents the statistical weight of the state with $N+1$ electrons. The average number of particle in the system, $n$, can be given a similar expression:

$$n = (1 - \omega)N + \omega(N + 1) = N + w \tag{3.13}$$

so that the total energy of this open atomic system is represented by a series of straight-line segments joining states corresponding to integer occupations of the atomic orbitals

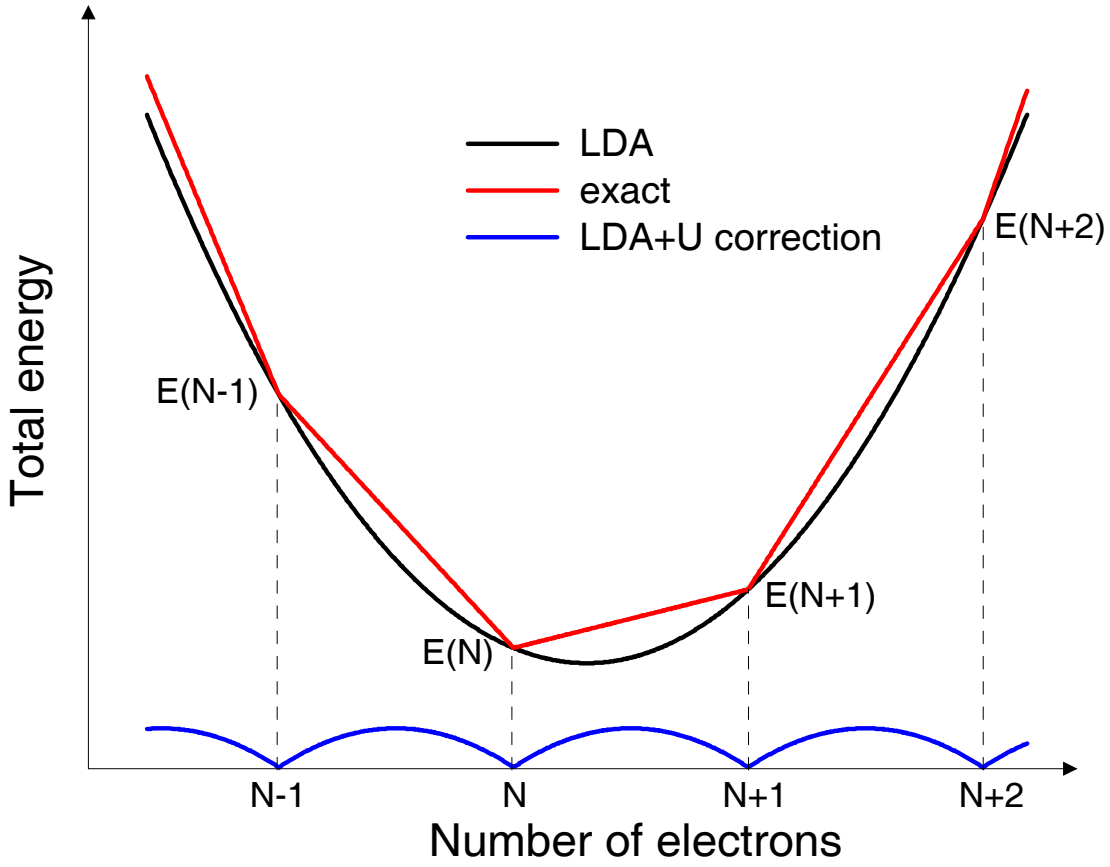


Figure 3.1: The total energy profile as a function of the number of electrons in the system. The curve in the bottom is the difference between the other two (the LDA energy and the "exact" result for an open system).

as depicted in fig. 3.1. In between, just one orbital is partially filled so that the slope of the corresponding straight-line segment is nothing but the eigenvalue which is getting filled:

$$\epsilon_i = \frac{dE}{dn_i}. \tag{3.14}$$

This situation is not well reproduced by the LDA approach which produces unphysical total energy minima in correspondence of fractional occupation of the orbital of the atomic system. Thus the picture given by LDA is not physically meaningful as, if we admit that the total energy of the open atomic system can be defined for fractional occupations and is also differentiable with respect to N, a paradox arises when the atoms get farther and farther from each other in the dissociation limit [10, 51]. Nevertheless,

if the occupation of the orbitals is constrained to integer values the LDA approach can reproduce the differences among the total energy of different states quite accurately [52]. (this is the reason for which the two curves in fig. 3.1 touch each other when the system contains integer numbers of electrons). However the physical situation (the straight-line segment curve) can be recovered, beside constraining the occupations to integer values, adding a correction which, vanishing for $n = N-1, N, N+1...$, eliminates the curvature of the LDA energy profile in every interval between two successive integer values of the occupation (bottom curve of fig. 3.1). This is what is done by eq. 3.11 which is based on the assumption that the curvature of the energy profile is not dependent on $n$. In this context the interaction parameter $U$ is the effective (unphysical) curvature of the energy as a function of $n$ which we want to eliminate. Equivalently, the quadratic dependence of the total energy on $n$ can be regarded as the self interaction of the particle which is being injected into the system. The Hubbard parameter results, in this context, the effective strength of this unphysical coupling of the electrons with themselves which has to be subtracted to the total energy of the system.

The situation is of course much more complicated in solids where fractional occupations of the atomic orbitals can occur because hybridization. But still the correlation is an atomic-like (on site) problem and the model in eq. 3.11 is expected to "measure" the atomic character of the valence wavefunctions and apply to them the same corrections that would be necessary for the corresponding atomic states.

The way this simple model works is equivalent to the one described at the beginning of the present section which can be recovered in the basis set where the occupation matrices are diagonal. In addition, the functional we choose retains the very appealing feature of rotational invariance (the physical occupancies are those in the diagonalizing basis set) so that the efficiency of the method does not depend on the basis set used to describe the atomic states.

In order to fully define how the model works and to calculate the Hubbard contribution to the potential, we have to fix a precise definition for the $n^{I,\sigma}_{m,m'}$ occupation matrix. In our implementation we define:

$$n^{I\sigma}_{mm'} = \sum_{\mathbf{k},v} f_{\mathbf{k}v} \langle \psi^{\sigma}_{\mathbf{k}v} | \varphi^{I}_{m'} \rangle \langle \varphi^{I}_{m} | \psi^{\sigma}_{\mathbf{k}v} \rangle \tag{3.15}$$

where $f_{\mathbf{k}v}$ is the weight of the electronic state $(\mathbf{k}v)$, $\varphi^I_m$ is the valence atomic orbital $|nlm\rangle$ of the atom sitting at site $I$ ($l = 2$ in our calculation and the same function is used for both spins), and $\psi^{\sigma}_{\mathbf{k}v}$ is the valence electronic wavefunction corresponding to the state $(\mathbf{k}v)$ with spin $\sigma$. The integrals defining the occupation matrix in eq. 3.15 select for

the localized orbital the Fourier components corresponding to the same **k**-vector which classifies the valence state $\psi^{\sigma}_{\mathbf{k}v}$. For this reason these integrals could equivalently be calculated using extended atomic wavefunctions constructed as Bloch sums of localized orbitals centered on translationally equivalent atomic sites:

$$\varphi^{I}_{m,\mathbf{k}}(\mathbf{r}) = \frac{1}{\sqrt{N}} \sum_{\mathbf{R}} e^{-i\mathbf{k}\cdot\mathbf{R}} \varphi^{I}_{m}(\mathbf{r} - \mathbf{R} - \tau_I). \tag{3.16}$$

These Bloch functions do not satisfy, in general, any orthonormality condition since functions of non equivalent sites may have non vanishing overlap. Using the Bloch sums of the atomic (localized) orbital is however one of the possible choices we could adopt to describe the atomic wavefunctions on which the occupation matrix has to be calculated. Other choices could be used as well as, for instance, orthogonalized atomic Bloch functions, Gaussian functions centered on the atomic sites, Wannier functions and so on. In principle, the particular choice of the (atomic-like) basis set used to describe the possible localization of the electrons should be not very relevant as far as the interaction parameters of the theory are defined in a way consistent with the definition of the localized basis (and thus of the occupation matrix). Different definitions for the occupation matrix will determine, in principle, different values of the parameter entering the LDA+U functional as it has been pointed out recently also by Pickett et al. in ref. [8].

In the next section this problem is discussed and a linear response approach is proposed as a possible scheme to evaluate the Hubbard $U$.

## 3.4 Calculating the Hubbard $U$

The theoretical approach we presented in the previous paragraph as the one chosen to be implemented in our plane waves code, needs to be completed with an appropriate definition of the interaction parameter (the Hubbard) $U$ entering its expression. In fact, in order to apply this theoretical scheme to generic systems (also non strongly correlated ones) and make it correctly reproduce their physical properties, we have to get rid of any aprioristic assumption about the choice of the effective on-site correlation for each material. In other words we want to extract $U$ from the the physical behaviour of the system under consideration in such a way it correctly "interprets" and then reproduces (and promotes) its tendencies toward strong correlation, electron localization, gap openings and so on. This requires this interaction parameter to be calculated in close consistency with the mathematical expression of the model and with the definition

of the $d$ level occupancies given in the previous section. In constructing this theoretical framework, in fact, we didn't use any "universal" definition of the quantities entering its expression nor a well fixed standard approach (if any exists) to the problem of correctly describing strong electronic correlations. What we did was giving the system new degrees of freedom (the possibility of modifying the $d$ level occupancies as defined in eq. 3.15) which could possibly be exploited to better account for on site correlations, so that now we have to tune the effective interaction associated to them in agreement with the real trends of the systems.

As it was explained in the previous paragraph, the Hubbard $U$ describes the spurious curvature of the total energy with respect to the number of electrons accommodated in the system due to the incomplete cancellation of the self energy in LDA. Equivalently, it can be defined as the first derivative of the last occupied eigenvalue with respect to its occupation. This is a well defined quantity in the atomic limit where just the highest energy orbital is partially occupied. It follows that the effective interaction parameter can be evaluated, in this case, considering the finite difference between the $3d$ energy eigenvalues when the number of electrons accommodated on the $d$ valence manifold is changed by one, and the system is free to screen the additional (constrained) charge on the $d$ states by (self consistent) modifications in the occupation of other levels and in the shape of the electronic wave functions [9]. This approach for calculating the Hubbard $U$ from first principle was also applied to the crystal case by Anisimov and coworkers in an early work on LDA+U [9]. The use of a localized basis set to construct the valence electronic states, as in the linear-muffin-tin-orbital (LMTO) method, allows to eliminate from the hamiltonian of the system the hopping terms among the atoms with a constrained $d$ population and the others. The problem is thus reduced to the one of an isolated atom embedded in a background which participates to the screening of the effective interactions. This extension to the crystal is based on the assumption that the screening of the Coulomb interactions is mainly performed by the $s$ or $p$ orbital on the same site where the charge is constrained, while the contribution from the other atoms is expected to be less important [9]. However this is not valid in general when we deal with crystals, since the strong overlap between the atomic orbitals may lead to a situation which cannot be described by the atomic limit. Thus, the finite difference method, based on a unitary variation of the on-site charge, cannot be applied because fractional occupations of the atomic states with possible continuous variations are to be expected as a consequence of hybridization and of possible degeneracies among the valence states driven by the symmetry of the crystal. Furthermore in a PW PP formalism

the atomic limit cannot be properly recovered as the hopping integrals among neighbor atoms cannot be explicitly eliminated from the expression of the hamiltonian.

Owing to this situation, in order to calculate the on-site interaction $U$ we adopted a linear response approach in which the $d$-level occupations, $n^{I\sigma}_{mm'}$, are forced to vary around the LDA (unconstrained) value. This method was inspired by the linear response scheme used by Pickett et al. in ref. [8] to compute the effective Hubbard parameter. However some differences with respect to that approach arose in our work and will be underlined later on.

In order to extract the Hubbard $U$ what we need is the LDA total energy as a function of the total $d$ level occupancy of one "Hubbard" site $E^{LDA}[n^{Id}]$. From this dependence we can (numerically) compute the second derivative $\partial^2 E^{LDA}/\partial(n^{Id})^2|_{n^{Id}=n^{Id}_{LDA}}$ which corresponds to the effective curvature of the LDA total energy. However this quantity is not directly the Hubbard $U$ we want to compute; in fact, if we had perturbed a non interacting system we would have obtained a quadratic behaviour of its energy as well, because the imposed $d$ charge variation would have determined a change in the kinetic energy of the system. This kinetic energy term, which involves also non directly perturbed sites because of hybridization of the atomic orbitals and the possible itinerant character of the valence states, should not be included in the calculation of the Hubbard $U$, nor in the screening of this effective coupling, because it does not originate from the electron-electron interaction. It rather comes from the band structure of the system which is correctly accounted for in the LDA functional so that including it in the on site $U$ parameter would lead to a double counting error.

Eliminating the band energy contribution from the calculation of the Hubbard parameter in our approach plays a role analogous to the cancellation of the hopping terms among the perturbed atom and the others in the LMTO approach of Anisimov and coworkers (see, for instance, ref. [5]). In the atomic limit the hybridization among the atomic orbital occurs because the very large interatomic distances, and the cutting of the hopping term between the perturbed atom and the others becomes an exact procedure. In our case the same situation is recovered because the single particle eigenvalues would eventually collapse to the corresponding atomic energies and the dependence of the (spurious) non interacting electron term of the total energy on the atomic occupation would result linear thus giving a vanishing contribution to the effective curvature we want to measure. Thus, in the atomic limit, the two methods are perfectly equivalent. In our approach, however, no aprioristic assumption is made about the mechanism of screening and the system is free to exploit all the degrees of freedom it contains to

redistribute the constrained charge. The system, in fact, has many more degrees of freedom than those we can describe with the $d$ levels occupancies, and when $d$ population is changed on one site, all of them take part to the response of the system, thus renormalizing the resulting interactions. In this context the "non-Hubbard" atoms (and the non "correlated" orbitals of the Hubbard atoms) play an important role in the screening of the charge fluctuation induced on the Hubbard atoms and described by the $n^{I\sigma}_{mm'}$. The role of the renormalizing background (as well as the one of the other Hubbard atoms) is, instead, completely neglected in the approach by Pickett et al. [8] where the linear response theory is applied treating the single angular momentum contributions to the atomic occupations of the perturbed atom as the effective perturbed degrees of freedom.

In our approach the total on-site occupation are considered and the effective Hubbard $U$ results:

$$U = \frac{d^2E^{LDA}}{d(n^{Id})^2} - \frac{d^2E_0^{LDA}}{d(n^{Id})^2} \tag{3.17}$$

where the second derivative of $E_0^{LDA}$ is the above mentioned independent electrons contribution we have to subtract from the full curvature of the LDA functional.

In actual calculations constraining the total $d$ orbital occupations is not very practical and what we do, instead, is to force them to vary adding to the effective potential a localized perturbation acting on the $d$ levels of a particular "Hubbard" site:

$$V^{constr} = V^{LDA} + \alpha P_d^I \tag{3.18}$$

where $V^{LDA}$ is the LDA potential (we always start from "normal" ($U = 0$) LDA calculations), $P_d^I$ represents the projector on the $d$ states manifold of the atom at site $I$:

$$P_d^I = \sum_{m=-2,2} |\varphi_m^I\rangle\langle\varphi_m^I| \tag{3.19}$$

and $\alpha$ is the amplitude of the potential shift we add to the $d$ levels of the chosen "Hubbard" atom to excite charge fluctuations on its orbitals. For a number of potential shifts around zero we solve the Kohn-Sham equations up to self consistency and what we finally obtain is:

$$E[\alpha] = \min_\rho\{E^{LDA}[\rho] + \alpha n_d^I\} \tag{3.20}$$

where $\rho$ is the electronic charge density of the system under consideration and the minimization is performed over an orthonormal set of electronic valence states. This expression is easily generalized to a set of perturbations acting on all the relevant Hubbard sites:

$$E[\{\alpha_I\}] = \min_\rho\{E^{LDA}[\rho] + \sum_I \alpha_I n_d^I\}. \tag{3.21}$$

From the solution of the Kohn-Sham equations we calculate the value of the total $d$ occupations on each "Hubbard" site corresponding to the ground state of the system, which are the quantities we would like to treat as the independent variables in our linear response study (instead of the $\alpha_I$). We can switch to an occupation-dependent energy functional by a Legendre transformation:

$$E[\{n_d^I\}] = \min_{\{\alpha_I\}}\{E[\{\alpha_I\}] - \sum_I \alpha_I n_d^I\} \tag{3.22}$$

where, at the minimum, the independent variable $n_d^I$ would correspond to $dE[\{\alpha_J\}]/d\alpha_I$. In this context the derivatives defining the effective interactions can be easily obtained from the expression 3.22:

$$\frac{dE[\{n_d^J\}]}{dn_d^I} = -\alpha_I(\{n_d^J\}) \tag{3.23}$$

$$\frac{d^2E[\{n_d^J\}]}{d(n_d^I)^2} = -\frac{d\alpha_I(\{n_d^J\})}{dn_d^I}. \tag{3.24}$$

that show that what is needed in order to compute the effective interaction parameter is the linear variation of the localized potential shift, $\alpha_I$, induced by a variation of the $d$-level occupation of the same site when all other occupations are unchanged with respect to their LDA value.

However, from eq. 3.21 the quantity that is directly accessible is the response function

$$\chi_{IJ} = \frac{dn_d^I}{d\alpha_J} \tag{3.25}$$

that measures the fluctuation of $n_d^I$ produced by $\alpha_J$ acting, in general, on a different "Hubbard" site. We can expect that this matrix strongly depends on the spatial arrangements of the atoms, the distances among each other, the symmetry of the system, the possible magnetization on the ions and so on. Using this response-function language, the effective interaction parameter $U$ can be recast as follows:

$$U = -\frac{d\alpha^I}{dn_d^I} + \frac{d\alpha^I}{dn_{d0}^I} = \left(\chi_0^{-1} - \chi^{-1}\right)_{II} \tag{3.26}$$

where the last expression on the right hand side of this equation represents the diagonal (on-site) term of the matrix in the brackets. The physical meaning of eq. 3.26 is clear: we force a fluctuation on the $d$ level occupancies on one site $I$ and observe its redistribution over the whole system (also non "Hubbard" sites take part to this relaxation) which is due to a shift of the energy levels on each site, and to electronic interactions which produce on-site correlation (thus introducing an energy cost to be paid when moving to

other strongly correlated sites with other particles already in their $d$ levels). As we are able to isolate the first contribution which is present also in a non interacting system, we subtract it from the total response of the system and what remains is the pure effect of local field interactions. This is reminiscent of a known result of the linear response theory in which the difference among the total and the bare response function describes the effect of local field interactions. The fact that we use integrated quantities (the $n_d^I$) as the effective degrees of freedom (instead, for instance, of the local charge density $n(\mathrm{r})$), implies that the resulting effective interaction we obtain from this procedure is averaged on the atomic region.

The matrix, whose diagonal term defines the Hubbard $U$, also contains non diagonal terms which correspond to inter site effective interaction in LDA. We do not use them in our model as we are interested in correcting the on-site (short range) electron-electron self interaction letting LDA account for inter-site terms.

In eq. 3.26 the fluctuation of the atomic occupations, $n_{d0}^I$, which defines the bare response function $\chi^0$, must be calculated without including the effect of the interparticle interactions. In practice we perform a well converged LDA ($U = 0$, $\alpha = 0$) calculation and, starting from its self consistent potential and the corresponding electronic wavefunctions, we add a series of potential shifts on each non equivalent "Hubbard" site, and let the system evolve to self consistency each time. At the first iteration of the perturbed run only the "bare" perturbation is included in the effective potential acting on the electrons. In other words, the density response obtained at the first iteration does not involve any effect of the electron-electron interaction and actually corresponds to the response of the independent electron system. The needed $n_{d0}^I$ and $\chi_0$ are thus obtained in the first iteration of the perturbed ($\alpha \neq 0$) run to self consistency, whereas the corresponding interacting (renormalized) quantities are calculated at the end, when electron-electron interactions have fully played their role in screening the effective couplings and charge distributions.

This is quite a different way to calculate the effective Hubbard $U$ than the linear response approach proposed by Pickett et al. [8]. In fact, they evaluate the bare contribution to the effective interaction directly calculating the second derivative, with respect to the atomic occupations, of the kinetic energy contained in the self consistent total energy, which produces unrealistically large results (the same authors could not use the obtained values in practical calculations). This is not the true independent electrons contribution to be subtracted from the total response function because a non interacting electron gas would have a different response in the kinetic contribution than an

interacting one.

Once we have studied the linear response of the system to perturbations applied to all possible non equivalent "Hubbard" sites, we have all the information we need to completely describe the response matrices $\chi$ and $\chi^0$. For symmetry reasons, given a pair of sites $IJ$ at a distance $l$ from each other, the corresponding element of $\chi$ (for example) $dn_d^I/d\alpha^J$ is the same we can obtain putting the perturbation on a site $J'$ equivalent to $J$ and studying the $d$ level occupation response on a site $I'$ whose distance from the $J'$ is $l$. We thus have in these matrices separate contributions coming from first, second, third neighbors and so on, and this provides some indications about the range of the screening and of charge redistributions. In order to properly calculate the effective interaction parameter $U$, a large enough number of neighbors of the perturbed atom has to be included in the unit (super)cell, so that the charge redistribution governing the screening can be completely accommodated within the considered volume. In practice, we have to repeat the perturbed calculations for larger and larger unit cells up to the point the resulting value of $U$ is reasonably converged. At each step of this study we add more and more distant shells of neighbors of the perturbed atom; thus the effect (and the relative importance) of adding first, second, third nearest neighbors (and sometimes even farther atoms) can be studied separately while increasing the size of the unit (super)cell. The background, corresponding to all degrees of freedom not described by the $n_d^I$ occupation numbers, also takes part in the screening of the effective interaction. Therefore, besides the Hubbard occupation numbers we deal with explicitly, it is useful to consider a charge reservoir which physically describes the $s$ and $p$ states of the strongly correlated atoms and the orbitals of possible interstitial ions. This translates in one more column (and one more row) in the linear response matrices. The matrix elements associated to this additional degrees of freedom are determined imposing overall charge neutrality of the perturbed system and absence of charge density variation upon perturbing the system with a constant potential. From a mathematical point of view both $\chi$ and $\chi_0$ matrices acquire a null eigenvalue corresponding to an eigenvector having $N+1$ equal components ($N$ being the number of strongly correlated sites):

$$\overrightarrow{\overrightarrow{\chi}}\,\overrightarrow{\beta} = \overrightarrow{\overrightarrow{\chi}}_0\,\overrightarrow{\beta} = \overrightarrow{0} \tag{3.27}$$

where $\overrightarrow{\beta} = \beta\overrightarrow{1}$. Thus the inverse matrices we need in eq. 3.26 are indeed ill defined. However, it can be shown that their singularities cancel out when computing the difference $\chi_0^{-1} - \chi^{-1}$. In fact, if we represent these matrices in block diagonal form (separating the eigenspace corresponding to the zero eigenvalue from the rest), we can single out

a $N \times N$ non singular block which is the one we need to invert in eq. 3.26. A simple trick to perform the necessary inversions without bothering for this singularity consists in shifting the null eigenvalue of both the $\chi$ and the $\chi_0$ matrices by the same amount, $\gamma$. This is easily done adding to both $\chi$ and $\chi_0$ a matrix built with $(N+1) \times (N+1)$ elements all equal to $\gamma/(N+1)$). Inverting both $\chi$ and $\chi_0$ we thus obtain, for each of them, a $N \times N$ block (corresponding to the inverse of the $N \times N$ non singular blocks of the starting response matrices), and the same result $(1/\gamma)$ on the remaining diagonal element. This latter term is canceled in the difference of eq. 3.26 while the physical interaction comes from the the two non singular $N \times N$ contributions to be subtracted one from the other. The numerical stability of this procedure has been tested and the final results was found to be independent on the chosen $\gamma$ over a wide range of possible values. It is worth notice that this procedure is not the same as directly computing $\chi_0^{-1} - \chi^{-1}$ with the row and column corresponding to the background removed; in fact we maintained the system neutral and the charge reservoir played a role in the screening that would be neglected otherwise.

We want to present now a possible extension of the approach described so far, which includes the spin degrees of freedom in the calculation of the on site interaction parameter. The way the spin of the electrons can be considered in the presented linear response approach, does not introduce any conceptual complication with respect to unpolarized case. In fact, this additional degree of freedom can be easily accounted for by potential shifts acting on the two $d$ states spin channels separately. We thus obtain $(2N+1) \times (2N+1)$ $\chi_0$, $\chi$ and "interaction" matrices; this latter contains the relevant informations in the diagonal (on-site) elements of each $N \times N$ block corresponding to the $\uparrow\uparrow$, $\uparrow\downarrow$, $\downarrow\uparrow$ and $\downarrow\downarrow$ spin arrangements between the perturbing potential shift at site $L$ $\alpha^{L\sigma}$ and the perturbed $d$ level occupation of the site $I$ $n_d^{I\sigma}$. This extended spin resolved procedure would correspond, ideally, to account for the exchange interaction parameter $J$ of the full rotational invariant LDA+U formulation (eqs. 3.5, 3.6). However, the expression we obtain for the interaction matrix can not always be mapped on this model. In fact, the LDA average contributions to the exchange and correlation which we obtained from our constrained calculations in the study of the magnetic system we present in this thesis are not the same for the two spin channels as predicted instead by eq. 3.6 which is perfectly symmetric upon exchanging the two spin components of the $d$ orbital occupations. In other words the two spin populations are treated on completely different grounds by the standard L(S)DA approach and completely different effective interactions are thus obtained in the two spin channels. Since the exchange parameter

$J$ cannot be obtained in this spin polarized linear response theory, the procedure used in the full rotational invariant LDA+U approach to extract the $Vee$ integrals of eq. 3.5 cannot be adopted. A possible alternative that does not rely on the spin symmetry in eq. 3.6 is to introduce in our simplified model a different Hubbard $U$ for each spin polarization. The simplified model described in eq. 3.11 is thus generalized as follows:

$$E_U[\{n^{I\sigma}_{mm'}\}] = \frac{1}{2}\sum_{I,\sigma} U^\sigma Tr[n^{I\sigma}(1-n^{I\sigma})]. \tag{3.28}$$

In this case, however, we neglect the role of the off diagonal spin blocks of the obtained interaction. On the other hand this is consistent with the spirit of our approach (where $U$ describes the spurious self interaction of the electrons) that does not contain off diagonal spin contributions. These off-diagonal interaction terms should be already properly taken into account in LDA in a way similar to the interaction between different sites, so that we don't need to correct them while modifying the on site correlations.

In practice, applying the described technique for the calculation of spin dependent interactions is quite problematic since the majority spin population is very delicate to probe (thus producing very unstable results for the effective interactions) upon numerical errors in the response matrices. This behaviour is due to the fact that the majority spin states are well below the Fermi level so that adding some charge on these orbitals is almost impossible (they are close to be completely filled in our atomic occupation language), and also extract even small amount of charge from them is particularly expensive. They thus tend to be particularly inert upon charge perturbations driven by the applied potential shifts, so that numerical differentiation is affected by large errors.

## 3.5 Implementation of the LDA+U approach in a PW PP code

Let us give at this point some technical details about the implementation of the described LDA+U functional within PW PP code. The use the ultrasoft (US) pseudopotentials (PPs) [23, 24], requires that the products appearing in eq. 3.15 are completed with the augmentation correction inside the ionic cores. So, for instance, instead of $\langle\varphi^I_{m\mathrm{k}}|\psi^\sigma_{\mathrm{k}v}\rangle$ we have $\langle\varphi^I_{m\mathrm{k}}|S|\psi^\sigma_{\mathrm{k}v}\rangle$ where $S$ is the overlap matrix defined in eq. 1.45.

Having fixed the definition of the atomic orbital occupations we can now derive the Hubbard contribution to the KS potential. To find the expression of $V_U|\psi^\sigma_{\mathrm{k}v}\rangle$ we first calculate the derivative of $E_U[\{n^{I\sigma}_{mm'}\}]$ with respect to $n^{I\sigma}_{mm'}$ and then the derivative of

this quantity with respect to $\psi^{\sigma *}_{\mathrm{k}v}$. The result is:

$$\begin{aligned} V_U|\psi^{\sigma}_{\mathrm{k}v}\rangle &= \frac{U}{2}\sum_{I,m'} S(|\varphi^I_{m'\mathrm{k}}\rangle - 2\sum_m n^{I\sigma}_{mm'}|\varphi^I_{m\mathrm{k}}\rangle)\langle\varphi^I_{m'\mathrm{k}}|S|\psi^{\sigma}_{\mathrm{k}v}\rangle) \\ &= \frac{U}{2}\sum_{I,m,m'} S|\varphi^I_{m\mathrm{k}}\rangle\left[(\delta_{mm'} - 2n^{I\sigma}_{mm'})\langle\varphi^I_{m'\mathrm{k}}|S|\psi^{\sigma}_{\mathrm{k}v}\rangle\right]. \end{aligned} \tag{3.29}$$

The ordinary result, eq. 3.4, is recovered just replacing $S$ with the unitary matrix. The contribution of $V_U$ does not correspond to the Hubbard energy (eq. 3.11) because the factor 2 in front of the atomic occupations in eq. 3.29. Furthermore, the resulting total energy of the system is not variational since the atomic occupations are updated at each iteration of the self-consistent run. The problem is similar to the one discussed in chapter 1 about the non variational contribution of the $Hxc$ potential to the band energy of the system. The sum of the eigenvalues results in a term which reads:

$$E^{LDA+U}_{band} = \sum_{\mathrm{k}v} f_{\mathrm{k}v}\epsilon^{LDA+U}_{\mathrm{k}v} = E^{LDA}_{band} + \frac{U}{2}\sum_I\sum_{m,\sigma}\{n^{I\sigma out}_{mm} - 2\sum_{m'} n^{I\sigma in}_{mm'}n^{I\sigma out}_{m'm}\} \tag{3.30}$$

where $f_{\mathrm{k}v}$ are the spectral weights of the electronic valence states of energy $\epsilon^{LDA+U}_{\mathrm{k}v}$, $E^{LDA}_{band}$ has been defined in eq. 1.16 (here we do not consider the non variationality of this term), and $n^{I\sigma in}_{mm'}$ and $n^{I\sigma out}_{mm'}$ represent, respectively, the atomic occupation matrices used to build the Hubbard potential and obtained from the last iteration. A corrections has now to be added to the sum of the eigenvalues which eliminates the undesired dependence of $E^{LDA+U}_{band}$ on $n^{I\sigma in}_{mm'}$ and also accounts for the double counting problem of the Hubbard contribution to the energy of the system:

$$\begin{aligned} \tilde{E}^{LDA+U}_{band} &= E^{LDA+U}_{band} - \frac{U}{2}\sum_I\sum_{m,\sigma}\{n^{I\sigma out}_{mm} - 2\sum_{m'} n^{I\sigma in}_{mm'}n^{I\sigma out}_{m'm}\} \\ &+ \frac{U}{2}\sum_I\sum_{m,\sigma}\{n^{I\sigma out}_{mm} - \sum_{m'} n^{I\sigma out}_{mm'}n^{I\sigma out}_{m'm}\} \\ &= E^{LDA+U}_{band} + U\sum_{I,m,m',\sigma}\left[n^{I\sigma out}_{mm'}\left(n^{I\sigma in}_{m'm} - \frac{1}{2}n^{I\sigma out}_{m'm}\right)\right] \\ &= E^{LDA}_{band} + \frac{U}{2}\sum_I\sum_{m,\sigma}\{n^{I\sigma out}_{mm} - \sum_{m'} n^{I\sigma out}_{mm'}n^{I\sigma out}_{m'm}\}. \end{aligned} \tag{3.31}$$

It can be noted in the final expression of this equation, that the resulting contribution of the Hubbard interaction to the band energy is the Hubbard energy given in eq. 3.11 written as a function of the only $n^{I\sigma out}_{mm'}$ occupation matrix.

# Chapter 4

# The LDA+U approach: application to some real systems

In this chapter the LDA+U method, introduced in the previous chapter, will be applied to the study of some real materials. Apart a brief investigation about the electronic structure of nickel oxide NiO, the same systems already studied within the conventional GGA approach will be taken into consideration so that a direct comparison will be possible between the results of that preliminary investigation and the ones obtained within the LDA+U method. The application of the LDA+U approach to the study of bulk iron, iron oxide and nickel oxide will give a good opportunity to test our theoretical scheme due to the availability of a reasonable number of experimental results about the electronic, magnetic and structural properties. The merits of our approach as well as some remaining problems will be underlined and discussed in comparison with other similar theoretical approaches that can be found in literature. Some possible (semiempirical) extensions of our simple functional (similar to other approaches used in literature) are, in fact, used to try to improve the description of the structural properties of bulk iron and iron oxides. The reliability of the method in describing the physical properties of real material which strongly depend on their structure is then discussed pointing out some still remaining problems. The study of fayalite within the LDA+U scheme is finally presented with a discussion about the results obtained for the electronic and magnetic properties.

## 4.1 Bulk iron

The application of the LDA+U method to the bulk iron (as to other transition metals) is rather unusual in the literature even if some consideration has been devoted to the role of electronic correlations on the physical properties of this material. On-site electronic interactions are expected to be important, for example, in reproducing the thermal expansion of iron (in particular the electronic contribution to it) [53], its magnetoelastic properties (incorrectly described by LSDA or GGA approaches) [54], or the features of its itinerant-electrons ferromagnetism such as ferromagnetic instabilities, effective local moments, and fluctuations in spin and charge [56]. In other works it is shown that the electronic correlations for the $3d$ electrons of iron are important to better reproduce the observed features of its band structure (obtained by photoemission spectra) [55], or are explicitly taken into consideration in ab initio calculations to study the magnetic anisotropy of this material as in ref. [57].

In this work some properties of bulk iron will be studied for which electronic correlations are believed not to play a major role. As evident from the results shown in chapter 2 (and also in other works as in ref. [26]), GGA can provide quite a good description of bcc FM bulk iron and good agreement can be obtained with experiments about the band structure (as already remarked in ref. [55]), the magnetic moments and the structural properties (lattice spacing and bulk modulus in particular). The LDA+U method can thus be tested on iron in order to check whether it is able, through the consistent calculation of the on-site interaction parameter (the Hubbard $U$), to preserve the good description of the GGA approach.

LDA+U calculations for iron are performed in the same conditions as the ones of the preliminary GGA calculations presented in chapter 2 (we used the same pseudopotential, the same $xc$ functional, the same energy cut-offs for electronic wavefunctions and charge density, and also the same k-point grid and smearing width for the Fermi distribution) so that a direct comparison is possible between the two sets of results. The presence of the Hubbard $U$ requires a larger cut-off for the wavefunctions than strictly necessary for ordinary GGA calculations because the $d$ level occupancies are defined as projections on atomic states which need a large cut-off to be described accurately (the $d$ atomic states are quite localized). Furthermore we also need to use a rather fine k-point grid in the BZ for reciprocal space integrations to avoid that atomic wavefunctions centered on a given atom have finite spurious overlap with their periodic replicas associated with the discreet BZ sampling. This determines the choice of the 40 Ry energy cut-off and the

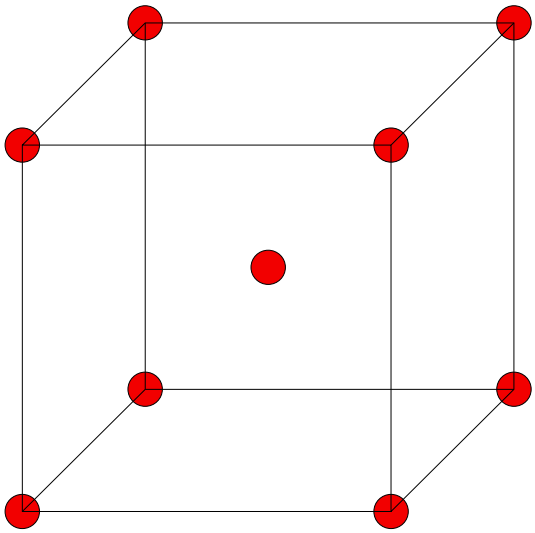

Figure 4.1: The two-atoms cubic supercell of iron.

8×8×8 grid we have used after having tested good convergence of the total energy upon increasing their values.

In its ground state bulk iron has a bcc unit cell. However the primitive unit cell (the one containing just one atom) cannot be used for calculating the Hubbard $U$ by the constrained LDA method described in chapter 3. A potential shift on the $d$ levels of all the atoms of the system would produce a variation of the $d$ levels occupancies poorly screened by the compensating background consisting of just the $s$ states of the ions. In order to properly take into consideration the effects of screening on the effective interactions, we need instead to observe how the perturbed atom redistributes its $d$ level charge to the $s$ states and among the nearest ions. Larger and larger supercells (containing one periodically repeated perturbed atom) are considered in order to describe an isolated perturbation.

We begin using a supercell of simple cubic (sc) shape (as the one depicted in fig. 4.1) containing the perturbed ion and one of its nearest neighbors. Then we consider a 2×2×2 bcc supercell which contains 8 atoms: 4 nearest neighbors and 3 second neighbors. The successive step is a 2×2×2 sc supercell with 16 atoms: 8 nearest neighbors, 3 second neighbors, 3 third neighbors and 1 fifth neighbor (the fourth neighbor is first neighbor of an atom which is translationally equivalent to the perturbed one). The largest cell we consider is a 4×4×4 bcc supercell with 64-atoms inside; we used this very large

cell just to extrapolate the results from the smaller ones as explained later on, and not in an explicit self consistent calculations. For each of the chosen supercells a series of self consistent calculations is performed with different potential shifts (symmetrically distributed around zero shift) applied to the $d$ levels of one of the iron ions (we always choose to perturb the atom at the origin for symmetry reasons). Then we used the resulting values of the total $d$ states occupancies to compute, by finite difference, the derivatives which define the response matrices $\chi$ and $\chi_0$ (see the discussion in section 3.4, eq. 3.25). Adding more and more atoms into the calculations of the $\chi$ and $\chi_0$ matrices, by using larger and larger supercells, allows to separate the contributions to the effective interactions coming from successive shells of neighbors. If, for instance, we suppose that the first nearest neighbor redistribution of the $d$ charge is sufficient to compute the effective interactions, we can use the result of the sc supercell containing 2-atoms (the one with the $d$ potential shifted and one of its nearest neighbors) in the eight time larger sc supercell with 16 atoms inside (8 of which are first neighbor of the perturbed one) just assigning the nearest neighbor contribution of the response according to the results of the 2-atom cell and putting the successive shell contributions to zero. Each of the eight nearest neighbor would be given, in this case, 1/8 of the corresponding response term calculated in the 2-atom sc cell, as the total amount of the charge flowing from the perturbed atom to its environment is equally distributed to the neighbors of the first shell. This extrapolation procedure is quite useful because it allows to appreciate the contributions coming from successive shells of neighbors (and their relative importance) to the calculation of the effective interactions. This is evident from the fig. 4.2 where the lines connect the results obtained extrapolating contributions up to a given shell of neighbors to larger supercells. At each supercell the distances among the different lines describe the importance of involving successive shells of atoms in the redistribution process of the perturbed charge. It can be observed that the extrapolation procedure gives good convergence of the calculated parameters and the result obtained from the sc 2-atom cell once inserted in the 64-atom supercell captures most of the effective interaction. The second and third nearest neighbors bring, of course, significant contributions in the resulting parameter and this is particularly evident by extrapolating their results to the largest supercell. However, while the difference with the (extrapolated) result of the sc 2-atom cell is quite relevant, the third neighbor contributions is not so different from the second neighbor ones, and, despite we did not check directly, we believe that contributions from further shells of atoms rapidly become very small. Thus, the main contributions can already be obtained within the sc supercell

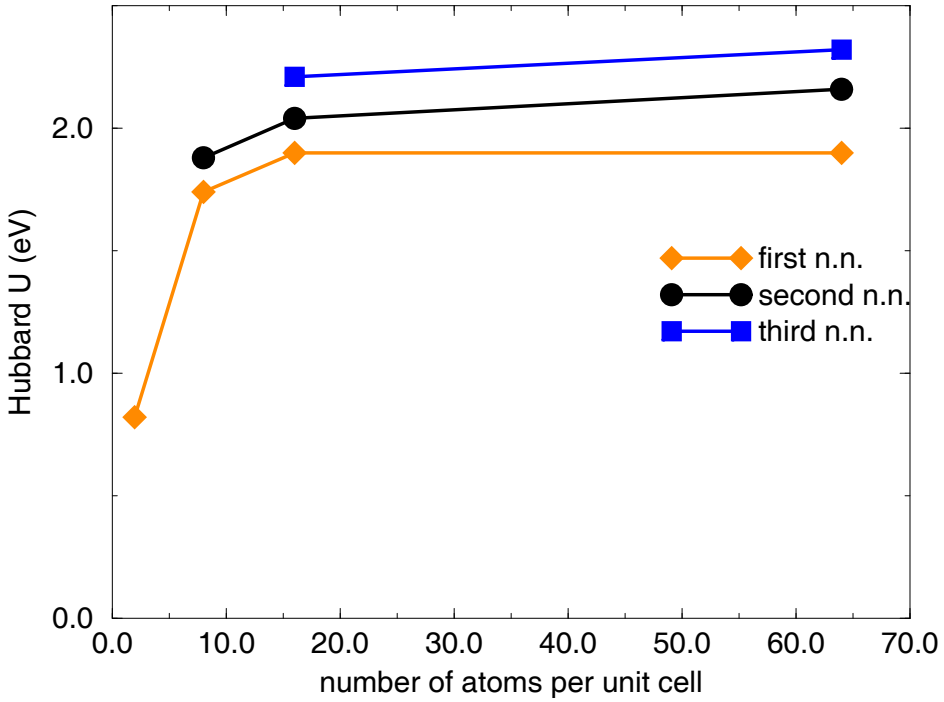


Figure 4.2: The calculated Hubbard $U$ for different supercells. The lines connect results from the "cell extrapolation" procedure (see the text) describing the contribution up to a given shell of neighbors of the perturbed atom.

containing 16 atoms. The extrapolation from this to the 64-atoms unit cell also brings minor variations which are indeed within the finite numerical accuracy of our simple scheme. Our estimate for the Hubbard $U$ will be made, therefore, using the supercell containing 16 atoms and corresponds to a value of 2.2 $\pm$ 0.2 eV at the experimental lattice spacing.

We have then performed an LDA+U calculation for bulk iron at the experimental lattice spacing using the computed value of $U$. The resulting band structure is shown in fig. 4.3 where the same experimental results already reported in chapter 2 are also present. As it can be easily noted by comparison with the results obtained in the preliminary GGA study the agreement with the experiments is now somehow worse than in that case (especially around $\Gamma$, P and H high symmetry points). The global effect of applying the on site repulsion $U$ mainly consists in a (almost) rigid downward shift of the majority spin bands of about 1eV while the minority states are maintained,

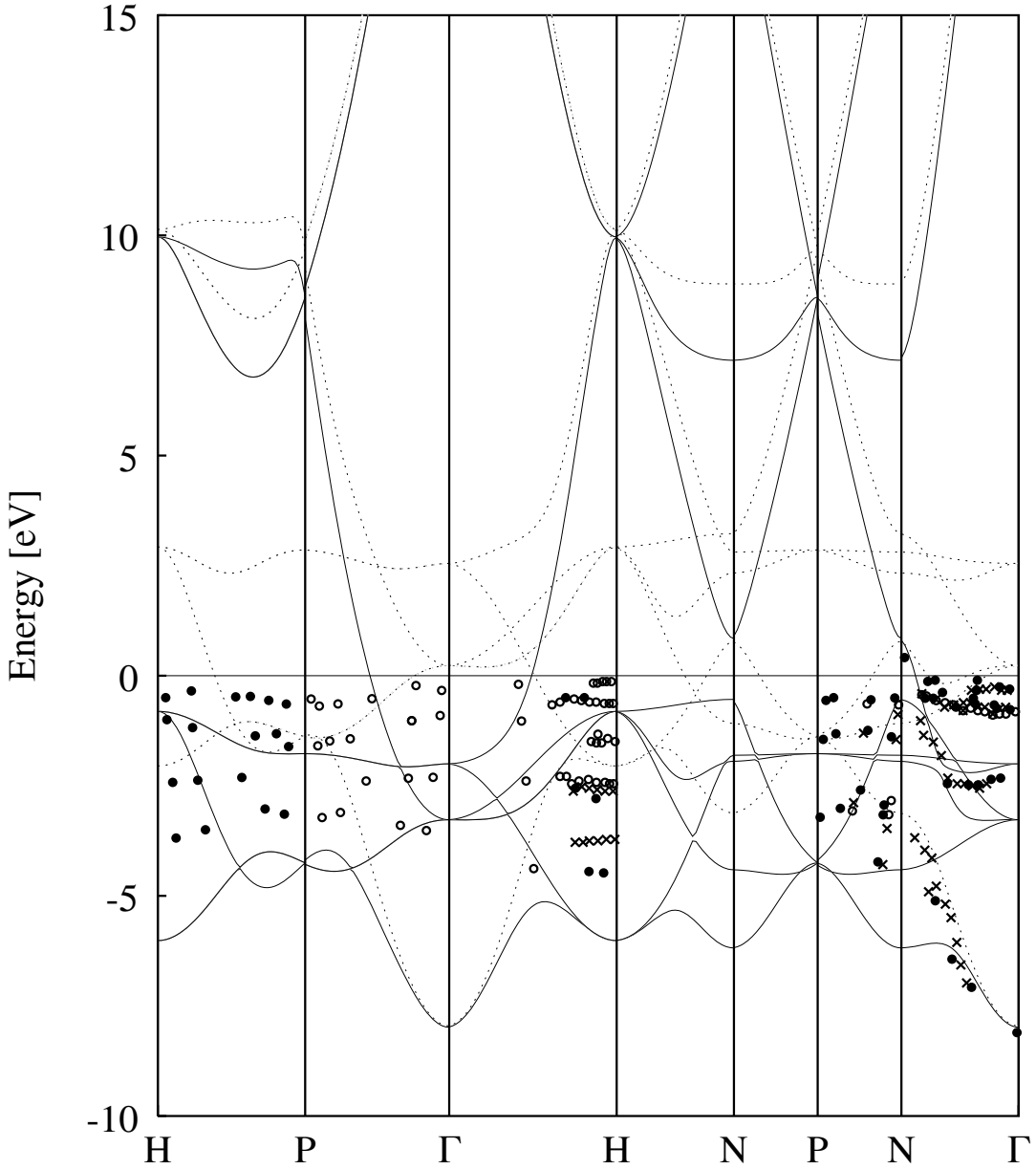


Figure 4.3: The band structure of bcc iron obtained within the LDA+U approach. Solid lines for majority spin bands, dotted lines for minority spin bands. The zero of the energy is set to the Fermi level.

with good approximation, at the same positions. The levels of $s$ character are also left unchanged by the application of the LDA+U method as it is demonstrated by the features at the bottom of the valence bands near the Γ point (still in good agreement with experiments) and the structure of the electronic levels far above the Fermi energy.

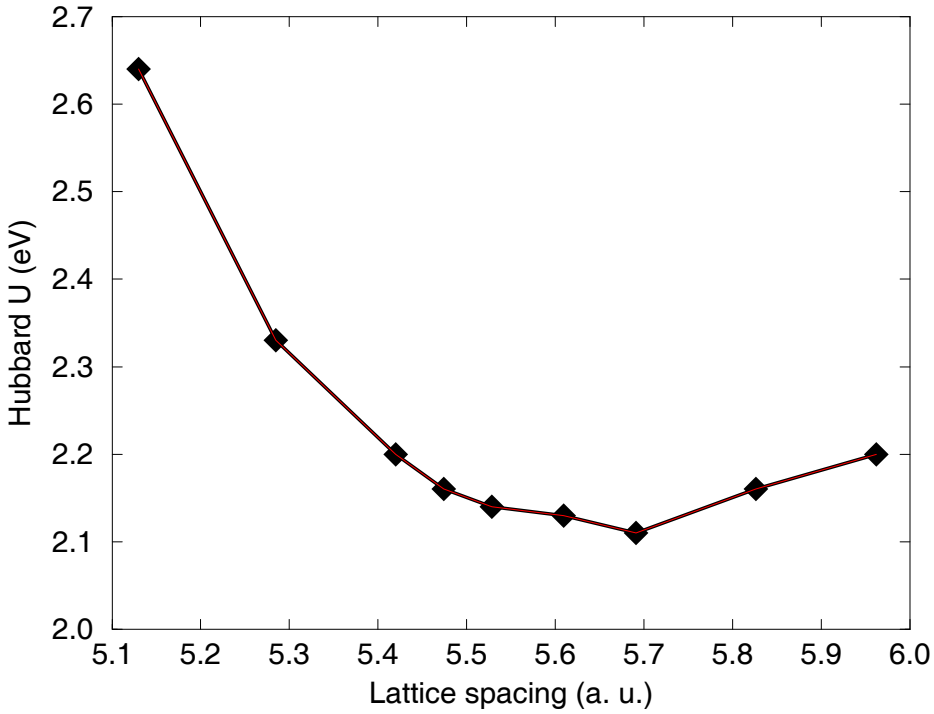


Figure 4.4: The dependence of the calculated Hubbard $U$ on the cubic lattice spacing.

This is consistent with the fact the Hubbard correction is applied just on the $d$ states of the materials.

Although quite evident, the observed disagreement in the band structure of iron may not be dramatically serious, also keeping in mind the fact that *i*) within DFT the single particle energy bands have no precise physical meaning; *ii*) the reliability of the approximations used to extract the experimental results has been questioned by some authors [58].

In order to further test the method on this material we investigate the structural properties studying the effect of the correlations introduced in our scheme at different lattice spacings. As the calculation of the Hubbard parameter has to be done on the same system it is used on, we have recalculated this quantity for each considered unit cell volume. The dependence of the calculated interaction parameter on the lattice spacing of the unit cell is shown in fig. 4.4 where a marked increase of the Hubbard $U$ can be observed when the lattice parameter is squeezed below its experimental value. Despite this may appear counterintuitive because correlation effects are expected to

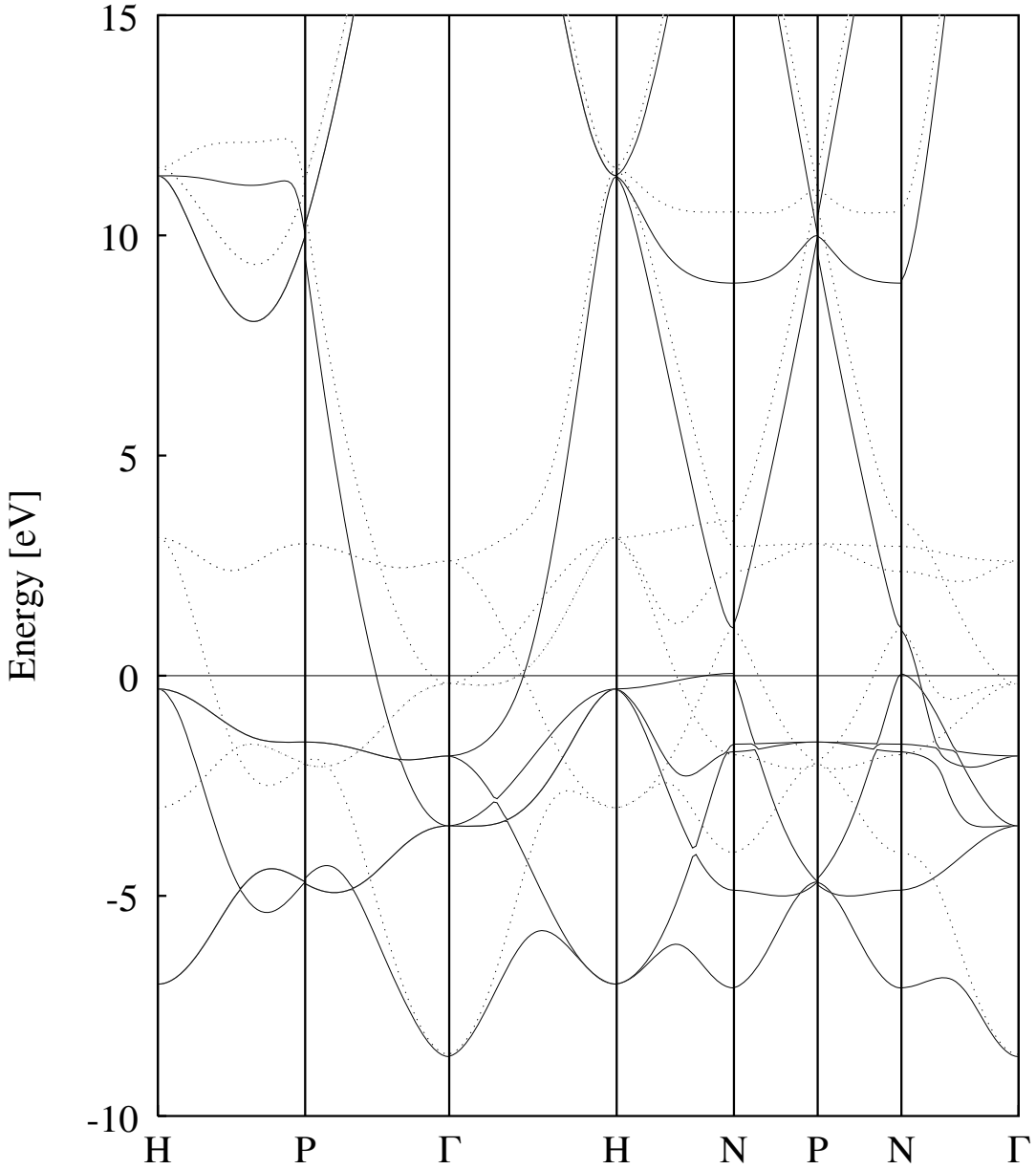


Figure 4.5: The band structure of bcc iron obtained within the LDA+U approach at a lattice spacing 5% smaller than the experimental value.

be less important when atoms get closer and closer to each other, actually it is not because, in a meaningful comparison, the increase of the interaction parameter should be compared with the increase of the bandwidth of the electronic levels around the Fermi energy. In fig. 4.5 the band structure of iron (obtained within our LDA+U approach) at a lattice spacing 5% smaller than its experimental value (the corresponding $U$ is 2.6

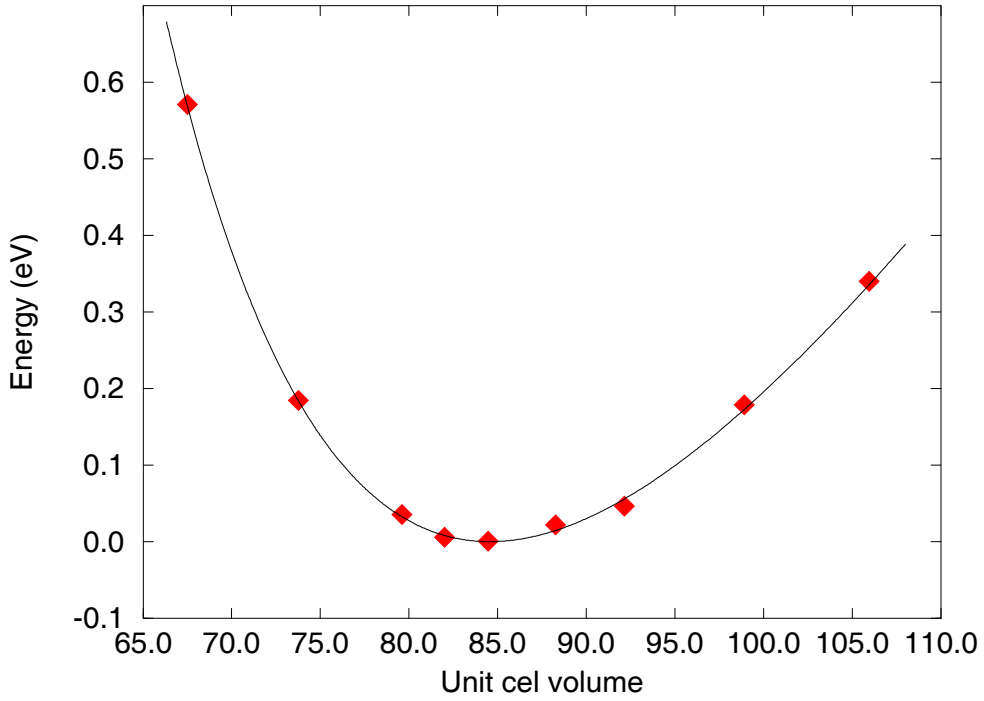


Figure 4.6: The total energy as a function of the unit cell volume and a Murnaghan fit to the calculated points. The zero of the energy is set to the minimum of the plot, while volumes are given in (a. u.)$^3$.

eV) is shown. It can be observed that the bandwidth of the $d$ states in both majority and minority spin channels has become of about 7 eV so that its increase, of about 2 eV, results much more pronounced than the one in the $U$ parameter (0.44 eV), and the metallic character of the system is actually reinforced as expected when squeezing under pressure. When the unit cell volume becomes larger than the experimental one (we now go back to fig. 4.4) a less pronounced increase of the $U$ parameter can be also observed probably motivated by the fact that the system is approaching the atomic limit where the screening is less efficient. Using the calculated values for the Hubbard parameters in LDA+U calculations at different lattice spacings we can study the effect of the LDA+U functional on the structural properties. The result is shown in fig. 4.6 where a Murnaghan fit to the calculated points is shown and used to extract the equilibrium lattice parameter and bulk modulus. A comparison with the experimental values for these quantities is presented in table 4.1. The agreement of LDA+U with the

Table 4.1: Calculated lattice constant ($a_0$), bulk modulus ($B_0$) and magnetic moment ($\mu_0$) in comparison with previous $\sigma$-GGA and experimental results [28]. LSDA results are also shown (from the same reference) to appreciate a comparable agreement with experiments as for LDA+U results.

| | $a_0$ (a.u.) | $B_0$ (Mbar) | $\mu_0$ ($\mu_B$) |
|---|---|---|---|
| LDA+U | 5.53 | 2.12 | 2.60 |
| $\sigma$-GGA | 5.42 | 1.45 | 2.46 |
| LSDA | 5.22 | 2.33 | 2.10 |
| Expt. | 5.42 | 1.68 | 2.22 |

experimental data for the lattice spacing is of the same order as the one obtained by LSDA (but of opposite sign) while GGA gives, in this case, perfect agreement. The bulk modulus obtained within this latter approach is, however, too soft while the LDA+U is intermediate (somewhat too hard if compared with the experimental result) and closer to experiments than the one obtained within LSDA. On the other hand, the magnetic moment is overestimated by the LDA+U approach which gives a worse result than both LSDA and GGA. The overall agreement of the obtained structural parameters with the experimental results is thus quite reasonable for our simple LDA+U scheme even if we could not improve on the results obtained within the GGA approach. The band structure at the equilibrium lattice spacing is shown in fig. 4.7 where the same agreement can be observed with the experimental results as the one reported for calculations performed at the experimental lattice spacing. The results presented in this section about bulk iron, although not completely negative, are not fully satisfactory in the perspective of a systematic use of LDA+U method, as we would expect that an useful approximation should improve the description of problematic systems without spoiling the description of "normal" ones.

Since the simplified LDA+U approach we have adopted here is slightly different from what is commonly used in the literature, we need to check whether extensions of the method frequently used in literature could help improving the obtained results.

The first attempt we made consisted in using the full rotationally invariant formulation of the LDA+U functional (which we call LDA+U+J) introduced by Anisimov and coworkers [6, 7] and described in section 3.2 (eqs. 3.5 and 3.6). The additional parameter we need in this approach, the exchange coupling $J$, cannot be easily calculated from

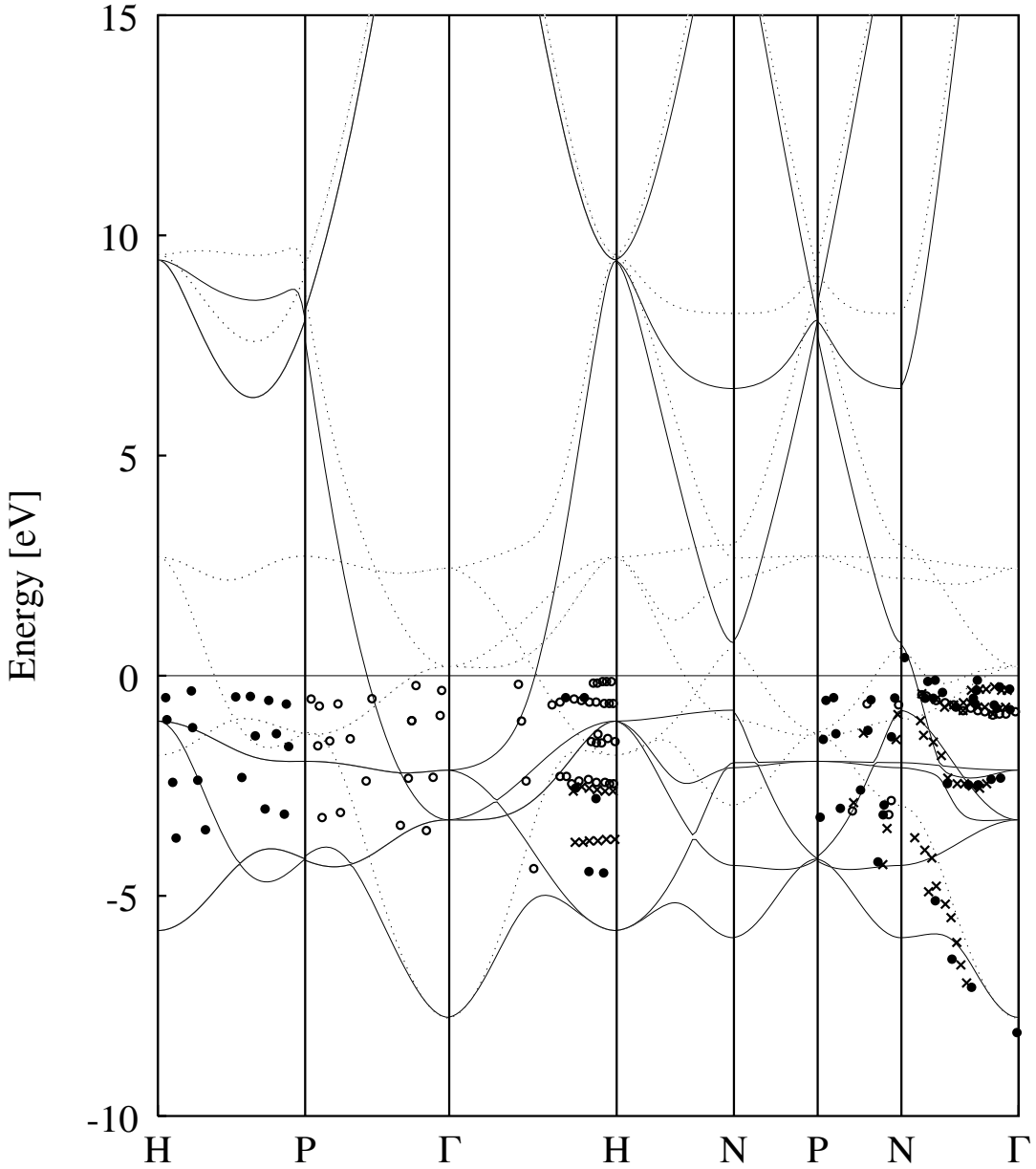


Figure 4.7: The band structure of bcc iron obtained within the LDA+U approach at the equilibrium lattice spacing.

first principle within our scheme as explained at the end of section 3.4. We therefore tried different values of $J$ (together with our calculated Hubbard $U$) seeking a good agreement with the photoemission results for the band structure of this material at the experimental lattice spacing. This semiempirical procedure is somehow equivalent to what is generally done in order to "compute" the values of the interaction parameters

entering the theory. The final choice for $J$ is 1.75 eV while for the Hubbard $U$ we use the ab-initio value of 2.20 eV. These values for the interaction parameters are somewhat larger than those used in ref. [57] (which are $U = 1.2$ eV, $J = 0.8$ eV); however we can notice that the difference $U - J$, which is sometimes used as an effective Hubbard $U$, is almost the same as in our calculations. Completely different values are instead obtained in ref. [59] ($U = 6.65$ eV, $J = 0.89$ eV) where the iron ion is treated as an isolated impurity in a MgO environment and the atomic limit is thus recovered.

The band structure resulting from our interaction parameters at the experimental lattice spacing is shown in fig. 4.8 where a similar agreement with experimental results as the one obtained within standard GGA can be observed. Some minor details differ in the two results (GGA and LDA+U+J) but it is not possible to clearly establish the best agreement to the photoemission measurements on the basis of the available experimental results. We then recalculated the structural properties of bulk iron to check whether the improvement obtained in reproducing the electronic band structure is able to produce better results also for the structural properties and the magnetic moment. In these calculations we assumed that $J$ remains fixed while for $U$ we used our calculated values. The results of these calculations are given in fig. 4.9 whereas in table 4.2 the resulting lattice spacing, bulk modulus and magnetic moments are compared with previous results and with experiments. A slight improvement can be observed for these quantities in comparison with LDA+U results, but the improvement is not significant. Thus, our simplified approach is practically equivalent to the method commonly used in literature for studying the structural properties. The systematic deviation of the calculated parameters from the experimental ones also means that reproducing the band structure with reasonable accuracy is not sufficient to guarantee that other physical properties can be well represented and we will have to take care of this fact when applying the LDA+U scheme to other compounds.

Another simplified approach commonly used in literature consists in considering just one interaction parameter (which we can call $U_{eff}$) corresponding to the difference $U_{eff} = U - J$ [31, 32], and using it in a theoretical approach which is formally equivalent to the LDA+U as it has been adopted in this thesis [43]. Keeping the $J$ fixed (to 1.75 eV), we evaluated the effective $U$ ($U_{eff}$) starting from the calculated values for $U$ and repeat the self consistent calculations at each considered lattice spacing. The results for the lattice spacing, the bulk modulus and the magnetic moment are given again in table 4.2. As it can be clearly observed there is an overall agreement between the LDA+U, LDA+U+J, and the LDA+$U_{eff}$ approaches about the structural properties

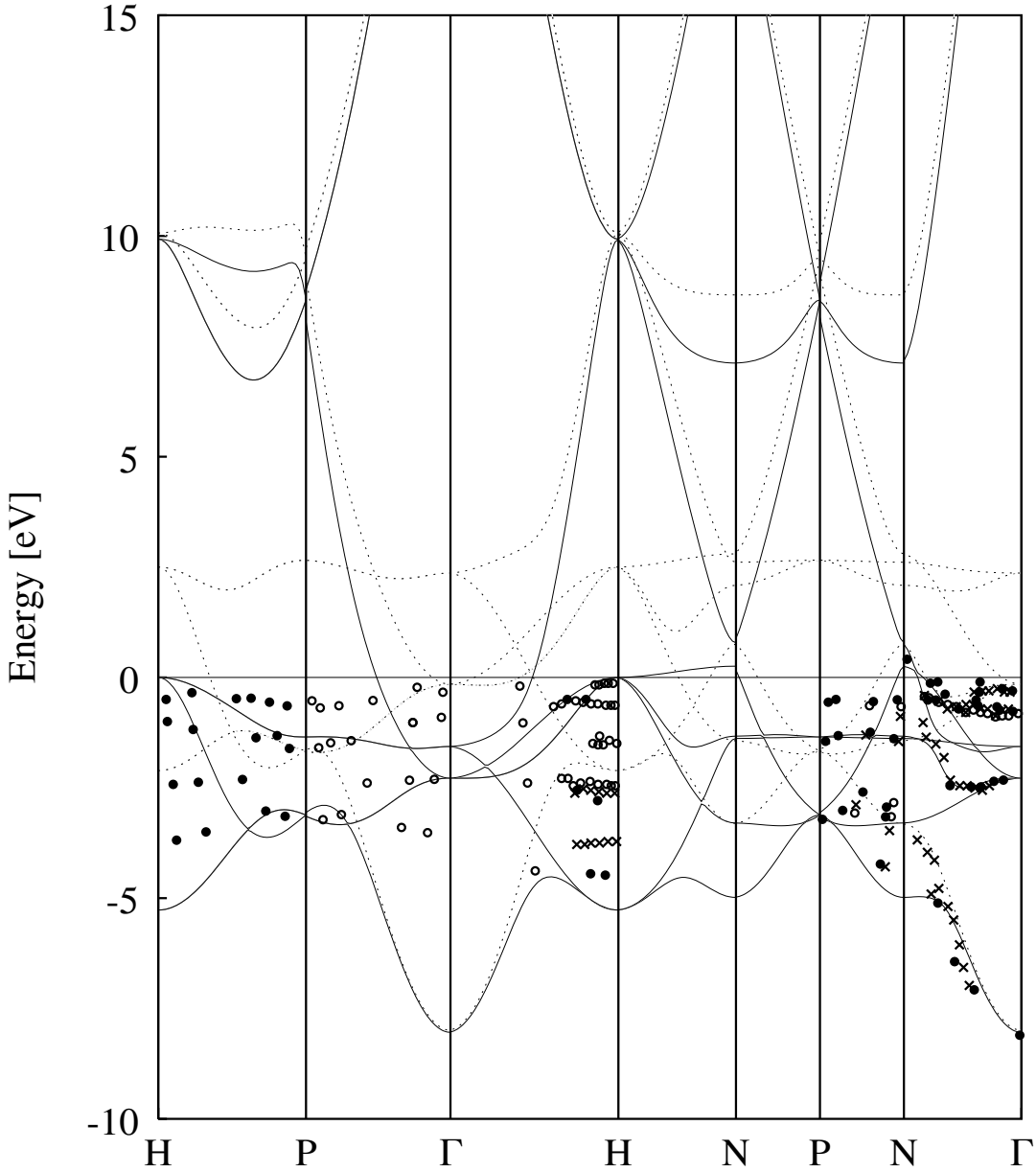


Figure 4.8: The band structure of bcc iron obtained within the LDA+U+J approach at the experimental geometry. $U = 2.2$ eV, $J = 1.75$ eV. Solid lines for majority spin bands, dotted lines for minority spin bands. The zero of the energy is set to the Fermi level.

of bcc FM bulk iron, and this confirms that, at least for this compound, they are practically equivalent when dealing with structural properties. The important feature of the considered theoretical schemes, which controls the description of the structural

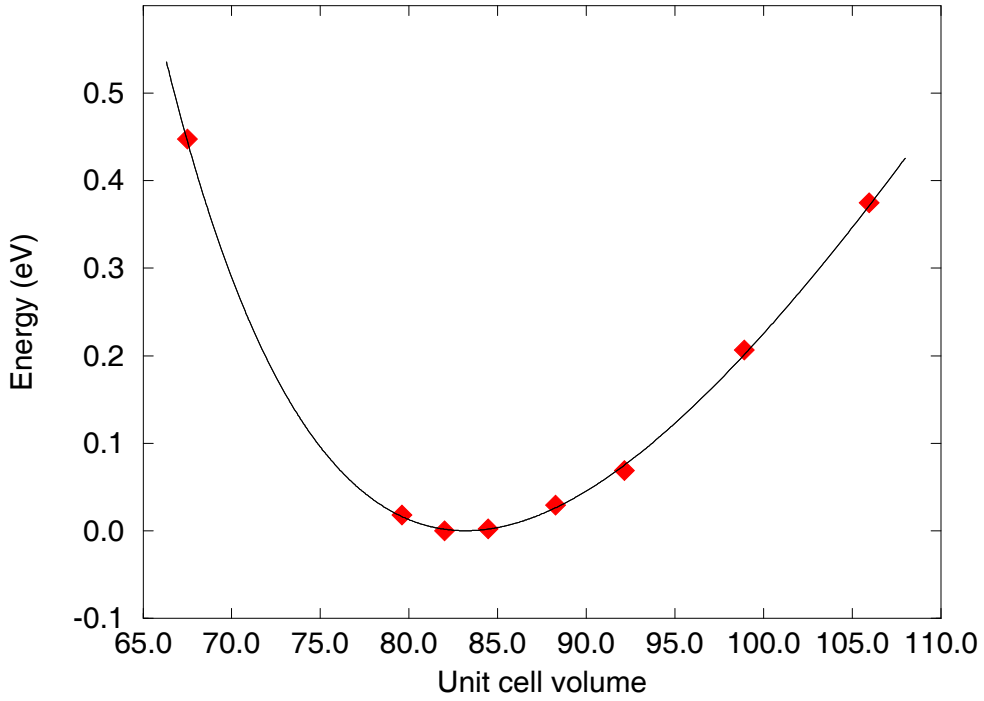


Figure 4.9: The total energy as a function of the unit cell volume and a Murnaghan fit to the calculated points obtained within the LDA+U+J approach. The zero of the energy is set to the minimum of the plot, while volumes are given in (a. u.)$^3$.

properties, is the variation of the Hubbard parameter $U$ with the lattice spacing (which is the same for these approaches) resulting from our calculations. Better results about the lattice parameter, the bulk modulus, and the magnetic moment could possibly be obtained calculating the exchange parameter $J$ at each lattice spacing and considering its variation as well.

In order to check the validity of this idea, we made a further attempt considering, within the full rotational invariant scheme, an exchange parameter $J$ which varies with the lattice spacing $a$ of the unit cell (LDA+U+J($a$) method). The dependence of of the exchange interaction on the cell parameter was modeled assuming that $J$ represented a fixed fraction of the (calculated) on-site Coulomb interaction $U$ at each considered lattice spacing. Using the empirical value of 1.75 eV determined for the experimental volume, we calculated the fixed ratio with the corresponding Hubbard $U$ (2.2 eV) and used this to rescale the value of the exchange parameter for each lattice spacing. A fit

Table 4.2: Calculated lattice constant ($a_0$), bulk modulus ($B_0$) and magnetic moment ($\mu_0$), obtained within the different LDA+U approaches described in the text, in comparison with previous LDA+U, $\sigma$-GGA, LSDA and experimental results.

| | $a_0$ (a.u.) | $B_0$ (Mbar) | $\mu_0$ ($\mu_B$) |
|---|---|---|---|
| LDA+U | 5.53 | 2.12 | 2.60 |
| LDA+U+J | 5.50 | 2.05 | 2.53 |
| LDA+$U_{eff}$ | 5.51 | 2.22 | 2.59 |
| LDA+U+J($a$) | 5.41 | 1.51 | 2.37 |
| LSDA | 5.22 | 2.33 | 2.10 |
| $\sigma$-GGA | 5.42 | 1.45 | 2.46 |
| Expt. | 5.42 | 1.68 | 2.22 |

to the Murnaghan equation of state of the total energies, calculated letting $J$ varying at different volumes, gave the results which are shown in table 4.2. It can be observed that, despite the arbitrary dependence of the exchange parameter $J$ on the lattice spacing, the results obtained within this LDA+U+J($a$) method represent a significant improvement with respect to the other LDA+U approaches and even give (slightly) better agreement with the experimental results (for the bulk modulus and the magnetic moment) than GGA does. This improvement in the description of the structural properties (but also in the electronic structure) of iron confirms our idea that, at least for this material, considering the exchange parameter and its variation with the volume (and in general with the geometry) of the unit cell is necessary to correctly reproduce the physical properties. We also notice that having an exchange interaction $J$ of comparable strength of the on-site Coulomb repulsion $U$ is consistent with the strong ferromagnetic and metallic character of this material. In fact, in a rough HF-like picture, $U - J$ is the effective electronic interaction in the like-spin channel to be compared with the pure $U$ for the unlike-spin one. This means that each ion tends to fill one population of spin, thus fulfilling the first Hund's rule and giving rise to a large on site magnetic moment, but also that, when the itinerant character of the electrons is pronounced, the ionic magnetic moments tend to align with each other to avoid the costly hopping of the valence electrons on opposite spin atomic orbital (itinerant ferromagnetism of iron).

The case of transition metal oxides is quite different. First, the distances among the transition metal ions are larger than in the corresponding bulk material so that

the $d$ states are more localized around the Fe ions. Second, the hybridization with the $s$ orbitals (which also contributes to the metallic behaviour in the bulk iron) is much less important as the presence of the oxygen ions usually strips electrons from the most external states of metals and pushes them far above the Fermi level. The last valence electrons are thus accommodated on very narrow, almost pure, $d$ states which, retaining their atomic-like character to a large extent, may likely generate an insulating behaviour of Mott-Hubbard type which is indeed observed in many cases.

Transition metal oxides are thus the prototype systems for which the LDA+U approach is expected to give a very important contribution. This is what we are going to test in the next sections where the study of FeO and NiO within our LDA+U approach will be presented.

## 4.2 Iron oxide

### 4.2.1 The electronic structure of FeO

The use of the LDA+U method for studying FeO is mainly motivated by the attempt to reproduce the observed insulating behaviour. However ferrous oxide has a quite rich phenomenology including structural phase transitions which seem to be intimately correlated with changes in the magnetic and the electronic properties.

FeO is a very interesting compound for geophysics as it is one of the candidate constituents for Earth's lower mantle and outer core. Thus the experiments have mainly concentrated on the phase transitions this system undergo at high pressure over a wide range of temperatures. It was found that an important transition from the cubic rocksalt structure to a rhombohedrally distorted phase occurs at room temperature at about 16 GPa in correspondence to the onset of the AFM order from the paramagnetic (PM) state [35, 36]. In fact the Neél temperature, which is 198 K at ambient pressure condition is found to increase with pressure and reaches the room value at about 16 GPa. Another structural phase transition is found to occur at 70 GPa when this compound transforms from B1 (cubic or rhombohedrally distorted) to B2 (hexagonal) phase while becoming metallic [31, 32, 35, 36].

The currently used numerical approaches (LDA or GGA) can give a good description for the high pressure phases of FeO where correlation effects are not very important [31, 32, 36]. Even in lower pressure regimes, where on site electronic correlations become stronger, despite failing in correctly reproducing the conduction properties, LDA and

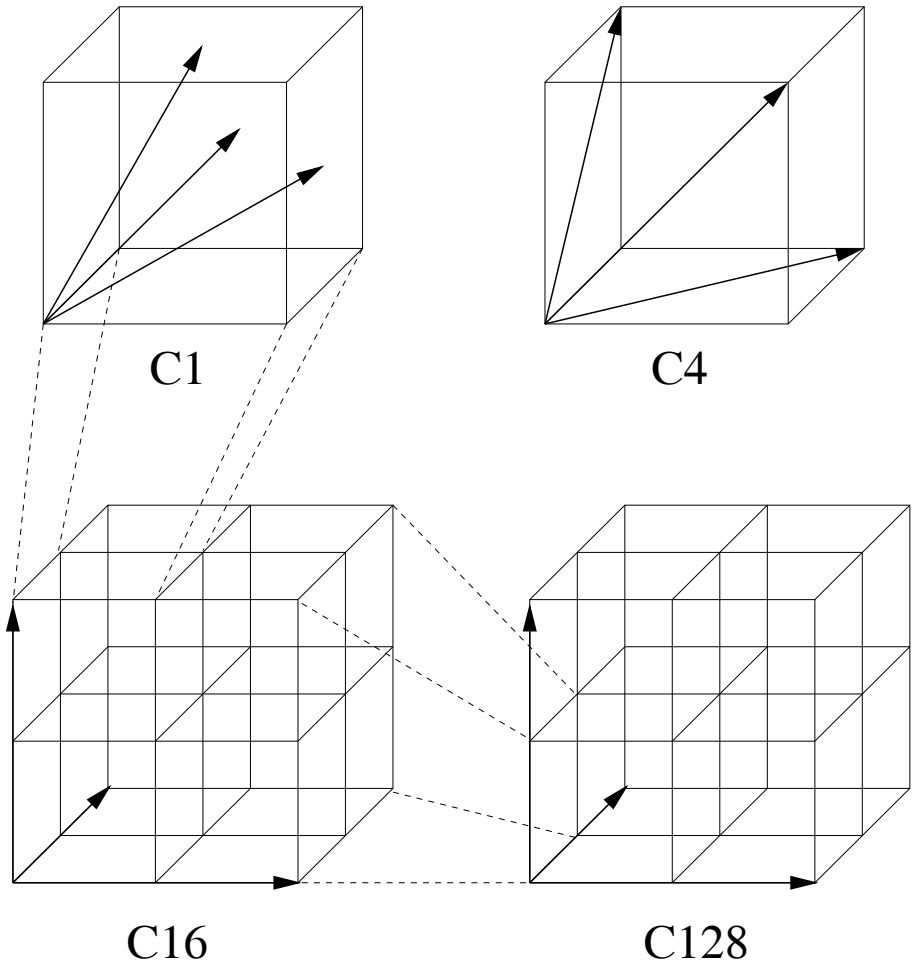


Figure 4.10: The supercells used in the calculation of the Hubbard $U$. C1 is the primitive cell (2 iron), C4 contains 8 iron ions, C16 contains 32 iron ions and C128 contains 256 iron ions. The arrows indicate the fundamental lattice vectors.

GGA can provide a reasonable description of its structural and magnetic properties and also predict qualitatively correct behaviour of the rhombohedral distortion with pressure as shown in chapter 2 (and in ref. [36]).

In this section the low pressure (rhombohedrally distorted B1) AFM phase of FeO is considered in order to study the possible role of correlations in both magnetic and structural properties. The stoichiometric compound is studied in this work despite it is never obtained in experiments due to its instability toward states with iron vacations which deeply influence the magnetic and the structural properties of this material.

Despite the structure is found to be rhombohedrally distorted from the cubic shape

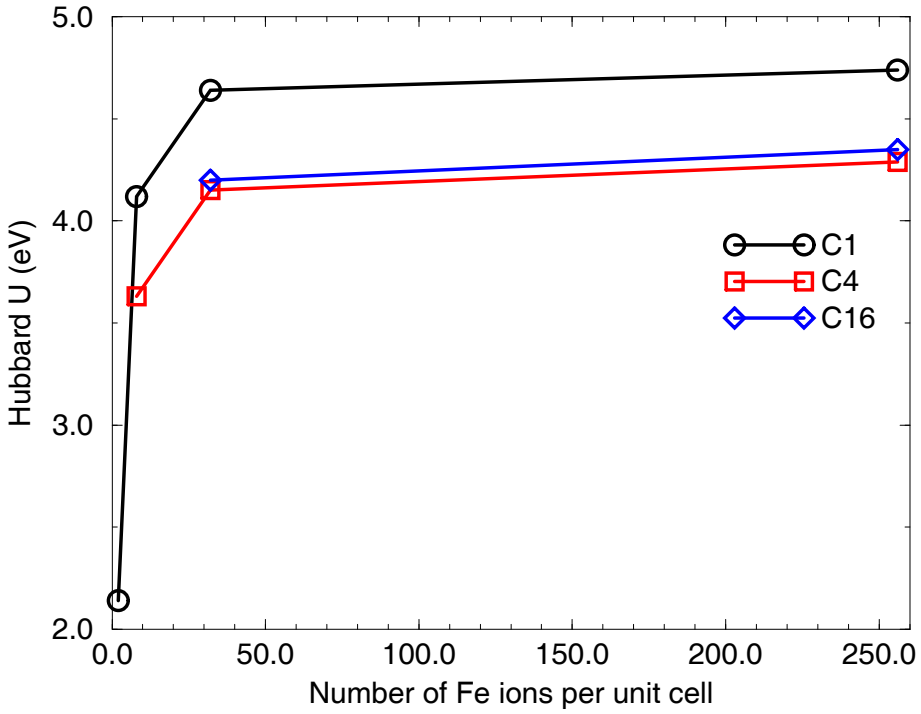


Figure 4.11: The different contributions to the Hubbard $U$ from farther and farther shells of neighbours and their convergence properties with size. C128 is just used to extrapolate results obtained using smaller supercells.

below the Neél temperature (and our calculations always correspond to low temperature conditions) we start considering the cubic cell with the antiferromagnetic order described in fig. 2.4, at the experimental lattice spacing. As already observed in the case of iron, the LDA+U approach required a larger energy cut-off (40 Ry) for the electronic wavefunctions, while the used 4×4×4 k-point grid is not denser than would be necessary in ordinary calculations as this method produces an insulating state. However, quite a small smearing width (0.005 Ry) of the Fermi distribution had to be used when calculating the effective on-site parameter in order to well account for the dynamics of the single particle energy levels around the Fermi energy which produces the charge redistribution.

In order to compute the Hubbard $U$ we adopted the same procedure used for bulk iron and shifted the potential acting on the $d$ states of one iron ion to study the response of the $d$ atomic occupations on the perturbed site and on the others atoms in the system.

When this perturbation is applied on one of the two ions of the primitive unit cell, the result is not very accurate because the redistribution of the charge can just involve the other iron, apart the compensating background (containing iron $s$ states and oxygen $s$ and $p$ states) so that the perturbation is not completely decayed. In practice, the perturbed atom strongly interacts with its nearest neighbours with the same spin which, being translationally equivalent to it, also have a shifted potential in the $d$ channel, so that the screening process is not completely efficient. We thus perform constrained GGA calculation perturbing the potential on the $d$ states of one particular ion in larger and larger supercells which are shown in fig. 4.10. The result about the convergence of the Hubbard $U$ with the number of iron ions contained in the supercell is shown in fig. 4.11. The larger supercell considered, C128, (containing 256 iron ions) is used just to extrapolate the results obtained from the smaller ones as it is too large to be used in direct calculations.

The result obtained using the primitive cell is quite distant from the converged value of the C16 supercell, but, if we consider its extrapolation to the largest C128 structure, we realize that the nearest neighbour contribution can already capture most of the effective interaction. The inclusion of the nearest neighbours with the same spin and of second nearest neighbours with opposite spin (C4 supercell) gives a finite (negative) contribution to the effective parameter as resulting from the full extrapolation to the C128 supercell of the results obtained with C4. Further shells of neighbours are instead irrelevant for the calculation of $U$ as demonstrated by the almost complete equivalence among the the relaxation of the results obtained for the C4 and the C16 supercells into the largest one. In practical calculations we thus performed constrained GGA runs using C4 and then extrapolated the result to C128 to obtain a full converged parameter. The final result is a Hubbard $U$ of 4.29 eV which is in good agreement with the values obtained (or simply assumed) in other works [31, 32]. We then used the computed interaction parameter in LDA+U calculations of some physical properties of this compound. The obtained band structure of the undistorted unit cell at the experimental lattice spacing is shown in fig. 4.12. A gap opens around the Fermi level whose minimal width is about 2 eV. The band gap is direct and located at the $\Gamma$ point. If we observe the (projected) density of states shown in fig. 4.13, we can easily realize that the effective gap appearing in the latter plot is larger than the one in the band structure. The reason for this is that the $\Gamma$ point transition is of Fe $d$ - O $p \rightarrow$ Fe $s$ kind and the contribution of the $s$ states to the projected density of states is not clearly visible on the scale of the plot of fig. 4.13. This implies that the above mentioned

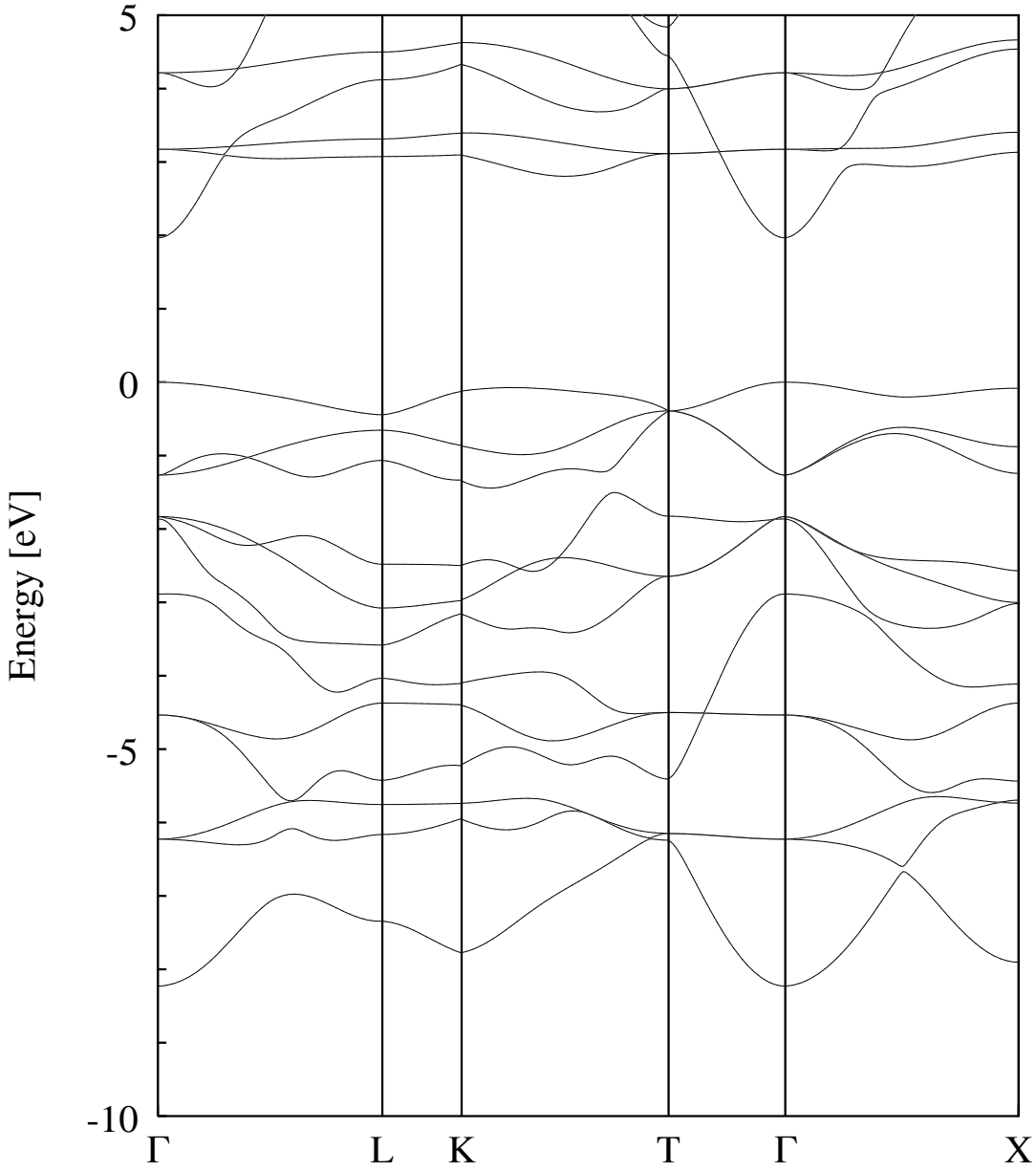


Figure 4.12: The band structure of FeO in the undistorted (cubic) cell at the experimental lattice spacing obtained with a Hubbard $U$ of 4.29 eV. The zero of the energy is set at the top of the valence band.

transition is very weak and this is in very good agreement with experiments reported in [60] where a weak absorption between 0.5 and 2.0 eV is reported. A stronger line (relative to the Fe $d$ - O $p \rightarrow$ Fe $d$ transition) is observed at 2.4 eV [60, 61, 62] which is also in quite good agreement with the width of the gap we obtain in the calculated

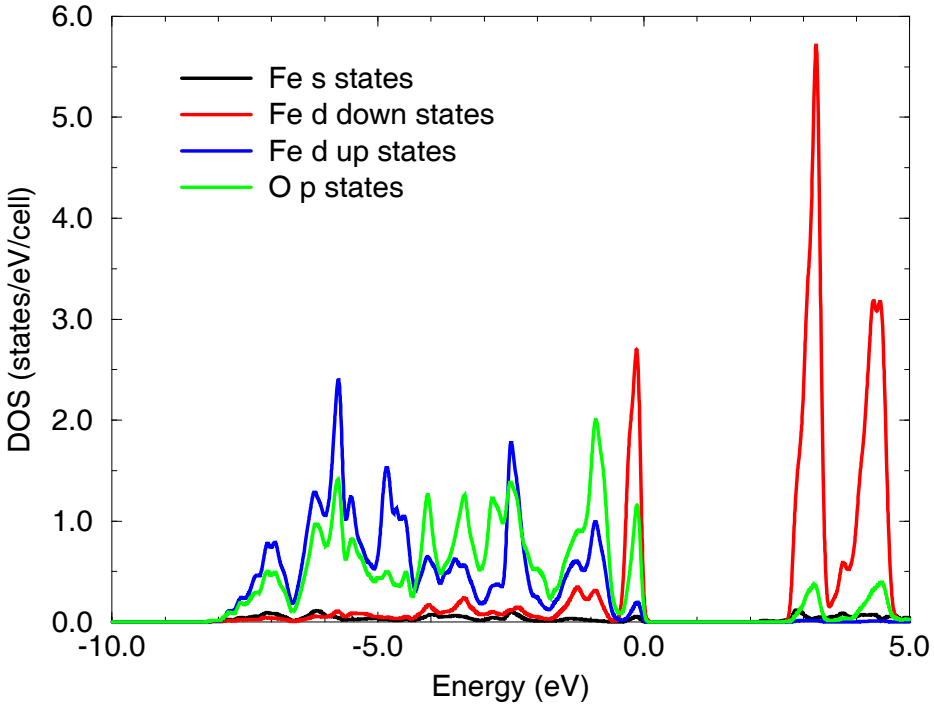


Figure 4.13: The projected density of states of AF undistorted iron oxide at the experimental lattice spacing obtained with $U = 4.29$ eV.

density of states (about 2.6 eV) and other theoretical results [33]. If we compare the density of states obtained within the LDA+U approach with the one we calculated using GGA the only difference which is worth to be underlined (besides the gap) is the fact that the oxygen $p$ states are mixed with the iron $d$ majority spin levels over a wide region of energy extending to almost the top of the valence band (for majority spin we mean the up spin if the magnetization of the considered ion is up and viceversa). In the GGA result (fig. 4.13), instead, the oxygen $p$ states are mainly concentrated below the majority spin $d$ states of iron except a rather isolated contribution on the top of the valence band. The photoemission experiments, however, predict the top of the valence band to be of mixed O $2p$ - Fe $3d$ character [63] which is obtained in both approach. Nevertheless the consequent interaction among the two atomic state groups is stronger in the LDA+U result (due to the larger region of overlap) which can be in better agreement with experiments predicting for FeO a moderate charge transfer character of the insulating state. The contribution of oxygen $p$ states at the top of the

valence band is quite large in our results, and also increases just below this region where the strong mixing with the Fe $d$ majority spin states is observed.

The calculated magnetic moment on the iron ions results to be of 3.73 $\mu_B$ which slightly improve the GGA result of 3.61 $\mu_B$ but is still quite far from the experimental value 4.20 $\mu_B$.

However, despite its simplicity, our LDA+U approach, with the consistent evaluation of the Hubbard $U$, works quite well in reproducing the width and the spectroscopic nature of the band gap of FeO. We want now to further investigate this aspect and test the accuracy of our approach on another paradigmatic transition metal oxide such as NiO.

### 4.2.2 The electronic structure of NiO

The reason for choosing NiO is that it is a well studied material in the family of transition metal oxides so that there exist a good number of works (here including some photoemission experiments) our results can be compared with. On the contrary of FeO, no compositional instability is observed for NiO so that the stoichiometric compound is easy to study thus resulting much better characterized than the iron oxide. Furthermore NiO is a more tractable system to be studied within ab initio techniques. It has cubic structure with the same AF spin arrangements of rhombohedral symmetry as FeO, but does not show tendencies toward geometrical distortions of any kind. Due to the presence of 8 electrons in the $d$ states of Ni (which completely fill, in the atomic limit, the majority spin and the minority spin $t_{2g}$ levels of each ion) and to the presence of a crystal field splitting (which separate the lower energy $t_{2g}$ states from other two of $e_g$ symmetry), it is described as an insulator within the standard GGA approach (which however predicts a smaller gap than experimentally observed), so that the $d$ states already have the correct order for the insulating state to take place. For NiO we did not perform any structural relaxation nor preliminary GGA investigation; we simply run calculations at the experimental lattice spacing for the cubic unit cell with rhombohedral AF magnetic order which is the ground state spin arrangement for this compound. We used the same energy cut offs (of 40 and 400 Ry respectively) for both the electronic wavefunctions and the charge density as for FeO and also the same 4×4×4 k-point grid for reciprocal space integrations. The pseudopotential for Ni is also of US kind and was built within the GGA scheme following the PBE prescription.

To calculate the Hubbard $U$ of NiO we followed the same procedure as for FeO without studying the converged properties of $U$ in this case. We performed a constrained

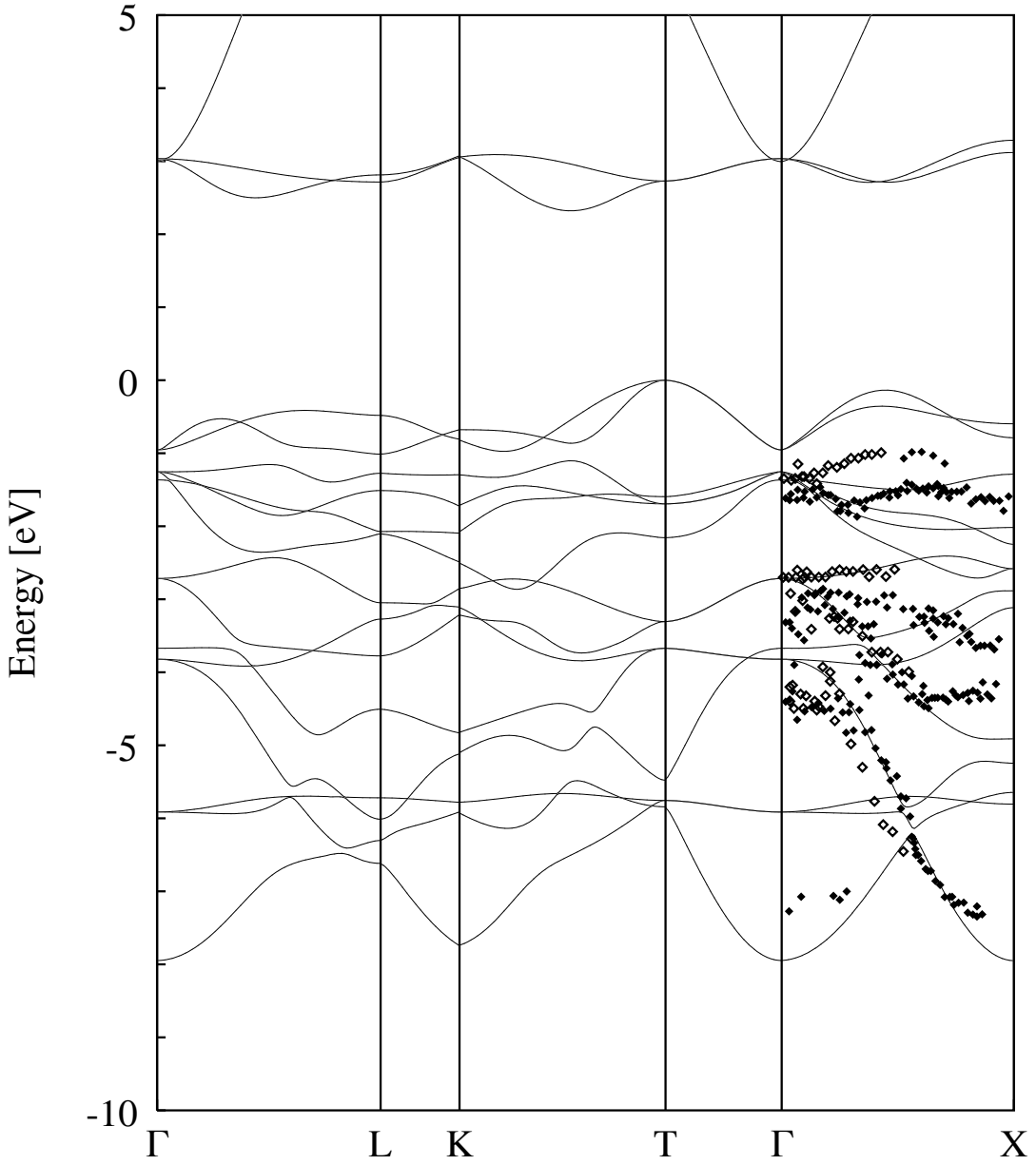


Figure 4.14: The band structure of NiO in the undistorted (cubic) cell at the experimental lattice spacing obtained with a Hubbard $U$ of 4.58 eV. The zero of the energy is set at the top of the valence band. The experimental results were taken from ref. [64] (hollow symbols) and [65] (solid symbols).

calculation in the C4 cell and then extrapolated the obtained result to the C128 supercell (see fig. 4.10) obtaining a final value for the $U$ parameter of 4.58 eV. In fig. 4.14 the band structure of NiO obtained with this value of $U$ is shown and compared with

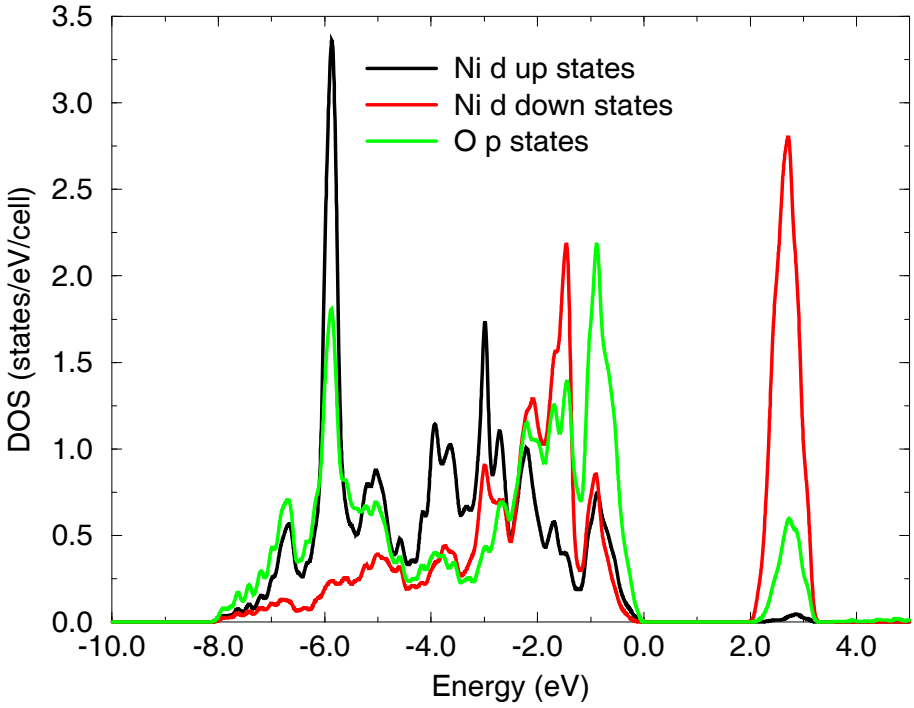


Figure 4.15: The projected density of states of AF undistorted nickel oxide at the experimental lattice spacing obtained with $U = 4.58$ eV.

the photoemission data in the ΓX direction extracted from ref. [64, 65]. Despite the agreement with the experimental results is not excellent, our band structure can reproduce some features of the photoemmission spectrum for this compound. Our theoretical value for the optical gap is $\approx 2.7$ eV around the T point. The fundamental gap, of about 2 eV, is in not in so good agreement with the experimental values exceeding 4 eV as reported in [61, 62, 66]. In ref [67], however, a wider range for the experimental value of the band gap of NiO is reported ranging from 3.0 to 4.4 eV. In the same work it is also reported that in practical LDA+U calculations the experimental value of the band gap is correctly reproduced in calculations using $U$ parameters of the order of 8 eV which are however found to give a worse description of other properties of the material. Using an Hubbard $U$ of 5 eV the same authors were able to obtain a gap of 2.8 eV which is closer to our result. The magnetic moment of the Ni ions is correctly described within our LDA+U approach which gives a value of 1.7 $\mu_B$ well within the experimental range of values ranging from 1.64 and 1.9 $\mu_B$ [67].

In fig. 4.15 the density of states of NiO obtained in our study is shown. The most important feature that is worth notice in the density of states of NiO is the fact that the $p$ states of oxygen dominate the top of the valence band while the bottom of the conduction band is mainly $d$-like thus producing a charge transfer insulator rather than a pure Mott-Hubbard one. This is in good agreement with experiments and other LDA+U calculations which predict the band gap to be of $p - d$ type and the charge transfer character to increase going from FeO to NiO.

### 4.2.3 The structural properties of FeO

Having obtained quite a good description of the electronic structure of FeO and NiO, we want now to use our LDA+U approach to investigate the structural properties of this compound and check whether it is able to correct the disagreement between the GGA results and the experiments about the rhombohedral distortion and its behaviour under pressure. In order to obtain this we followed the same procedure already adopted in the GGA case (chapter 2): we considered a number of rhombohedral distortion, centered around the undistorted cubic structure, and for each of them we performed self consistent calculations at different lattice spacings in order to properly sample the behaviour of the total energy with respect to the volume of the unit cell. In the case of LDA+U calculations, however, a further amount of work is to be done because the Hubbard $U$ parameter has to be recalculated for each distortion and for each considered lattice spacing. This has been done using the same procedure described in the first paragraph of this chapter extrapolating the (distorted) C4 result for the $\chi$ and $\chi_0$ matrices to a C128 supercell with the same considered distortion. The result of these calculations is presented in fig. 4.16 where a Murnaghan fit is shown for the calculated points at each value of the rhombohedral distortion $\alpha_r$. We now extract, for each Murnaghan fit, the pressure dependence of the total energy and repeat the same analysis already done for the GGA case. We thus chose a number of values in the pressure range from 0 to 250 kilobars and for each of them we made a quadratic fit to describe the dependence of the total energy on $\cos(\alpha_r)$. The minimum for this fit at each considered value of pressure produces the behaviour of the rhombohedral angle which is shown in fig. 4.17 where the GGA results and the experimental points already reported in chapter 2, are also considered. The dependence of the rhombohedral angle on pressure which we obtained within our LDA+U approach is not in agreement with the experimental results, nor with the ones obtained within GGA. It even introduces a worse description with respect to the GGA results because it predicts the unit cell to be contracted ($\alpha_r > 60°$) along the

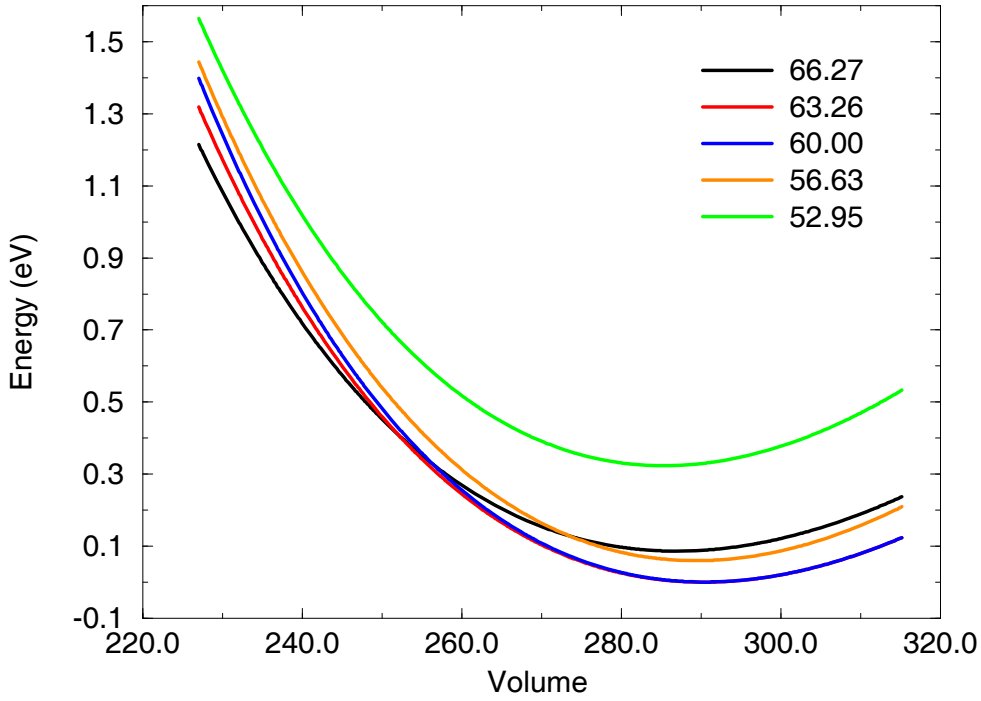


Figure 4.16: The Murnaghan fits for different distorted structures obtained within the LDA+U approach. Angles smaller than 60° correspond to rhombohedral stretching distortions along the [111] direction.

[111] body diagonal (instead of being stretched) and also shows a qualitatively wrong behaviour of the deformation with pressure.

In order to try to improve the description of the structural properties (in particular the rhombohedral distortion) of FeO under pressure loading, we made some attempts to include in our LDA+U functional some additional degrees of freedom (interaction parameters) which were not considered up to this moment. For this compound, however, we don't have any photoemission experiment the calculated electronic band structure can be compared with, as it was the case for iron. To fix the value of the additional parameter we tried to anchor our calculations to the experimental results for the rhombohedral distortion and the lattice spacing obtained at ambient pressure in ref. [34]. In order to obtain the (equilibrium) structural parameters (lattice spacing and rhombohedral distortion) for the stoichiometric compound, we extrapolated the experimental dependence of the structural parameters on iron content reported in the same ref. [34].

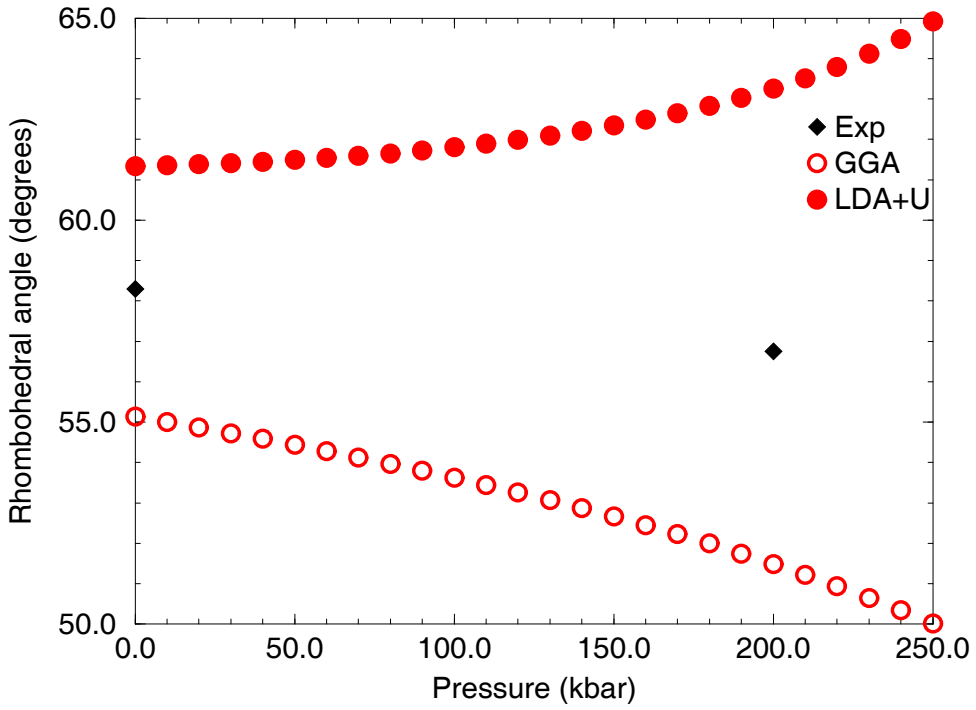


Figure 4.17: The rhombohedral angle as a function of pressure for both GGA and LDA+U approaches. Two experimental points are also shown, which were extracted from refs. [34, 35] as explained in the text.

As this particular distortion was not considered so far, we needed to calculate the Hubbard $U$ parameter for this considered geometry of the unit cell and for a number of different lattice spacings used in the structural relaxation.

The first attempt we made was, as in the case of bulk iron, to use the full rotational invariant LDA+U approach (3.5, 3.6) that we named previously LDA+U+J. In order to fix the value of $J$ we attempted several values for this parameter and, holding it fixed and considering the calculated values for the $U$ parameter, we computed the structural properties at the experimental rhombohedral distortion. Unfortunately we found that increasing $J$ from 0 to 2 eV the equilibrium lattice spacing, that was about 0.7 % smaller than the experimental value, decreases even further so that the best agreement is obtained for $J = 0$, that is our simplified LDA+U approach.

However, in the case of iron, considering the exchange parameter $J$ as a function of volume could improve very much the description of the structural properties of that

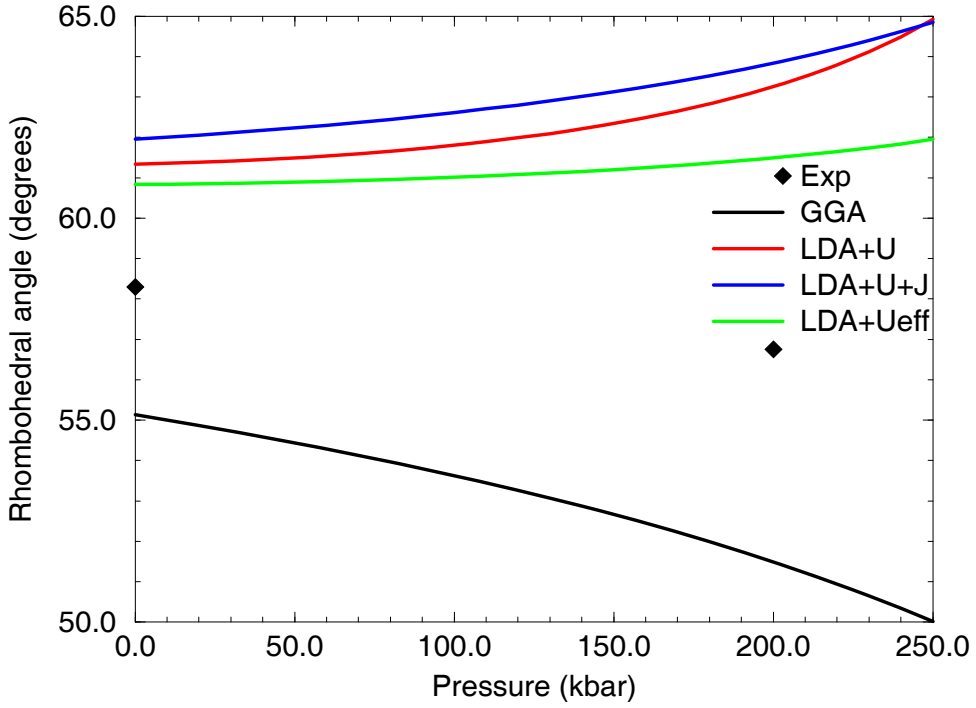


Figure 4.18: The rhombohedral angle as a function of pressure for all the considered LDA+U, LDA+U+J, LDA+$U_{eff}$ approaches in comparison with the GGA and the experimental results.

material. Thus, we wanted to make a similar attempt for FeO and, after arbitrarily fixing for the experimental undistorted structure a $J$ of 2 eV, we assumed that the ratio between $U$ and $J$ remained fixed while changing the lattice parameter and the rhombohedral distortion. Calculating this ratio from the starting undistorted unit cell (the corresponding $U$ is 4.29 eV) we could obtain a value for the exchange interaction in correspondence to each lattice spacing and distortion considered in the structural relaxation. The functional containing the additional exchange parameter $J$ was chosen in two ways: in the first we used the rotational invariant formulation (LDA+U+J), in the second we considered, within the simplified approach, an effective $U$ equal to the difference $U - J$ (LDA+$U_{eff}$). Performing structural calculations for a set of different distortions according to the same procedure illustrated above for the simplified LDA+U scheme we obtained the results shown in fig. 4.18 where the LDA+U and GGA curves are also given in comparison with two experimental results. As it can be observed from

this figure the two extended methods are not equivalent as in the case of bulk iron. The rotational invariant approach gives results which are comparable, or even slightly worse, than the ones obtained within the simplified LDA+U scheme; the LDA+$U_{eff}$ method improves the description of the other two but the agreement with experiments does not change significantly and the rhombohedral distortion still has the wrong sing. Despite the choice of the exchange interaction $J$ was completely arbitrary, we could show that considering this additional parameter in the model may improve the description of the structural properties of real compounds as also happened in the case of iron. However, in the case of FeO, the details about the dependence of $J$ on the structural parameters and, above all, about the way this additional interaction is treated into the model are very important. Thus, calculating the exchange interaction from first principle would be very useful even if, from our results, we do not expect a great improvement in the description of the structural properties of FeO, unless the dependence of the calculated $J$ on the structural parameters would result very different from that found for the Hubbard $U$.

To summarize our experience, the use of the simplified LDA+U approach described in this thesis or of some of the extended approaches including the exchange parameter results useful in the study of the electronic structure of strongly correlated materials as it is able to realize the observed insulating behaviour, to open a gap of width comparable with experimental results and to produce the correct ordering of the bands around the energy gap. However, the use of this approach to study the structural properties of the same compounds is problematic, as demonstrated by the case of FeO, and the quality of the obtained results is critically dependent on the value of the effective interactions, on their variation with the structural parameters and, above all, on the theoretical details and approximations used to build the model. This latter difficulty is probably due to the simplicity of this kind of approaches which does not allow them to properly take into consideration the many degrees of freedom governing the electronic charge distribution and thus the structural properties. The same conclusion we arrive at is also suggested in ref. [68] where a structural study about NiO using GGA and LDA+U metods produced a charge distribution in not very good agreement with the experimental one.

## 4.3 $Fe_2SiO_4$ fayalite

In this section we present the results of the application of the LDA+U scheme to fayalite. The main purpose of this calculation is to study the possible gap opening in the band structure of this compound and the nature of the resulting insulating state. In fact,

as we realized in the study of FeO, the LDA+U approach is quite efficient to study the electronic band structure of strongly correlated materials, but not reliable enough to correctly describe their structural properties. Thus, this latter issue will not be addressed for this material and we will focus our attention on the electronic and magnetic properties studied at the experimental geometry.

The technical details about our practical calculation are slightly different from the ones used in the LDA and GGA studies presented in chapter 2. Thus, to compare the results obtained from the LDA+U scheme with those produced by standard DFT methods, it will be necessary to repeat the GGA calculation at the experimental structure with the same set of parameters required by the LDA+U approach. The same pseudopotentials (ulstrasoft fo Fe and O, norm-conserving for Si) used in the preliminary GGA investigation were also adopted in this case. To calculate the Hubbard parameter we decided to use a smearing width of 0.005 Ry as for bulk iron and iron oxide (smaller than required in standard calculations) to be accurate in describing the region around the Fermi levels where dynamics of levels controlling the charge redistribution in the constrained calculation takes place. Larger energy cut off than used in the calculations reported in chapter 2 were required for both the electronic wave functions and charge density (we used values of 36 and 288 Ry respectively) to obtain a good accuracy in describing the atomic states. A smaller k-point with 8 inequivalent vectors in the IBZ (corresponding to a 2×4×4 Monkhorst-Pack grid) is instead sufficient in the present case to give a good convergence of the total energy and the atomic forces.

As the primitive unit cell of fayalite is quite large, we did not perform the (direct) constrained calculation in larger superstructures (which would be very expensive from a computational point of view) supposing that a large enough number of neighbors, (representing the possible degrees of freedom for the charge redistribution), is already included in the primitive one. Thus, larger supercell were just used to extrapolate the obtained results according to the same procedure illustrated for bulk iron and iron oxide. We considered four supercells. The first is the primitive one (containing 8 iron ions) which is used in the constrained calculation. The second one icludes 16 iron ions and has been obtained by duplicating the primitive one along the $y$ direction (1×2×1 supercell) which is the one along which the dispersion of the (GGA) band structure (and thus the mobility of the electrons) is larger. A third supercell, containing 64 magnetic ions was obtained by duplicating the primitive structure in each direction (2×2×2 supercell). The biggest one is a 4×4×2 supercell and contains 256 iron ions. To calculate the Hubbard parameter we pertub separately the two different families of iron (Fe1 and Fe2). We thus

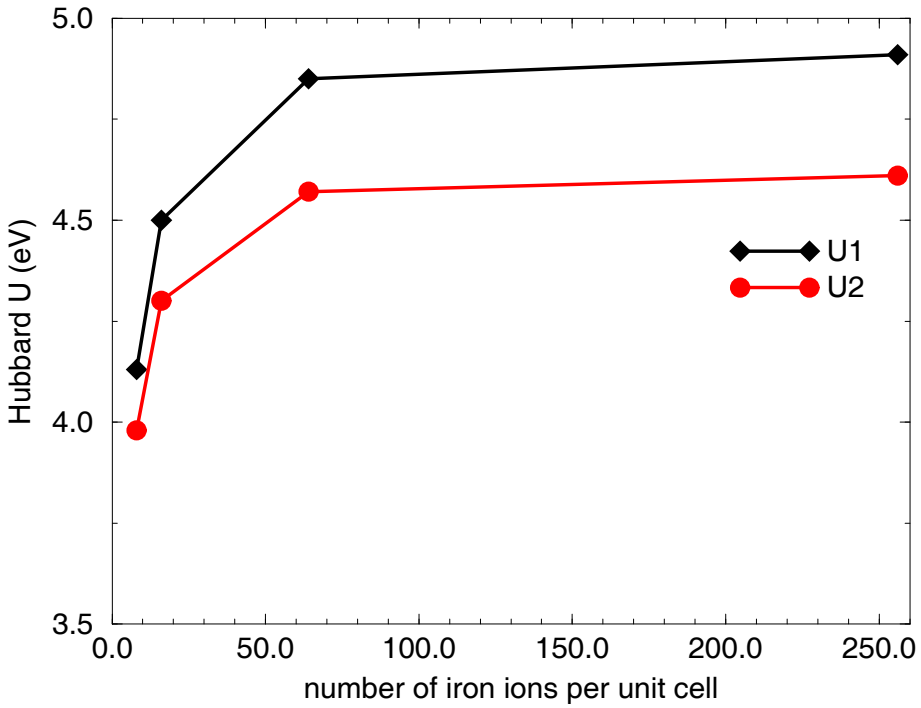


Figure 4.19: The convergenge of the Hubbard parameters with the number of iron included in the supercell. U1 is for Fe1 ions, U2 for Fe2.

obtain two different values for the interaction parameters whose convergence properties with the number of neighbors in larger and larger supercell is shown in fig. 4.19. The final results for the on-site Coulomb parameters are 4.9 eV for Fe1 ions and 4.6 eV for Fe2, which are much larger than the rough estimation we made in chapter 2.

Some preliminary results obtained from a GGA calculation for fayalite at the experimental structure which is considered in this section have to be shown in order to be compared with the ones obtained within the LDA+U approach in the same conditions. The GGA band structure of fayalite is shown in fig. 4.20. The same qualitative considerations done for the GGA study in chapter 2 are still valid here, while a more extended energy range in the plot of the band structure allows some further observations about the relation among the $d$ states of iron and the levels originated from the atomic states of other ions.

A rough classification of the electronic states in three groups can be made from the plot in fig. 4.20. The first group of levels, that lies in the region at the top of the

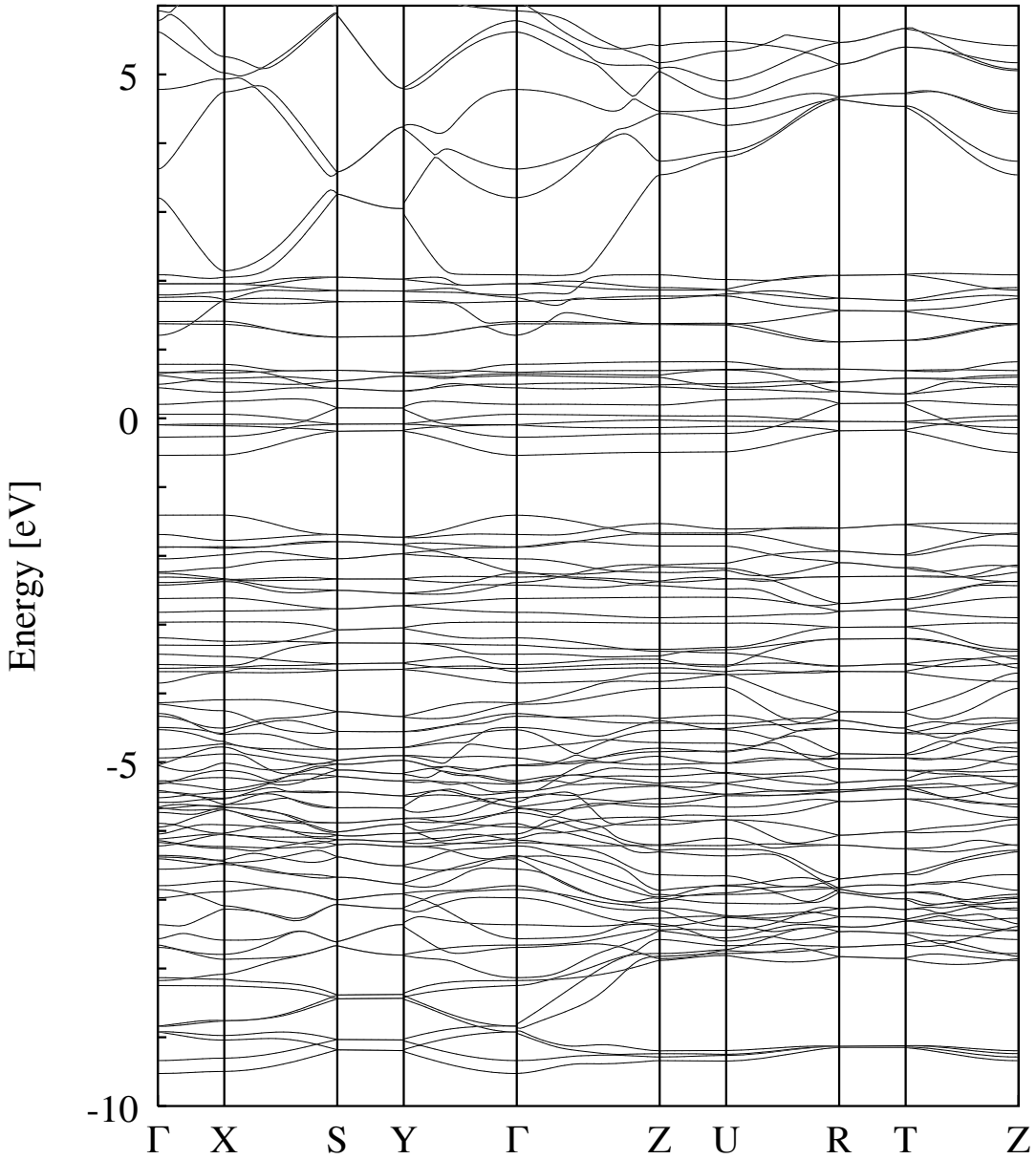


Figure 4.20: The band structure of fayalite obtained within GGA. The zero of the energy is set to the Fermi level of the system. Different lines were used to distinguish the two spin groups of levels but, due to the antiferromagnetism of the system, the states with different spins are completely degenerate.

considered energy window, well above the Fermi energy, display a marked dispersion which suggests they mainly consist of the $s$ states of iron and silicon. The central block of states, ranging from (approximately) 5 eV below the Fermi level to 2 eV above,

consists instead of rather flat bands, that reveal the atomic-like character of the $d$ states of iron. A further distinction of this manifold into two subgroups is also evident and separates the lower energy bands, which lie, completely filled, from 5 to 1.5 eV below the Fermi level (corresponding to the majority spin states of each iron), from the higher energy group of states which crosses the Fermi level and extend from -0.5 to 2 eV, consisting in the minority spin states group of each magnetic ion. As discussed in chapter 2 this separation of the $d$ bands of iron is the origin of the magnetic moment of each ion of this kind while an equal number of sites with opposite magnetization ensures the ground state of the system to correspond to an AF spin configuration. The third group of bands lies from 10 to 5 eV below the Fermi level (it actually cannot be clearly separated from the second) and is characterized by a somewhat larger dispersion than the one observed in the second block which reveal the $p$ nature of these states.

This crude distinction of the energy levels is confirmed by the density of states shown in fig. 4.21. In this plot we considered, for clarity, just the $d$ states of one Fe1 iron and the $p$ levels from one of the oxygens. The contributions to the density of states coming from other atomic levels of the same kind would, in general, be different from the one plotted in this picture, but the qualitative behaviour and the relative importance of the different atomic contribution were found to remain the same and we decided to show just a representative case. Other atomic contributions are also escluded from the plot as, for instance, the $s$ states of iron or the $s$ and $p$ states of Silicon. The reason for this is that they are not important in the physical picture we want to describe: the former states lie well above the Fermi level, whereas the latters give a negligeble contribution in the whole energy window of the plot (the Si ions are almost completely spoiled of their outer electrons). Another set of states, consisting in the oxygen $s$ states, is not considered here; however they are concentrated in a small energy region around 20 eV below the Fermi level where only a small overlap with the Si $s$ and $p$ states can be observed. As it was anticipated in the above introduction, and also observed in the analougus sudy in chapter 2, the Fermi level cuts the minority spin $d$ manifold of iron thus producing a metallic behaviour. This is the main wrong result produced by GGA in representing the conduction properties of this material which is experimentally observed to be an insulator of supposedly Mott-Hubbard type. Another aspect of the density of states which is worth notice is the separation among the majority spin $d$ states of iron and the oxygen $p$ states below the Fermi level. Except for some small overlap, the two groups of states are mainly concentrated in two adiacent regions of energy thus confirming the classification of the states made above.

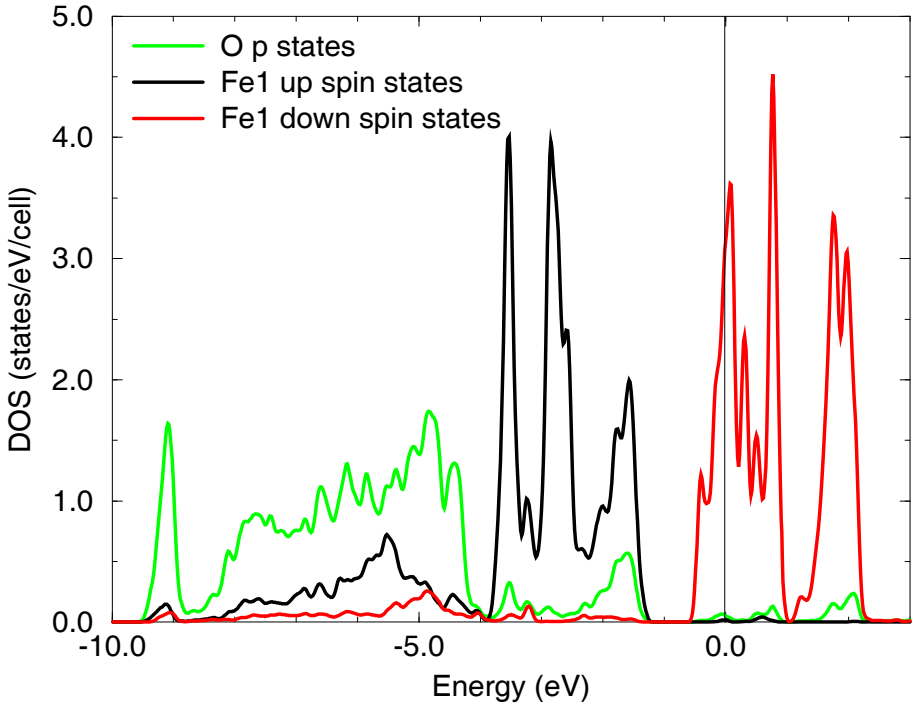


Figure 4.21: The projected density of state of fayalite obtained within GGA. Contributions from the majority (up) and the minority (down) spin $d$ states of one of the Fe1 iron ions and from the total $p$ manifold of one oxygen are shown.

We now want to compare the GGA results with the picture obtained within our simplified LDA+U method using the calculated interaction parameters. The band structure in this case is shown in fig. 4.22. A band gap now separates the valence manifold from the conduction one. The obtained width of about 3 eV overstimates the experimental results at zero pressure which report an energy gap of about 2 eV [69]. However, we have to take into consideration that the experimental structure is not the equilibrium one in our approach. An estimate of the stresses acting on the unit cell showed a tendency toward contraction which could lead to a partial reduction of the calculated band gap due to the widening of the $d$ bands of iron (as already observed for bulk iron). Furthermore the inclusion of the exchange interaction parameter $J$, which is neglected in this case, could lead to a pronounced modification of the electronic band structure as it was observed for bulk iron and the gap could be considerably reduced. The classification of levels introduced within the GGA approach looses its validity in this case. The minority

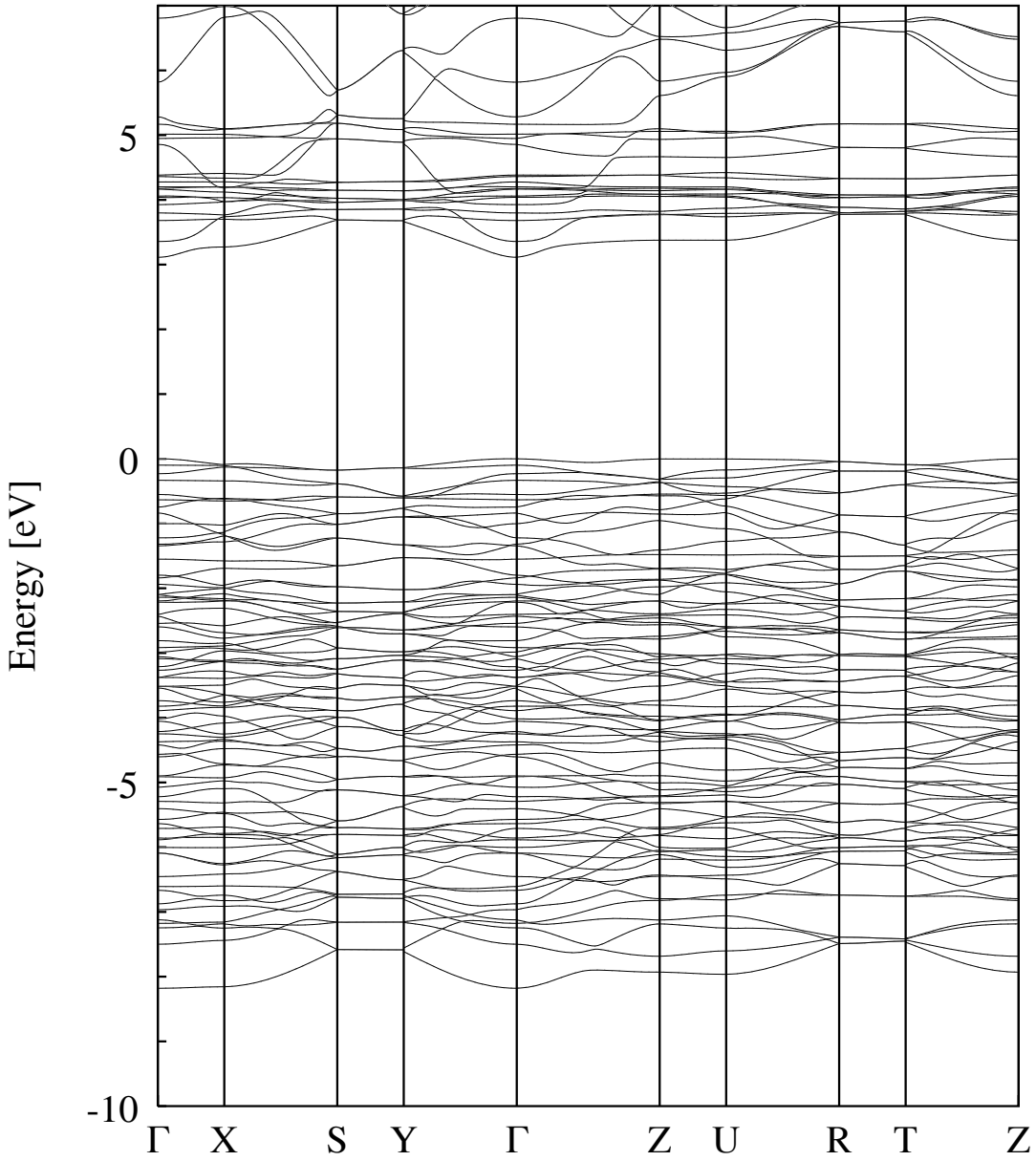


Figure 4.22: The band structure of fayalite obtained within the LDA+U approach. The zero of the energy is set to the top of the valence band. Completely degeneracy among spin up and spin down states can be observed also in this case.

spin manifold is separated into two subgroups by the gap opening and the higher energy $d$ states are shrinked in a smaller energy region and moved above the bottom of the iron $s$ states band which remains almost unaffected. The lower energy minority spin $d$ states, instead, are immerged in the group below the Fermi level where the two sets

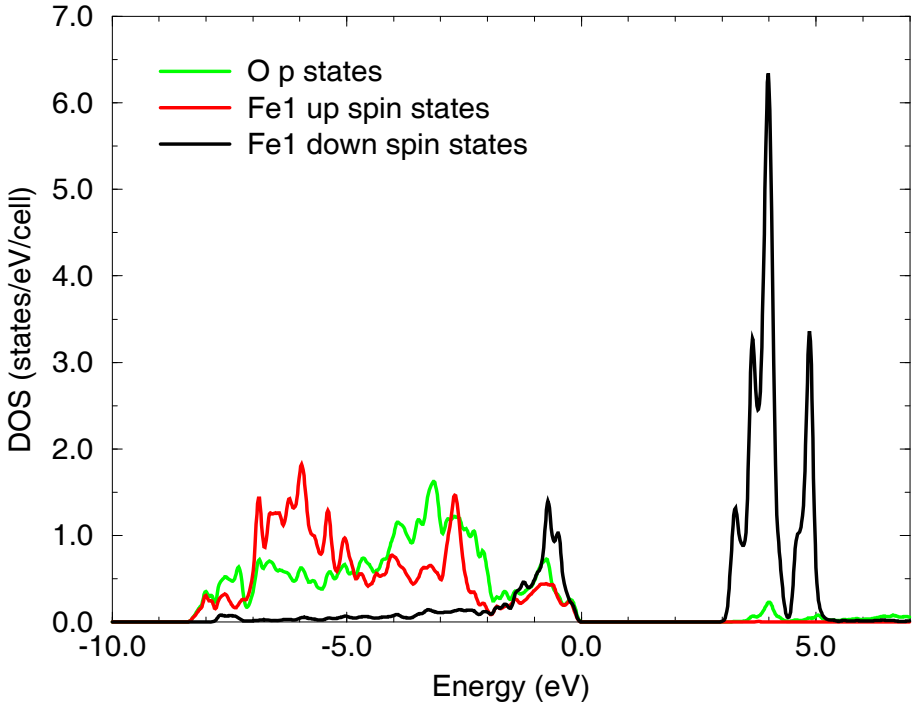


Figure 4.23: The projected density of state of fayalite obtained within the LDA+U approach. Contributions from the majority (up) and the minority (down) spin $d$ states of one of the Fe1 iron ions and from the total $p$ manifold of one oxygen are shown.

of states (belonging to iron and oxygen respectively), distiguished in the GGA results, collapsed into a unique block. The most evident consequence of the gap opening mainly consists in the pronounced shrinking of the $d$ states of iron which, once separated into two groups, become flatter than in the GGA case. This is evident on the top of the valence band, but also for the states well below this energy level, which thus reveal a more pronounce atomic-like behaviour. In this region (extending up to 8 eV below the top of the valence band) the same distinction made within GGA is not possible anymore as we observe a unique block of very flat states. Some mixing has thus occurred among the $d$ states of iron and the $p$ states of oxygen which is indeed confirmed by the projected density of states plotted in fig. 4.23. Beside the gap opening between the two groups of the minority spin states, we can notice, in fact, that a strong mixing occurs among the oxygen $p$ states and the iron $d$ level over the rather large region extending for 8 eV below the top of the valence band. In particular a finite contribution of the oxygen

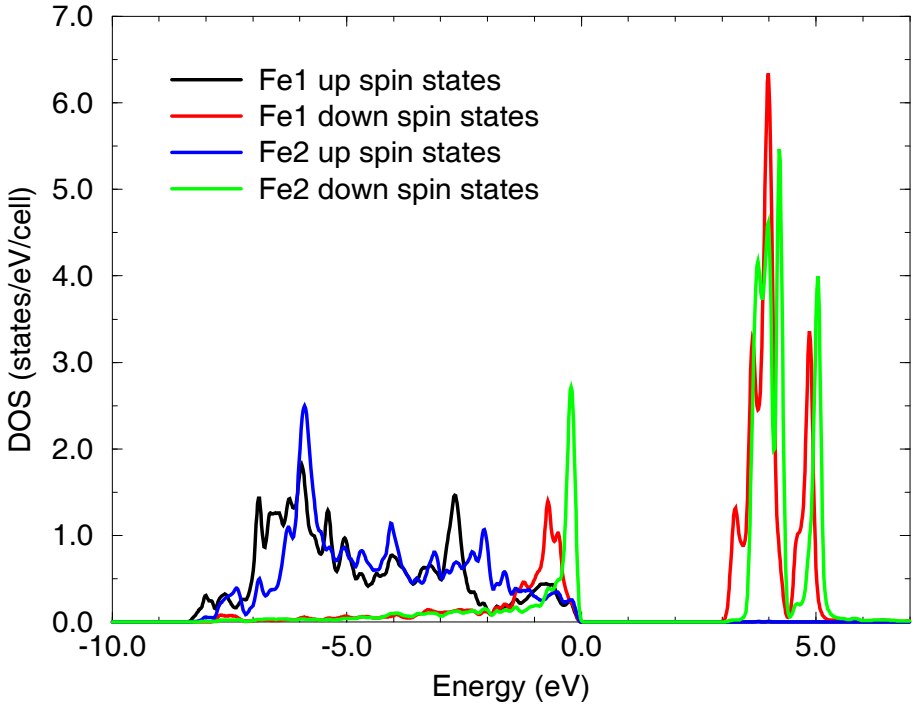


Figure 4.24: The projected density of state of fayalite obtained within the LDA+U approach. Contributions from the majority (up) and the minority (down) spin $d$ states of one of the Fe1 iron ions and from the total $p$ manifold of one oxygen are shown.

states is present at the top of the valence manifold thus suggesting that, as in the case of FeO and NiO, a charge transfer mechanism is responsible for the observed insulating behaviour rather than a Mott Hubbard one. In fig. 4.24 the projected density of states describing the contributions from the $d$ levels of Fe1 and Fe2 ions is shown. The most important feature which is worth notice is the fact that the gap opens among the $d$ states belonging to ions of different kind. The minimum energy transition accross the gap implies the hopping of electrons from Fe1 to Fe2 irons.

Regarding the magnetic structure of fayalite we did not investigate the two possible spin configuration studied in chapter 2 and just took into consideration the spin arrangement obtained, within GGA, as the ground state one. The magnetic moment on each iron, however, is now found to be 3.9 $\mu_B$ which is in closer agreement with its spin-only value (4 $\mu_B$) of the experimental result (4.4 $\mu_B$) than the one obtained in GGA (3.8 $\mu_B$). This increase is probably due to the enhancement of the atomic-like character of

the iron $d$ states which is concenquence of the gap opening.

In conclusion, the LDA+U method gives a quite good description of the electronic band structure of fayalite reproducing the observed insulating behaviour with a reasonable value for its fundamental band gap. Unfortunately, the unreliability of this theoretical approach forbides, for the moment, to investigate the possible consequences of the improvement in the description of electronic structure on the structural properties of this material and on the important phase transitions it undergoes upon pressure loading. These issues are thus left inexplored at the moment.

# Chapter 5

# Conclusions

In the present thesis the accuracy and potential of the LDA+U method in the description of the structural, magnetic and electronic properties of real materials has been analyzed in detail applying this approach to some iron compounds. We have implemented the full rotational invariant LDA+U formalism [6, 7] as well as a simplified approach where, while maintaining the appealing feature of rotational invariance of the parent model, the exchange contribution to the effective electronic interaction is neglected and a direct connection of the correction term with the spurious electronic self-energy present in LDA is made.

The practical implementation of these schemes in a plane wave pseudopotential formalism was realized introducing localized $d$ level occupation matrices as projections of the occupied electronic manifold on suitable atomic states.

In order to make the approach non-empirical, a method for the ab-initio calculation of the interaction parameter $U$ in a plane wave pseudopotential formalism was introduced so as to be consistent with the assumed definition for the occupation matrices. This was done studying the response of the system under consideration to localized perturbations of the Hubbard ions and properly extracting from the total response function the local interaction term. In practical calculations this study has to be performed in larger and larger supercells in order to correctly extract the contribution for an isolated perturbation. In order to study the convergence properties of the effective interactions with the size of the considered unit structure an extrapolating technique of the results of the small supercell to the very large ones was introduced and found to be accurate.

A possible extension of this method to include spin degrees of freedom in the determination of the interaction parameter (which would allow to calculate the exchange interaction $J$) was considered. It was, however, never used for actual calculations be-

cause it resulted affected by large numerical errors due to the encountered difficulties in modifying, with a perturbing potential, the occupancy of the completely filled majority spin states. The very large stiffness of the corresponding response function made the numerical differentiation and the inversion of the corresponding matrix very unstable and unreliable.

The method was applied to both "normal" and "correlated" iron compounds in order to analyze its usefulness as a general approach.

The application of our simplified approach to bulk iron was mainly done in this spirit as it is known that standard GGA (and also LDA) functionals can give a good description of its physical properties and we wanted to check whether the LDA+U method was able to preserve the success of the former approach. The results obtained for bulk iron could not improve the GGA picture, but remained within the same range of agreement with the experimental results already fixed by LDA. The effect of the Hubbard-like interactions on the electronic structure of this material mainly consists in a rigid downward shift of the majority spin states which made worse the agreement with the photoemission results. However, the shift could be eliminated, and the agreement with the experiments reestablished, by considering an exchange parameter in the Hubbard functional treated as in the full rotational invariant approach. Assuming that the exchange parameter scales with the lattice spacing as a constant fraction of the calculated Hubbard $U$ we were able to give a good description of the structural properties of this material, also slightly improving the agreement of the GGA results with experiments for bulk modulus and magnetic moment. Our simplified approach, instead, produced a systematic overestimating of the equilibrium lattice spacing and bulk modulus. Similar overestimating were obtained using a rotational invariant formalism with a fixed $J$ for all the explored unit cell volumes. Thus, at least for iron, including the exchange parameter in the model is important and considering its variation with the volume is necessary to correctly describe the structural properties of this material.

The use of the LDA+U approach to the study of transition metal oxides (which are generally strongly correlated materials), as FeO and NiO, is instead more "natural" because the (almost pure) $d$ bands are very narrow and the overlap among the atomic states is small due to larger interatomic distances. The application of our simple LDA+U method to both FeO and NiO gave good results in describing the electronic structure as it reproduced the band gaps (of the observed width in the case of FeO) with the correct (observed) spectroscopic nature of the associated transitions. The band gap of NiO was indeed obtained to be smaller than the experimental value, but in agreement with

other theoretical approaches. The structural properties of FeO, however, could not be represented very well within this scheme because the rhombohedral distortion of the AF phase upon increasing pressure was obtained to have quite large discrepancies with the experiments and even a qualitatively wrong dependence on pressure. The GGA method could instead reproduce, at least, the correct qualitative trend of this quantity under pressure loading. Also for FeO we considered, beside our simplified LDA+U approach, a number of variations of the method described in the literature but no significant improvement could be achieved in the description of the structural properties, thus confirming that our simplified scheme shows the same problematic behaviour of other more complicated approaches when used for structural calculations. This situation may be possibly traced back to the inability of the LDA+U method to describe the electronic charge distributions which in NiO, for instance, has already been documented in literature [68], while the small variation of the Hubbard parameter with the structural properties is probably not responsible for the obtained wrong behaviour under pressure loading.

The application of LDA+U to $Fe_2SiO_4$ fayalite was mainly motivated by the possibility of studying the gap opening in the band structure (this material is also observed to have an insulating behaviour driven, probably, by a Mott-Hubbard mechanism) and the spectroscopic nature of the possible electronic transitions across it. A gap, about 3 eV wide, is obtained in the band structure (somewhat larger than the experimental one measured at ambient pressure) which makes this compound acquire the observed insulating character. The analysis of the electronic density of states reveals that the oxygen $p$ states give a finite contribution to the top of the valence band so that the mechanism leading to the insulating behaviour is, to some extent, of charge transfer type rather than purely Mott-Hubbard. The stronger atomic-like character of the $d$ states produced by the gap results in a much flatter valence manifold and is probably the origin of the obtained enhancement of the magnetization of each iron ion.

In conclusion our analysis shows that LDA+U method(s) can give quite good results in the description of the electronic properties of strongly correlated materials and can reproduce the observed band gaps and their spectroscopic nature. In the case of transition metals it is somewhat less accurate than for strongly correlated systems but can correctly reproduce the increase of the metallic character upon squeezing under pressure. However, the application of this simple scheme to study the structural properties of real materials is generally problematic and the reason seems not to be related with the simple approximation our model relies on. A possible improvement upon its results can

sometimes be obtained using the original full rotational expression and considering, as in the case of iron, the variation of the additional exchange parameter with the unit cell volume. However this procedure does not lead to systematic improvements and the case of FeO is paradigmatic. In order to better assess the potential of the LDA+U method for structural calculations a consistent and reliable procedure to calculate the exchange parameter $J$ is needed. In any case we believe that, even in this case, the simplified way strong electronic correlations are treated in the model can hardly be successful in describing, with the same accuracy, the different electronic, magnetic and structural properties of real materials. The examples presented in this thesis, in fact, show that using LDA+U it is possible to correctly describe the electronic structure of real (problematic) systems without, however, the guarantee that other physical properties can receive an accurate description as well.

# Bibliography


[1] P. Hohenberg and W. Khon, *Phys. Rev.* **136**, B864 (1964).

[2] W. Khon and L. J. Sham, *Phys. Rev.* **140**, A1133 (1965).

[3] V. I. Anisimov, J. Zaanen, O. K. Andersen, *Phys. Rev. B* **44**, 943 (1991).

[4] V. I. Anisimov, I. V. Solovyev, M. A. Korotin, M. T. Czyzyk, G. A. Sawatzky, *Phys. Rev. B* **48**, 16929 (1993).

[5] I. V. Solovyev, P. H. Dederichs, V. I. Anisimov, *Phys. Rev. B* **50**, 16861 (1994).

[6] A. I. Liechtenstein, V. I. Anisimov, J. Zaanen, *Phys. Rev. B* **52**, R5467 (1995).

[7] V. I. Anisimov, F. Aryasetiawan, A. I. Liechtenstein, *J. Phys.: Condensed Matter* **9**, 767 (1997).

[8] W. E. Pickett, S. C. Erwin, E. C. Ethridge, *Phys. Rev. B* **58**, 1201 (1998).

[9] V. I. Anisimov, O. Gunnarson, *Phys. Rev. B* **43**, 7570 (1991).

[10] J. P. Perdew, R. G. Parr, M. Levy, J. L. Balduz, *Phys. Rev. Lett.* **49**, 1961 (1982).

[11] M. Born, J. R. Oppenheimer, *Ann. Phys. (Leipzig)* **84**, 457 (1927).

[12] W. E. Pickett, *Comput. Phys. Rep.* **9**, 115 (1989)

[13] J. P. Perdew, K. Burke, M. Ernzherof, *Phys. Rev. Lett.* **77**, 3865 (1996).

[14] A. Baldereschi, *Phys. Rev. B* **7**, 5212 (1973); D. J. Chadi, M. L. Cohen, *Phys. Rev. B* **8**, 5747 (1973); H. J. Monkhorst, J. D. Pack, *Phys. Rev. B* **13**, 5188 (1976); **16**, 1748 (1977).

[15] Stefano de Gironcoli, *Phys. Rev. B* **51**, 6773 (1995).

[16] C. L. Fu, k. M. Ho, *Phys. Rev. B* **28**, 5480 (1983).

[17] N. Marzari, D. Vanderbilt, A. De Vita, M. C. Payne, *Phys. Rev. Lett.* **82**, 3296 (1999).

[18] M. Methfessel and A. T. Paxton, *Phys. Rev. B* **40**, 3616 (1989).

[19] D. R. Hamann, M. Schlüter, C. Chiang, *Phys. Rev. Lett.* **43**, 1494 (1979).

[20] G. Kerker, *J. Phys. C* **13**, L189 (1980).

[21] A. Zunger, M. L. Cohen, *Phys. Rev. B* **18**, 5449 (1978); **20**, 4082 (1979).

[22] L. Kleinman, D. M. Bylander, *Phys. Rev. Lett.* **48**, 1425 (1982).

[23] D. Vanderbilt, *Phys. Rev. B* **41**, 7892 (1990).

[24] K. Laasonen, A. Pasquarello, R. Car, C. Lee and D. Vanderbilt, *Phys. Rev. B* **47**, 10142 (1993).

[25] T. C. Leung, C. T. Chan, B. N. Harmon, *Phys. Rev. B* **44**, 2923 (1991).

[26] A. Dal Corso, S. de Gironcoli, *Phys. Rev. B* **62**, 273 (2000).

[27] A. M. Rappe, K. M. Rabe, E Kaxiras, J. D. Joannopoulos, *Phys. Rev. B* **41**, 1227 (1990).

[28] E. G. Moroni, G. Kresse, J. Hafner, J. Furthmüller, *Phys. Rev. B* **56**, 15629 (1997).

[29] A. M. Olés, G. Stollhoff, *Phys. Rev. B* **29**, 314 (1984).

[30] K. Terakura, T. Oguchi, A. R. Williams, *Phys. Rev. B* **30**, 4734 (1984).

[31] Z. Fang, I. Solovyev, H. Sawada, K. Terakura, *Phys. Rev. B* **59**, 762 (1999).

[32] Z. Fang, K. Terakura, H. Sawada, T. Miyazaki, I. Solovyev, *Phys. Rev. Lett.* **81**, 1027 (1998).

[33] I. I. Mazin, V. I. Anisimov, *Phys. Rev. B* **55**, 12822 (1997).

[34] B. T. M. Willis, H. P. Rooksby, *Acta Cryst.* **6**, 827 (1953).

[35] T.Yagi, T. Suzuki, S. Akimoto, *Journ. of Geophys. Res.* **90**, 8784-8788 (1985).

[36] D. G. Isaak, R. E. Cohen, M. J. Mehl, D. J. Singh, *Phys. Rev. B* **47**, 7720 (1993).

[37] Q. Williams, E. Knittle, R. Reichlin, S. Martin and R. Jeanloz, *Journal of Geophys. Res.* **95**, 21549 (1990).

[38] H.K. Mao and P.M. Bell, *Science* **176**, 403-406 (1972).

[39] H. Fuess, O. Ballet, and W. Lottermoser in "Structural and Magnetic Phase Transitions in Minerals", S. Ghose, J.M.D. Coey, E. Salje (Ed), Springer-Verlag, (1988).

[40] R.W.G. Wyckoff, *Crystal Structures*, 2nd ed. (Krieger, Florida , 1981), Vol. 3, chapter VIII,b10.

[41] D. Pines, and P. Nozières, *The Theory of Quantum Liquids*, 1966, vol. **1**, (Perseus Books Publishing).

[42] T. Oguchi, K. Terakura, A. R. Williams, *Phys. Rev. B* **28**, 6443 (1983).

[43] S. L. Dudarev, G. A. Botton, S. Y. Savrasov, C. J. Humpreys, A. P. Sutton, *Phys. Rev. B* **57**, 1505 (1998).

[44] J. Bouchet, B. Siberchicot, F. Jollet, A. Pasturel, *J. Phys.: Condensed Matter* **12**,1723 (2000)

[45] I. G. Austin and N. F. Mott, *Science* **168**, 71 (1970).

[46] A. K. McMahan, R. M. Martin, S. Satpathy, *Phys. Rev. B* **38**, 6650 (1988).

[47] M. S. Hybertsen, M. Schluter, N. E. Christensen, *Phys. Rev. B* **39**, 9028 (1989).

[48] M. T. Czyzyk, G. A. Sawatzky, *Phys. Rev. B* **49**, 14211 (1994).

[49] I. V. Solovyev, N. Hamada, K. Terakura, *Phys. Rev. B* **53**, 7158 (1996).

[50] H. Sawada, Y. Morikawa, K. Terakura, N. Hamada, *Phys. Rev. B* **56**, 12154 (1997).

[51] J. P. Perdew, M. Levy, "Density functional theory for open systems" in the proceedings of the workshop on *Many-body phenomena at surfaces*, ed. by D. Langreth and H. Suhul in 1983.

[52] R. O. Jones, O. Gunnarsson, *Rev. of Mod. Phys.* **61**, 689 (1989).

[53] Y. Kakehashi, J. H. Samson, *Phys. Rev. B* **34**, 1734 (1986).

[54] M. Fähnle, M. Komelj, R. Q. Wu, G. Y. Guo, *Phys. Rev. B* **65**, 144436 (2002).

[55] A. M. Turner, A. W. Donoho, J. L. Erskine, *Phys. Rev. B* **29**, 2986 (1984).

[56] A. M. Oleś, G. Stollhof, *Phys. Rev. B* **29**, 314 (1984).

[57] I. Yang, S. Y. Savrasov, G. Kotliar, *Phys. Rev. Lett.* **87**, 216405 (2001).

[58] M. M. Steiner, R. C. Albers, L. J. Sham, *Phys. Rev. B* **45**, 13272 (1992).

[59] M. A. Korotin, A. V. Postnikov, T. Neumann, G. Borstel, V. I. Anisimov, M. Methfessel, *Phys. Rev. B* **49**, 6548 (1994).

[60] I. Balberg, H. L. Pinch, *J. Magn. Magn. Mater.* **7**, 12 (1978).

[61] G. Lee, S. J. Oh, *Phys. Rev. B* **43**, 14674 (1991).

[62] P. Wei, Z. Q. Qi, *Phys. Rev. B* **49**, 10864 (1994).

[63] P. S. Bagus *et al.*, *Phys. Rev. Lett.* **39**, 1229 (1977).

[64] Z. X. Shen, C. K. Shin, O. Jepsen, W. E. Spicer, I. Lindau, J. W. Allen, *Phys. Rev. Lett.* **64**, 2442 (1990).

[65] H. Kuhlenbeck, G. Odörfer, R. Jaeger, G. Illing, M. Menges, Th. Mull, H. J. Freund, M. Pöhlchen, V. Staemmler, S. Witzel, C. Scharfschwerdt, K. Wennemann, T. Liedtke, M. Neumann, *Phys. Rev. B* **43**, 1969 (1991).

[66] A. B. Shick, A. I. Liechtenstein, W. E. Pickett, *Phys. Rev. B* **60**, 10763 (1999).

[67] O. Bengone, M. Alouani, P. Blöchl, J. Hugel, *Phys. Rev. B* **62**, 16392 (2000).

[68] S. L. Dudarev, L. M. Peng. S. Y. Savrasov, J. M. Zuo, *Phys. Rev. B* **61**, 2506 (2000).

[69] Q. Williams, E. Knittle, R. Reichlin, S. Martin, R. Jeanloz, *Journ. of Geophys. Res.* **95**, 21549 (1990).